

https://dspace.org/

Magmatic stratigraphy of the Tweespalk Section towards potential correlation with the other known Bushveld Complex sequences north of the Thabazimbi-Murchison Lineament

Marx, Daniel George

2021

https://hdl.handle.net/10539/33193

Downloaded from a DSpace repository. https://dspace.org/



UNIVERSITY OF THE
WITWATERSRAND,
JOHANNESBURG

Magmatic stratigraphy of the Tweespalk Section towards potential correlation with the other known Bushveld Complex sequences north of the Thabazimbi-Murchison Lineament.

Daniel George Marx

Supervisors: Prof J.A. Kinnaird and Dr M.A. Yudovskaya

Department of Geology

School of Geosciences

University of the Witwatersrand

October 2021

Declaration

I, Daniel George Marx, declare that this research report is my own original work and that the appropriate measures have been taken to appropriately reference and acknowledge the work of other authors where relevant. This research report submitted in partial fulfilment of the requirements for the degree of Master of Science in Economic Geology at the School of Geosciences, University of the Witwatersrand.



Signature of Candidate

06/10/2021

Date

Abstract

The northern limb of the Bushveld Complex forms part of one largest repositories of PGE-Ni-Cu in the world in the world. The limb has historically received significantly less attention when compared to the eastern and western limbs of the Bushveld, and until more recently has been left largely underexplored. The discovery of the now world-renowned Platreef sparked an increase in the economic potential of the area, with the heightened exploration focus on the limb resulting in the identification of a diverse array of mineralisation types and styles not accounted for in the Platreef definition (ss). This includes the Aurora and Waterberg deposits located further to the north of the observed Platreef extension. The Tweespalk property is situated towards the middle of the northern limb, within a ~10 km section between the Witrivier and Nonnenwerth properties. This section is notably depleted with regards to PGE or Ni-Cu sulphide mineralisation when compared to the high grades seen throughout the Platreef to the south, as well in both the Aurora and Waterberg projects further north. This study has shown that the magmatic stratigraphy at Tweespalk correlates with the conventional northern limb stratigraphy and is representative of both Upper and Main Zones. However, the presence of the local granite gneiss basement high that rises northwards, forms the northern edge of the basin and has resulted in the impeded development of the full Bushveld stratigraphy at Tweespalk. The succession shows an observed but discrete transition from predominantly MZ lithologies through to more felsic and magnetite-rich UZ lithologies, with the UZ-MZ boundary being placed at a depth of 566.1 m, which is ~24.9 m below the first cumulus magnetite-bearing unit. No specific marker horizon (troctolite or pyroxenite markers) was observed within the ~182.2 m MZ at Tweespalk, suggesting that the magmatic stratigraphy in the area comprises a small portion of upper MZ and a thick UZ portion above. In terms of mineralisation within the stratigraphy, the study highlights the absence of two major processes that typically enhance the likelihood of mineralisation within the stratigraphy. The first is the lack of contamination of the intruding magma as a result of limited interaction with the relatively impermeable Archaean granite gneiss basement. In contrast to northern limb stratigraphies that are underlain by various Transvaal Supergroup basement rocks, which contributed significantly towards the development of economic mineralisation. The second is the lack of evidence to support mixing between the new UZ magma influx and residual magma in the chamber during formation. The study concludes that the Tweespalk stratigraphy compares with the typical geology of the northern limb as well as the rest of the Bushveld Complex. The development of the full MZ and underlying RLS however, was inhibited by the local granite gneiss basement high which in turn led to lack of any significant economic mineralisation within the area.

Acknowledgements

I would like to acknowledge and thank a number of people for their contribution to this study. Firstly, many thanks to my supervisors Judith Kinnaird and Marina Yudovskaya for making the project possible. My most sincere thanks go to my parents, Ginny and Gary, and my brother Oliver, for their unwavering support throughout this journey. This degree would never have been possible without your guidance, motivation and backing. I would also like to express a great deal of appreciation to my colleague Andy Vuthuza. Your encouragement and support have been ever-present and I can't thank you enough. Thanks must go to the School of Geosciences at the University of the Witwatersrand for the provision of access to microscope, sample preparation and geochemical analysis facilities, as well as to the laboratory technicians in the department for all of their help. A final thanks to Nicky, Bis and Matt at home, as well as all of my friends and family.

Table of Contents

Declaration i
Abstract ii
Acknowledgements iii
List of Figures vii
List of Tables x
Chapter One 1
1.1. Preamble 1
1.2. Scope of the Research 3
1.3. Aims and Objectives 5
Chapter Two 6
2.1. Introduction to the Bushveld Complex 6
2.1.1. The Rooiberg Group 9
2.1.2. The Rustenburg Layered Suite (RLS) 10
2.1.3. The Lebowa Granite Suite 11
2.1.4. The Rashoop Granophyre Suite 12
2.2. Palaeotectonic Setting 12
2.3. Age of the Bushveld Complex 16
2.4. The Transvaal Supergroup 17
2.5. Magmatic Stratigraphy 18
2.5.1. The Marginal Zone (MZN) 19
2.5.2. The Lower Zone (LZ) 20
2.5.3. The Critical Zone (CZ) 21
2.5.4. The Main Zone (MZ) 23
2.5.5. The Upper Zone (UZ) 24
Chapter Three 26
3.1. Introduction 26
3.2. Magmatic Stratigraphy 28
3.3. The Platreef 32
3.4. The Aurora Project 35
3.5. The Waterberg Project 36
3.6. Mineralisation in the Northern Limb 37
3.6.1. Lower Zone Mineralisation 38
3.6.1.1. South of the Ysterberg-Planknek fault 38

3.6.1.2. North of the Ysterberg-Planknek fault 39
3.6.2. Platreef Mineralisation 39
3.6.2.1. GNPA member south of the Ysterberg-Planknek fault 39
3.6.2.2. Southern Sector (Ysterberg-Planknek to Turfspruit) 40
3.6.2.3. Central Sector (Tweefontein to Zwartfontein) 41
3.6.2.4. Northern Sector (Zwartfontein to Witrivier) 42
3.6.3. Main Zone Mineralisation 43
3.6.4. Upper Zone Mineralisation 44
Chapter Four 45
4.1. Introduction 45
4.2. Core Logging Features 46
4.2.1. Rock Classification 46
4.2.2. Mineralisation 47
4.2.3. Mineralogy 49
4.2.4. General stratigraphy of the Tweespalk area 49
4.2.4.1. The Footwall (Granite Gneiss) 49
4.2.4.2. Main Zone 50
4.2.4.3. Upper Zone 51
4.2.4.4. Sedimentary Cover 53
4.3. Local Geology 53
Chapter Five 57
5.1. Introduction 57
5.2. Methodology and Analytical Techniques 57
5.2.1. Sample Selection 57
5.2.2. Sample preparation for polished thin sections 57
5.2.3. Petrography 58
5.3. Petrologic Features 58
5.3.1. Gabbro 58
5.3.2. Magnetite Gabbro 59
5.3.3. Gabbronorite 60
5.3.4. Magnetite- and/or Olivine-bearing Gabbronorite 62
5.3.5. Anorthosite 63
5.3.6. Feldspathic Harzburgite 64
5.3.7. Pyroxenite/Feldspathic Pyroxenite 65
5.3.8. Norite 67

5.3.9. Granite Gneiss (Footwall) 69
Chapter Six 71
6.1. Introduction 71
6.2. Whole Rock Geochemistry 71
6.2.1. Sample preparation for geochemical analysis 73
6.3. Geochemical Results 73
6.3.1. CIPW Normative Mineralogy Classification 73
6.3.2. Major Element Oxides 74
6.3.3. Geochemical Variations with Depth 76
Chapter Seven 81
7.1. Discussion 81
7.2. Conclusions 86
References 88
Appendix 1 101
Appendix 2 108

List of Figures

Figure 1.1. *A simplified geological map of the Bushveld Complex, highlighting the locations of the various limbs and lithological exposures (Adapted from Eales and Cawthorn, 1996).* *1*
Figure 1.2. *Location of the Tweespalk farm property within the northern limb of the Bushveld Complex, with the farm area highlighted in red (After Ashwal et al., 2005).* *4*
Figure 2.1. *A simplified geological map of the Bushveld Complex, highlighting the locations of the various limbs and lithological exposures (Adapted from Kinnaird et al., 2005).* *7*
Figure 2.2. *A schematic north-south cross-section of the eastern limb from Dulstroom to Steelpoort, illustrating the relationship between Rustenburg Layered Suite's chamber expansion from magma addition and the Pretoria Group (After Harmer and Sharpe, 1985).* *8*
Figure 2.3. *A schematic diagram of the Rogers Model for the estimated timing of amalgamation, formation and breakup of major continental land masses between 3.0 and 0.3 Ga, and more specifically the evolution of Rodinia, the first supercontinent (After Robb, 2005).* *13*
Figure 2.4. *The location of the Bushveld Complex PGE deposit within the Kaapvaal Craton, as well as the relation between the Kaapvaal and Zimbabwe Cratons (After Maier and Groves, 2011).* *15*
Figure 2.5. *A generalised stratigraphic succession through the RLS of the Bushveld Complex, highlighting the major subdivisions, dominant rock types, major marker horizons and appearance of the various cumulus phases throughout. Also shown are the major integration and differentiation evolutionary phases of the Complex discussed in section 1.2.1.2. (Adapted from Robb, 2005).* *19*
Figure 3.1. *A geological map of the northern limb of the Bushveld Complex, showing the geology of the northern limb as well as the locations and boundaries of farm properties therein (After van der Merwe, 1976).* *26*
Figure 3.2. *A schematic illustration of the stratigraphic columns of the Rustenburg Layered Suite in the northern limb relative to the Western and Eastern Limbs of the Bushveld Complex. The illustration shows the inferred correlation between the Merensky Reef in the Eastern and Western Limbs and the Platreef in the northern limb (Adapted from McDonald and Holwell, 2005).* *28*
Figure 3.3. *The general stratigraphy of the northern limb of the Bushveld Complex (After McDonald et al., 2005 and Smith et al., 2014).* *30*
Figure 3.4. *A geological map of the of the northern limb of the Bushveld Complex, highlighting Platreef development by the red line and the ~10 km sector south of Nonnenwerth where Platreef mineralisation has not developed (Adapted from Grobler et al., 2018).* *33*
Figure 3.5. *A schematic south-north cross-section of the northern limb showing the complex geographic and stratigraphic relationships between the various farm and deposit localities, with the Tweespalk farm location specifically illustrated to the north of Witrivier (Adapted from Kinnaird and McDonald, 2018).* *38*
Figure 4.1. *Locations of seven of the nine borehole collars drilled on the Tweespalk farm with borehole TW1 highlighted by the black rectangle. The generalised surface geology of the area is also shown, with the purple and blue colours representing the Upper and Main Zones respectively (Adapted from Visser and McWha, 2005).* *45*
Figure 4.2. A) *The QAPF double triangle modal classification diagram for plutonic rocks (based on Streckeisen (1976)).* ***B)*** *Modal classification Plag-Px-Ol ternary diagram of Gabbroic rocks* ***C)*** *Modal classification Plag-Opx-Cpx ternary diagram of Gabbroic rocks. (Adapted from Le Maitre et al., 2002).* *47*
Figure 4.3. *Photos of the Tweespalk core TW1 showing* ***A)*** *Main Zone Gabbronorites overlying the Granite Gneiss Basement.* ***B)*** *A sharp contact between Melagabbronorite and the Granite Gneiss Basement.* ***C)*** *The leucocratic Granite Gneiss Basement rock.* *50*
Figure 4.4. *Main Zone rock types observed in the Tweespalk core of TW1.* ***A)*** *A fine-grained Feldspathic Harzburgite that transitions into Olivine-bearing Melanorite* ***B)*** *A section of Olivine-bearing Gabbronorite, Feldspathic Pyroxenite and Gabbronorite* ***C)*** *A range of MZ rock types from Gabbronorite, to Feldspathic Pyroxenite, to a patchy textured Leuconorite.* ***D)*** *A homogeneous Gabbronorite towards Melanorite.* *51*
Figure 4.5. *Upper Zone rock types observed in the Tweespalk core of TW1.* ***A)*** *Magnetite Gabbro and Anorthosite with magnetite patches or oikocrysts.* ***B)*** *Normal Gabbro with the presence of Granitic Veining.* ***C)*** *Magnetite Gabbro towards magnetite-bearing Leucogabbro.* ***D)*** *A range of UZ rock types including Anorthosite, Magnetite Gabbro, Olivine- and Magnetite-bearing Feldspathic Pyroxenite, as well as a pegmatoid and altered pegmatoid.* *52*

Figure 4.6. *Unconsolidated alluvium and weathered sedimentary cover, as well as highly weathered gabbro overlying Magnetite Gabbro of the Upper Zone in core TW1.* *53*
Figure 4.7. *Full stratigraphic log of borehole TW1 from Tweespalk, showing the different lithologies observed at various depths.* *54*
Figure 5.1. *The photomicrographs **A)** and **B)** display a medium-grained gabbro from TW1-17 (339.8 m), showing two large grains of clinopyroxene and orthopyroxene surrounded by plagioclase grains and smaller clinopyroxene grains (PPL and XPL). Photomicrographs **C)** and **D)** show a slightly more leucocratic gabbro of TW1-18 (390 m), showing coarse grains of orthopyroxene and plagioclase with medium-grained clinopyroxene grains (PPL and XPL).* *59*
Figure 5.2. *The photomicrographs **A)** and **B)** shows plagioclase, clinopyroxene and orthopyroxene grains with intercumulus magnetite and minor biotite in a typical magnetite gabbro sample from TW1-1 (30.2 m) (PPL and XPL). Photomicrographs **C)** and **D)** also show the magnetite gabbro from TW1-1 (30.2 m), but the sample displays a small volume of disseminated sulphides with biotite and other accessory minerals forming around the sulphide grains as well as at the boundary between orthopyroxene and magnetite grains (PPL and reflected light).* *60*
Figure 5 3. *Photomicrographs **A)** and **B)** of TW1-26 (584.3 m) exhibit a coarse-grained to pegmatoidal leucogabbronorite, with a large orthopyroxene grain that hosts inclusions of finer-grained orthopyroxene, surrounded by large grains of plagioclase (PPL and XPL). Photomicrographs **C)** and **D)** show a more typical gabbronorite sample of TW1-31 (627.6 m) that is generally more equigranular with large proportions of clinopyroxene and plagioclase with lesser orthopyroxene (PPL and XPL). Photomicrographs **E)** and **F)** are representative of the largely homogeneous gabbronorites observed towards the base of the succession, displaying a largely equigranular texture with limited plagioclase and speckles of sulphides throughout the TW1-39 (686.1 m) sample (PPL and XPL).* *62*
Figure 5.4. *Photomicrographs **A)** and **B)** show the melagabbronorite sample of TW1-27 (595.5 m) which contains small grains of cumulus magnetite amongst the plagioclase, orthopyroxene, clinopyroxene and biotite (PPL and XPL). Photomicrographs **C)** and **D)** are images of the olivine-bearing and homogeneous gabbronorite sample TW1-28 (603.3 m) (PPL and XPL).* *63*
Figure 5.5. *Photomicrographs **A)** and **B)** show a medium-grained magnetite-rich anorthosite of TW1-8 (166.5 m) with largely euhedral cumulus plagioclase grains and anhedral intercumulus magnetite grains with minor biotite at the grain boundaries (PPL and XPL). Photomicrographs **C)** and **D)** show a more typical anorthosite of TW1-11 (206.6 m), largely dominated by medium-grained plagioclase with some intercumulus magnetite (PPL and XPL).* *64*
Figure 5.6. *Photomicrographs **A), B), C)** and **D)** show the olivine-bearing feldspathic harzburgite sample TW1-22 (544.2 m), which comprises largely of medium-grained orthopyroxene, olivine and plagioclase with lesser clinopyroxene (PPL and XPL).* *65*
Figure 5.7. *Photomicrographs **A)** and **B)** show the coarse-grained and olivine-rich pyroxenite of TW1-12 (210.5 m) that has undergone moderate alteration (PPL and XPL). Photomicrographs **C)** and **D)** show sample TW1-23 (567.5 m) which is reclassified as a norite on the basis of both cumulus plagioclase and pyroxenes being present (PPL and XPL). Photomicrographs **E)** and **F)** show the highly altered feldspathic pyroxenite of TW1-13 (212.8 m) which shows quartz reaction rims around the rounded magnetite grains as well as altered olivine grains in association with chlorite (PPL and PPL).* *67*
Figure 5.8. *Photomicrographs **A), B)**, **C)** and **D)** are all images of sample TW1-30 (618.2 m) which is a melagabbronorite, generally containing a higher proportion of clinopyroxene to orthopyroxene, and olivine-bearing (PPL and XPL). **E)** and **F)** show sample TW1-24 (568.1 m) which contains high proportions of plagioclase and clinopyroxene, is reclassified as an anorthosite from a leuconorite.* *69*
Figure 5.9. *Photomicrographs **A)** and **B)** show fine- to medium-grained quartz and altered feldspars in an interlocking texture of the granite gneiss sample TW1-40 (698.6 m) (PPL and XPL).* *70*
Figure 6.1. *Modal classification **A)** Plag-Px-Ol and **B)** Plag-Opx-Cpx ternary diagrams with the CIPW norm calculations for all forty samples plotted on each (Adapted from Streckeisen, 1976 and Le Maitre et al., 2002).* *74*
Figure 6.2. *Major element geochemical plots of **A)** Al_2O_3 vs MgO **B)** CaO vs Al_2O_3 **C)** Al_2O_3 vs MgO + Fe_2O_3 and **D)** CaO vs MgO + Fe_2O_3 for the TW1 samples, showing the compositions of the different rock types compared to the endmember minerals of plagioclase, orthopyroxene, clinopyroxene and olivine.* *75*

Figure 6.3. *Major element oxide geochemical variations with depth in borehole TW1,* ***A)*** *SiO_2 /Al_2O_3* ***B)*** *Al_2O_3* ***C)*** *CaO* ***D)*** *Mg#* ***E)*** *Fe_2O_3* ***F)*** *Al_2O_3/FeO + MgO* ***G)*** *TiO_2* ***H)*** *CaO/Al_2O_3. ..... 77*
Figure 6.4. *Major and trace element geochemical variations with depth in borehole TW1,* ***A)*** *Sr/Al_2O_3* ***B)*** *Ni* ***C)*** *Cu* ***D)*** *V* ***E)*** *Co* ***F)*** *Cr. Symbols as in seen in Figure 7.3. ..... 79*
Figure 7.1. *Simplified core logs representing and comparing the general stratigraphy of the northern limb at Tweespalk, Waterberg (After Huthmann et al., 2018), Aurora (After McDonald et al., 2017) and Bellevue (After Ashwal et al., 2005). 84*

List of Tables

Table 2.1. *The currently accepted standard nomenclature and subdivisions of the four major magmatic suites within the Bushveld Complex (After Cawthorn et al. (2006)). 9*
Table 4.1. *Collar co-ordinates, orientations and the number of samples taken for each the boreholes drilled on the Tweespalk farm (Adapted from Visser and McWha, 2005). 48*
Table 4.2. *Specific mineralised intersections from the Tweespalk boreholes (Adapted from Visser and McWha, 2005). 49*
Table 6.1. *A list of the TW1 samples with their respective depths and lithologies. 72*

Chapter One

Introduction

1.1. Preamble

The Bushveld Igneous Complex (*Figure 1.1)* is the largest and most well-known mafic to ultramafic layered intrusion on Earth and is the principal repository of platinum-group element (PGE) resources within the Earth's crust observed to date (Eales and Cawthorn, 1996; Kinnaird *et al*., 2005; Scoates and Friedman, 2008; McDonald and Holwell, 2011). Situated in northern South Africa, the intrusion spans approximately 600 km by 400 km and crosses into three different provinces within the country.

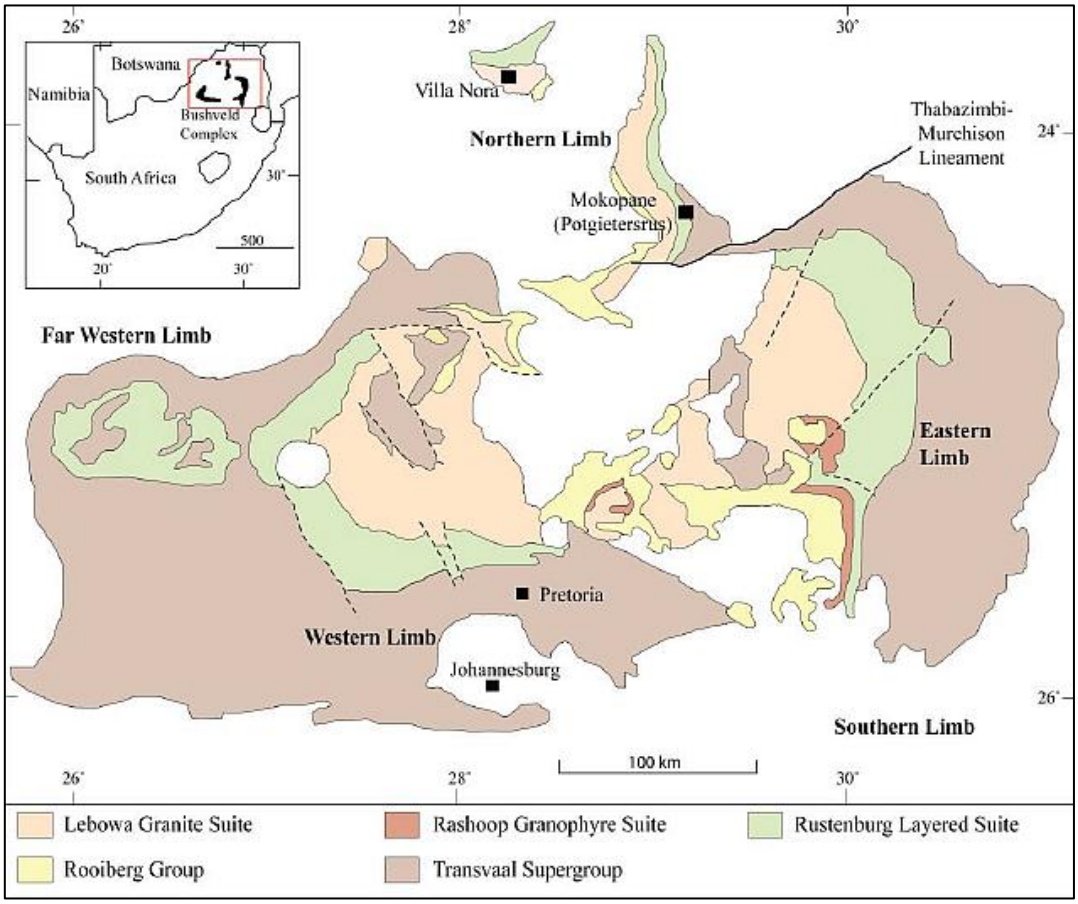

Figure 1.1. *A simplified geological map of the Bushveld Complex, highlighting the locations of the various limbs and lithological exposures (Adapted from Eales and Cawthorn, 1996).*

The Bushveld Complex and its surrounding aureole is host to a multitude of world-class magmatic mineral deposits (Kinnaird *et* al., 2002; Scoates and Friedman, 2008; McDonald *et al*., 2017). The Complex serves as the principal repository of the world's Platinum Group Element (PGE)-rich magmatic ore deposits, and the Large Igneous Province (LIP) has therefore been extensively explored,

studied and mined since the discovery of platinum in 1924, with exploration and mining focussing specifically on PGEs, Cr, Cu, Ni and V as commodities of interest (Van Der Merwe, 1976; Cawthorn *et* al., 2006; McDonald *et al*., 2017).

The PGE mineralisation occurs predominantly within the stratiform reef-type deposits of the Merensky Reef as well as in the Upper Group 2 (UG2) chromitite layer in the Critical Zone of the eastern and western limbs of the main Bushveld Complex. It also occurs within the Platreef of the northern limb as a Merensky Reef-style mineralisation hosted within pyroxenites and harzburgites, as massive sulphide bodies at the base or in marginal/contact disseminated hybrid rocks (Cawthorn, 1999; Kinnaird, 2005; McDonald and Holwell). In 2011, geophysical and drilling exploration carried out by Platinum Group Metals (PTM) north of the Hout River Shear Zone (HRSZ) resulted in the discovery of one of the most globally significant and a Tier 1 classified palladium deposit covered by Waterberg sedimentary rocks that lay to the north of the exposed area of the northern limb (Kinnaird *et al*., 2012; McCreesh, 2016; Kinnaird *et al*., 2017; Huthmann *et al*., 2018). This extended exploration led to the discovery of numerous intervals of continued economic mineralisation to the north of the exposed northern limb. Furthermore, the mineralisation occurred in parts of the magmatic stratigraphy that had not previously been regarded as having potential for mineralisation (Kinnaird *et al*., 2017).

The northern limb is one of the most significant mineral provinces of the Bushveld Complex, and has more recently received increased interest, study and exploration for PGEs and base-metal sulphides (BMS). The northern limb is host to the world renowned Platreef which is a 10 m to 400 m thick package of largely pyroxenites and gabbros that are PGE-enriched (Kinnaird, 2005). The Platreef of the northern limb was subdivided – on the basis of observed footwall lithology, following the work of Merensky (1925) – into three geographical sectors by Kinnaird *et al*. (2005), namely: the southern, central and northern sectors. The majority of early exploration work was carried out on what was thought to be the thickest section of the Platreef, the central sector (Merensky, 1925; Kinnaird *et al*., 2005). As a result of this focussed exploration and active mining, scientific literature of the Platreef was largely founded on this central sector, much of which may not be applicable to sections of the Platreef both to the south and north as a result of varying footwall compositions (Kinnaird *et al*., 2005; McDonald and Holwell, 2011).

The definition of the Platreef, as will be discussed in greater detail in *Chapter 3*, is a broadly accepted characterisation of a lithologically variable, contaminated and frequently xenolthic-rich unit of mafic to ultramafic rocks that contains irregular mineralisation of PGE and Ni-Cu base-metal sulphides (Kinnaird *et al*., 2005; Kinnaird and McDonald, 2005; Armitage, 2011; McDonald and Holwell, 2011). The Aurora Project deposit, of which mineralisation was first observed from initial Cu and Ni soil

geochemical anomalies recognised during exploration between 1974 and 1992, was considered to be a representation of the northern contact facies of the Platreef and therefore an extension of both the Platreef and the northern limb (Maier *et al*., 2008; Venmyn-Rand, 2010; McDonald *et al*., 2017). This description of the deposit as Platreef and thereby ensued suggestion of Platreef strike extension by both Naldrett (2005) and Maier *et al*. (2008) – on the basis of both petrological and geochemical differences observed when compared with typical Platreef sections – has subsequently been disputed and deemed unlikely and largely untenable based on a number of factors (McDonald and Harmer, 2010; McDonald *et al*., 2017).

1.2. Scope of the Research

The Tweespalk Project study area is located on the *Tweespalk 773 LR* property, which is situated in the northern limb of the Bushveld Complex, within the Limpopo Province of South Africa (*Figure 1.2.*) (PTM Annual Report 2012). The Tweespalk property which covers 2177 ha in extent and is surrounded by the *Atlatsa Resources* Kwanda North and Central Block project properties, lies approximately 55 km to the north of the town of Mokopane (formerly Potgietersrus) and is centred on the coordinates of 23˚ 42’ (S) and 28˚ 54’ (E) (PTM Annual Report, 2004; Furness, 2004).

In terms of the scope and context of this research, a great deal is known and understood with regards to the Platreef in the northern limb, as a result of numerous studies as well as ongoing exploration and mining in the area. There is also a fair amount of literature on the Aurora and Waterberg projects located further north towards the northern-most extent of the northern limb (Huthmann *et al*., 2016; Harmer *et al*., 2017; McDonald *et al*., 2017; Kinnaird *et al*., 2017). However, little scientific interest has been shown in the short ~10 km strike length, upper middle section of the northern limb between the farms of Witrivier and Nonnenwerth, where the Upper Zone has transgressed through the Main Zone and lies directly on the basement granitic gneiss of the intrusion (Maier *et al*., 2007). This is primarily a result of the disappearance of Platreef and the lack of any significant economic mineralisation within this section of observed transgression. The Tweespalk farm is the focus area of this study, with the research centred on the comparison of the geology at Tweespalk with the rest of the geology elsewhere in the northern limb.

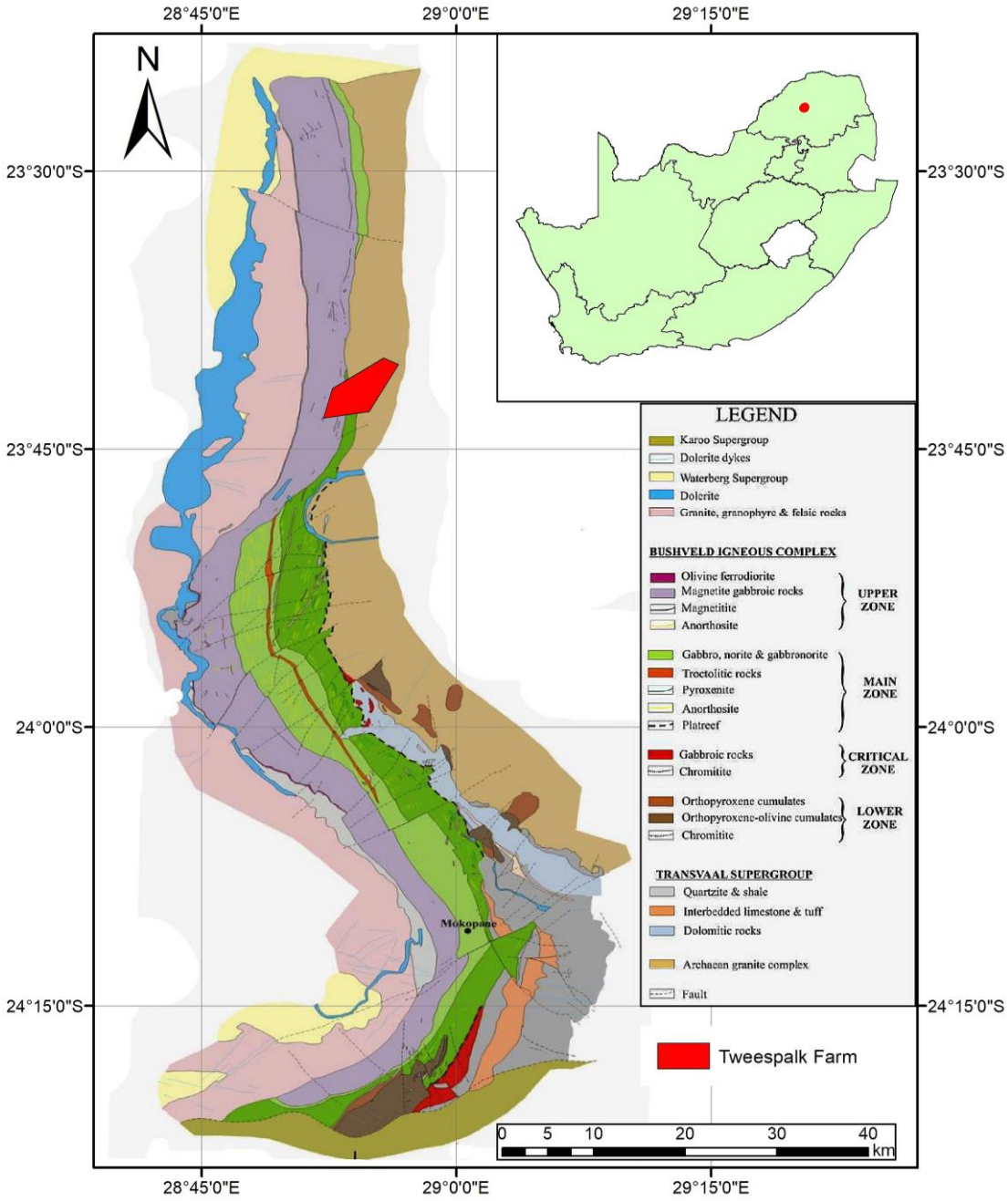

Figure 1.2. *Location of the Tweespalk farm property within the northern limb of the Bushveld Complex, with the farm area highlighted in red (After Ashwal et al., 2005).*

The premise of this thesis is to understand the nature, origin, and development of the relatively unknown and understudied Tweespalk magmatic sequence, and to compare the local geology with the geology of rest of the northern limb. An essential question is the position of the Main Zone-Upper Zone boundary within the stratigraphy and an attempt has been made to understand the factors behind the development of this largely unmineralized section within a limb that contains extensive economic mineralisation throughout. This project therefore looks to contribute further to the understanding of the magmatic history and its relationship to the formation of northern limb.

1.3. Aims and Objectives

There are two main aims of this thesis:

1) To establish the geochemical characteristics of the area and correlate the magmatic stratigraphy of the Tweespalk area with the rest of the known magmatic sequences of northern limb and the Waterberg project area further to the north.
2) To determine the stratigraphic position and style of mineralisation in the Tweespalk drill core and compare this with the mineralisation observed in the Platreef, Main Zone and Upper Zone sequences throughout the northern limb as well as the adjacent Waterberg segment.

The study looks to investigate the stratigraphy and PGE mineralisation of the Tweespalk area, making use of the research objectives defined below:

- Core logging and collection of appropriate core samples, with photographic analysis of the different rock types observed in the core.
- Production of a detailed stratigraphic log of the TW1 drill-core to investigate the general stratigraphy of the northern limb Bushveld rocks in this region.
- Optical petrographic studies to identify the constituent minerals of the various rock types for confirmation of the rock taxonomy given to the core and to identify the style of mineralisation present.
- Whole-rock geochemical analyses for major and trace elements to investigate the correlation of geochemical characteristics with other known sequences of the northern limb.

Chapter Two

Geology of the Bushveld Complex

2.1. Introduction to the Bushveld Complex

The Palaeoproterozoic Bushveld Complex formed as a result of multi-staged magma injections (Kinnaird, 2005; Smith *et al*., 2014). It has a combined area of greater than ~90 000 km^2, far greater than the approximate area of 65 000 km^2 as extensively stated in previous literature (Tankard *et al*., 1982; Eales and Cawthorn, 1996; Cawthorn, 1999), as earlier literature did not account for the full extent of the northern limb which extends underneath the Waterberg and Karoo sedimentary units as far as the Palala shear zone to the north of the Thabazimbi-Murchison Lineament (TML) (van der Merwe, 1976; von Grunewaldt *et* al., 1985; Finn *et al*., 2015; Kinnaird *et al*., 2017).

The Complex is located within the borders of South Africa and is spatially comprised of four sectors that are exposed at the surface, these include: the western limb, far western limb, eastern limb and northern limb, with another unexposed limb referred to as the south-eastern Bethal limb covered by younger sediments making up the fifth limb of the complex (*Figure 2.1.*) (Eales and Cawthorn, 1996; Kinnaird, 2005). The five major limbs or lobes of the Bushveld were initially interpreted to have been discrete, unconnected magmatic bodies (Cousins, 1959; Meyer and De Beer, 1987), however, more recent studies have re-interpreted the Complex to ultimately be connected at depth with single chromitite layers or packages as well as the Merensky Reef being traceable for at least ~350 km around the complex (Cawthorn and Webb, 2001; Kinnaird *et al*., 2002; Barnes and Maier, 2004). The limbs eastern and western limbs generally dip towards the centre of the intrusion at between 10˚ and 20˚ (Cawthorn and Webb, 2001), whereas the exposed northern limb dips westwards at typically 45° towards the centre of the unexposed limb (van der Merwe, 2008).

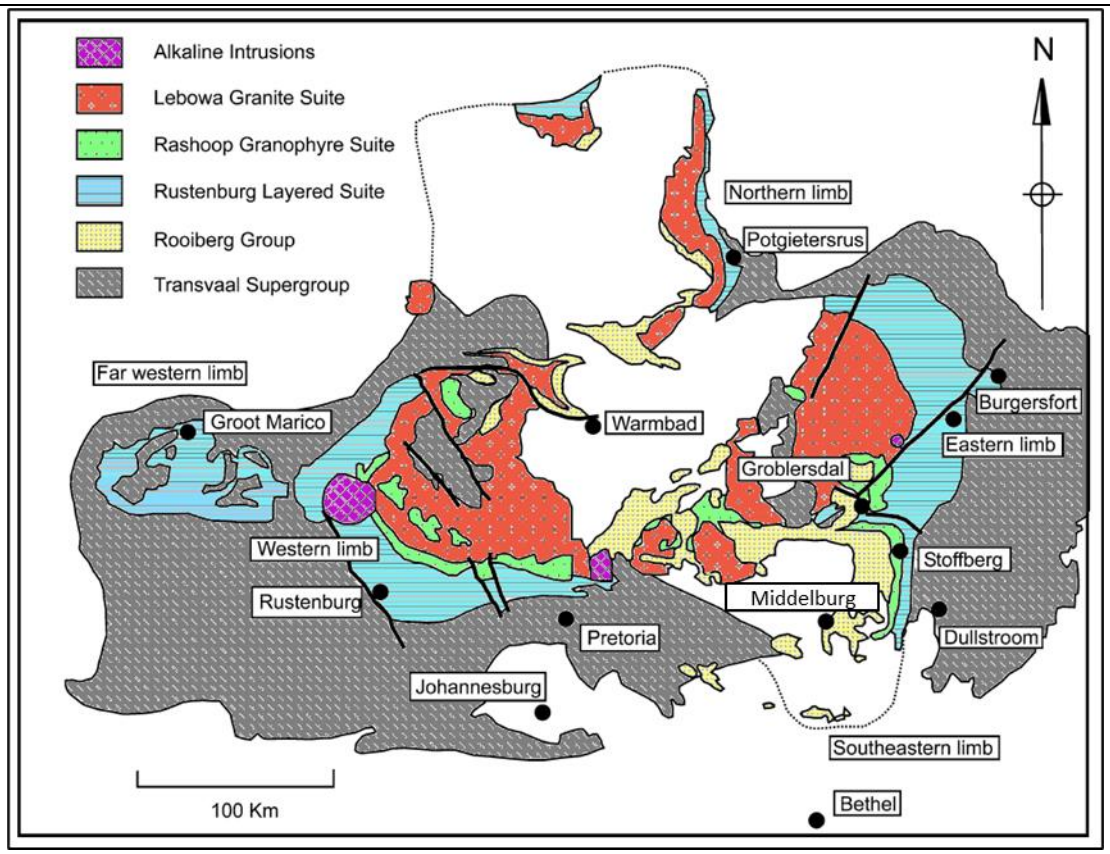

Figure 2.1. *A simplified geological map of the Bushveld Complex, highlighting the locations of the various limbs and lithological exposures (Adapted from Kinnaird et al., 2005).*

The entire Complex, located in the north-eastern region of South Africa, stretches between the four provinces of Mpumalanga, Limpopo, Gauteng and the Northwest, from just north of the town of Bethal in the south, to Villa Nora as the northern-most extent and to the towns of Burgersfort and Zeerust in the east and west respectively (Eales and Cawthorn, 1996; Cawthorn *et al*., 2006). The layered igneous suite of rocks within the Complex has a typical maximum thickness ranging between ca. 6 km and 8 km and generally exhibit a tabular shape, with some of the layers tracing along strike up to and further than 150 km (South African Committee for Stratigraphy, 1980; Walraven *et al*, 1990; Eales and Cawthorn, 1996; Cawthorn *et* al., 2006; Zeh *et al*., 2015). The overall estimated volume of the entire intrusion is approximately between 370 000 km^3 and 600 000 km^3 (Eales and Cawthorn, 1996; Cawthorn and Walraven, 1998; Ashwal *et al*., 2005). The Bushveld Complex is host to approximately 75% of the world's resources of platinum (Naldrett, 2004), as well as a large concentration of BMS, with these metals being concentrated in the three-principal aforementioned stratigraphic units of the UG2 chromitite, the Merensky Reef and the Platreef (McDonald and Holwell, 2011; Huthmann *et* al., 2018).

The relatively unusual LIP broadly referred to as the Bushveld Magmatic Province, stems from the first and original Bushveld Plutonic Series introduced by Molengraaf (1898). Subsequently, the term

changed to the Bushveld Plutonic Complex in order to signify the variety of intricately related intrusive components within the Province (Armitage, 2011). The later accepted term of the Bushveld Igneous Complex came into general use, as this preferred term highlighted the Bushveld cyclicity of both the intrusive and volcanic rocks within the Complex (Hatch and Corstorphine, 1905; Armitage, 2011). Modern literature has seen the qualifying term of 'igneous' become largely discontinued with the Bushveld Complex being the customary term (Armitage, 2011). Like much of the contested issues in literature that arose during the expansive study of the Complex over the last century – such as the tectonic setting of the Complex, the source of parental magmas, the mechanism(s) leading to the emplacement of the Complex, the overall structure of the Complex, and the nature and distribution of mineralisation –, the definitions of the lithology and stratigraphic subdivision of the suites of rocks encompassed within the Complex have changed and been adapted over time with a multitude of different definitions having been proposed (Eales and Cawthorn, 1996; Kruger, 1990; Kruger, 2005; Cawthorn *et al*., 2006; Wilson, 2012).

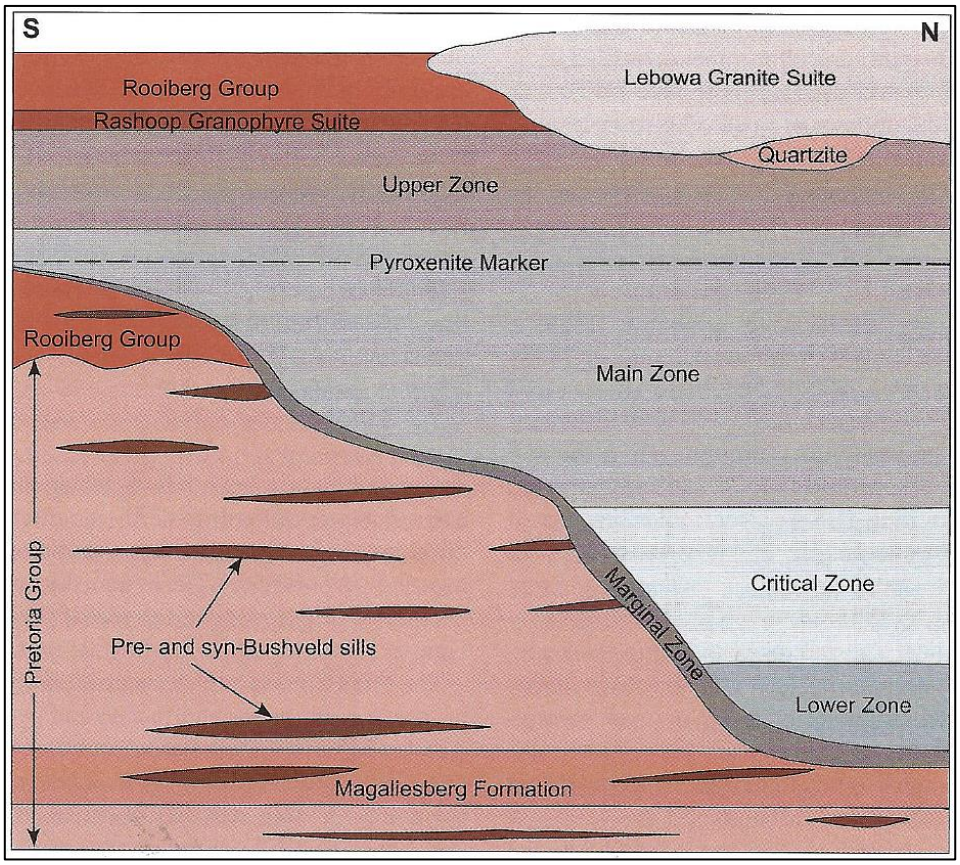

Figure 2.2. *A schematic north-south cross-section of the eastern limb from Dulstroom to Steelpoort, illustrating the relationship between Rustenburg Layered Suite's chamber expansion from magma addition and the Pretoria Group (After Harmer and Sharpe, 1985).*

The poor understanding of the Rooiberg Group and its connection to the Bushveld Complex led to the initial three-fold subdivision of the Complex into the mafic-ultramafic rocks of the Rustenburg Layered

Suite (RLS), the Rashoop Granophyre Suite (South African Committee of Stratigraphy, 1980), and the Lebowa Granite Suite (Tankard *et al*., 1982; Walraven, 1985; Walraven and Hattingh, 1993; Kinnaird *et al*., 2005; Cawthorn *et al*., 2006), as proposed by the South African Committee of Stratigraphy (1980). Hatton and Schweitzer (1995) thereafter revised this suggested definition with the addition of the felsic volcanic rocks of the Rooiberg Group, a set of marginal both pre- and syn-Bushveld sills and the inclusion of the outer disparate satellite intrusions, with the currently accepted subdivision and nomenclature of the Complex shown in *Table 2.1.* (Cawthorn *et* al., 1991; Eales and Cawthorn, 1996; Cawthorn *et al*., 2006; Smith *et al*., 2014). As suggested by Hatton and Schweitzer (1995) and Cawthorn *et al*. (2006), the Rooiberg Group lavas represent immediate precursors to the Rustenburg Layered Suite mafic intrusions that intruded below or into the Group, with the Pretoria Group rocks representing the predominant portion of roof-rocks to the Complex coupled with younger post-Bushveld volcanic and sedimentary rocks of the Karoo Super Group (*Figure 2.2.*) (Hall, 1932; Coertze *et* al., 1977; Cheney and Twist, 1991; Schweitzer *et al*., 1995; Kinnaird *et al*., 2005).

Table 2.1. *The currently accepted standard nomenclature and subdivisions of the four major magmatic suites within the Bushveld Complex (After Cawthorn et al. (2006)).*

Lebowa Granite Suite	Nebo, Makhutso, Klipkloof, Bobbejaankop, and Verena Granites	
Rashoop Granophyre Suite	Stavoren and Diepkloof Granophyres, Rooikop Porphyritic Granite, Zwartbank Pseudogranphyre	
Rustenburg Layered Suite	Upper Zone	Subzone C (Ol-Ap diorite) Subzone B (Ol-Mt gabbronorite) Subzone A (Mt gabbronorite)
	Main Zone	Upper Subzone (gabbronorite) Lower Subzone (gabbronorite, norite)
	Critical Zone	Upper Subzone (norite, anorthosite, pyroxenite) Lower Subzone (pyroxenite)
	Lower Zone	Upper Subzone Harzburgite Subzone Lower Subzone
	Marginal Zone (norite)	
Rooiberg Group	Schrikkloof Formation (flow-banded rhyolite) Kwaggasnek Formation (massive rhyolite) Damwal Formation (dacite, rhyolite) Dullstroom Formation (basaltic andesite)	

2.1.1. The Rooiberg Group

The felsic volcanics of the Rooiberg Group which lie predominantly above the Rustenburg Layered Suite, although are also found at the base of the Suite, is subdivided on the basis of lithology and

geochemistry into several volcanic unit formations that have a maximum vertical thickness of approximately 400 m and are interbedded with laterally extensive, thin sedimentary strata (Harmer and von Gruenewaldt, 1991; Buchanan, 2006; Cawthorn *et al*., 2006). These formations from the base to the top of the Group are: the Dullstroom Formation, Damwal Formation, the Kwaggasnek Formation and the Schrikkloof Formation (Hatton and Schweitzer, 1995; Buchanan, 2006; Cawthorn *et al*., 2006). The rock types of the Dullstroom formation range from mafic to intermediate basalts and basaltic andesites to more felsic volcanic units of dacites and rylolites, with the bulk of the succession comprising of siliceous volcanic rocks with shale and sandstone intercalations throughout (Buchanan, 2006; Cawthorn *et al*., 2006).

The Rooiberg Group represents the youngest, most voluminous and most silicic volcanic unit linked to the larger Bushveld Complex magmatic event (Twist and French, 1983; Hatton and Schweitzer, 1995; Eriksson and Reczko, 1995; Eriksson *et* al., 2005). A single-zircon age of 2061 ± 2 Ma was produced for a felsic volcanic rock within the Rooiberg Group, with the Group having magmas considered to be intrusive and time-equivalent to that of the Rashoop Granophyre Suite magmas (Walraven, 1987a; Lenhardt *et al*., 2017). The uppermost rhyolitic section of the Rooiberg Group is geochemically similar to that of the Stavoren Granophyre of the Rashoop Granophyre Suite – supporting the time-equivalent link and genetic relationship between the two Suites (Walraven, 1987b; Hatton and Schweitzer, 1995; Cawthorn *et al*., 2006). The resulting age-dating correlation between the Rooiberg Group and the RLS by Harmer and Armstrong (2000), led to the consideration of the Rooiberg Group being representative of the initial magmatic phase of the Bushveld Complex rather than the latter stages of the Transvaal Supergroup (Hatton and Schweitzer, 1995).

2.1.2. The Rustenburg Layered Suite (RLS)

The Rustenburg Layered Suite within the Bushveld Complex, comprises a package of rocks that highlights a complete differentiation sequence of a basic magma with the rock types varying from dunite and pyroxenite, norite, gabbro and anorthosite, through to magnetitite and diorite, and in its entirety, represents the mafic component of the Complex (Eales and Cawthorn, 1996; Kinnaird *et al*., 2005; Cawthorn *et al*., 2006; Zeh *et al*., 2015). This Suite has been subdivided into five different zones on the basis of the traditional zonal stratigraphy, mineralogical changes produced from magma differentiation, as well as the order of appearance or disappearance of cumulus minerals, with the zones from the bottom to the top being the noritic Marginal Zone (MZN), the ultramafic Lower Zone (LZ), the ultramafic to mafic Critical Zone (CZ), the gabbronoritic Main Zone (MZ) and finally the ferrograbbroic Upper Zone (UZ) (Hall, 1932; Kinnaird *et al*., 2005; Cawthorn *et al*., 2006). Wilson (2015) also noted and described a basal ultramafic unit of magnesian pyroxenites, harzburgites and dunites

below the MZN referred to as the Basal Ultramafic Sequence (BUS). The formal lithostratigraphic classification of the RLS adopted by the South African Committee of Stratigraphy (1980) subdivided the RLS using nomenclature on the basis of geographic names (Cawthorn *et al*., 2006). The widely known informal zonal subdivision that makes use of the traditional zonal stratigraphy within the RLS has generally been favoured in more recent literature as a result of widely separated areas within the Bushveld Complex – on which the proposed stratigraphy was originally based –, displaying similar rock types and stratigraphy (Cawthorn *et al*., 2006).

Layering within the Suite is present throughout, with this laterally continuous layering ranging on all vertical scales, from millimetres through to hundreds of metres (Eales and Cawthorn, 1996). The general order of occurrence of the cumulus minerals olivine, orthopyroxene, chromite, (olivine), plagioclase, (chromite), clinopyroxene, magnetite, iron-rich olivine, (orthopyroxene), and apatite, in terms of their appearance and/or disappearance within Suite, is the basis of the stratigraphic subdivision (Cawthorn *et al*., 2006). The evolution of the Bushveld Complex magma chamber is proposed to have occurred within two major stages, the first being the initial evolutionary phase of the lower, open-system 'Integration Stage' characterised by a multitude of magma influxes of differing isotopic compositions that involved concomitant mixing, crystallisation and deposition of cumulates leading to the formation of the Lower, Critical and Lower Main Zones (Kruger, 2005; Smith *et al*., 2014). These primary magmatic injections and depositional events led to the deposition of the main mineralisation units on top of or near to a stratigraphic unconformity (Eales and Cawthorn, 1996; Kruger, 2005).

In regard to the lithostratigraphy, Kruger (2005) noted that the larger magma influxes that are marked by sustained isotopic shifts, distinct mineral assemblage changes as well as unconformity development correspond with boundaries of stratigraphic zones and subzones within the RLS. The upper, closed-system 'Differentiation Stage' was without any major magma influxes with the thick magma layers forming as a result the extensive secondary magmatic process of differentiation and fractional crystallisation, possibly contributing to the concentration of mineralisation (Kruger, 1992; Kruger, 1999; Kinnaird *et al*., 2002; Kruger, 2005).

2.1.3. The Lebowa Granite Suite

There are four main granite intrusions of the Lebowa Granite Suite that occur within two large semi-circular groups or lobes in the arcuate eastern and western limbs of the Bushveld Complex respectively (Cawthorn *et al*., 2006). The principal granites of this Suite being the Nebo, Bobbejaankop, Klipkloof and Makhutso granites (Cawthorn *et al*., 2006). Another granite type known as the Verena Granite is also present within the Suite, but is considered to be of a different origin in relation to the typical

Bushveld granites (Robb *et al*., 2005; Cawthorn *et al*., 2006). The Lebowa Granite Suite was thermally metamorphosed by the intrusion of the RLS, where it was metasomatically altered throughout (Buchanan, 2006; Lenhardt and Eriksson, 2012). This alteration that led to the deposition of secondary cassiterite, tourmaline and carbonate, was particularly significant in the north-western sections of the Suite (Buchanan, 2006; Lenhardt and Eriksson, 2012).

2.1.4. The Rashoop Granophyre Suite

Despite being significantly smaller than the typically voluminous Rooiberg Volcanics, the 2053 ± 12 Ma Bushveld Complex granophyric rocks of the Rashoop Granophyre Suite occur extensively between the RLS (above which they intruded) and the overlying Rooiberg Volcanics (Coertze *et al*., 1978; Walraven, 1987b; Cawthorn *et al*., 2006). The granophyric rocks of the Suite make up a significant proportion of the acid phase of the Bushveld Complex, with the rocks occurring either above and/or below the Lebowa Granite Suite depending on the area (Cawthorn *et* al., 2006). As recognised by Walraven (1985), the Rashoop Granophyre Suite is a grouping of two types of granophyre on the basis of petrography, one group being intrusive and the other being metamorphic.

The more predominant magmatic group of granophyres referred to collectively as the Stavoren Granophyre (Lenthall, 1973), may represent both the shallow intrusive facies of magma below the Rooiberg Group rhyolite roof or Pretoria Group sediments, as well as the volcanic pile formed from extrusive facies of magma (Walraven, 1985; Walraven, 1987b; Kinnaird *et* al., 2005). The magmatic group of granophyres is largely characterised by micrographic intergrowths of alkali feldspar and quartz that are well developed throughout (Walraven, 1985; Cawthorn *et al*., 2006). The metamorphic group of granophyres on the other hand, comprises the Zwartbank Pseudogranophyre, the Diepkloof Granophyre and the Rooikop Porphyritic Granite (Walraven, 1985; Walraven, 1987; Cawthorn *et al*., 2006). The origin of this group of metamorphic granophyres is the result of extensive contact metamorphism of the Pretoria Group and Rooiberg Group rocks due to the emplacement of both the mafic and granitic rocks of the Bushveld Complex (Walraven, 1985; Cawthorn *et al*., 2006).

2.2. Palaeotectonic Setting

The amalgamation, form and evolution of the first supercontinent is still highly debated and largely speculative, however it is agreed that the first supercontinent widely referred to as Rodinia amalgamated and diachronously came into existence during the Proterozoic Eon (*Figure 2.3.*) (Robb, 2005; Li *et al*., 2008). A number of studies have postulated the formation and break-up of old supercontinents/continents throughout the history of the earth, ranging from the Archaean (Vaalbara) to the Palaeoproterozoic (Columbia), to the Neoproterozoic (Rodinia) and finally, the

youngest and most well documented supercontinent of Pangea, which formed at the end of the Palaeozoic era (Robb, 2005; Letts *et al*., 2011).

The paleogeographic reconstruction of the continental geometry and timing of amalgamation and dispersal, however, is still contested and differs amongst all literature with only the continental configuration and paleogeography of the major continents Gondwana, Laurentia and Pangea being generally accepted (Robb, 2005; Letts *et al*., 2011). As illustrated in the schematic diagram of *Figure 2.3.*, that on the basis of the Rogers Model by the end of the Archaean at 2500 Ma there would have been an inferred Archaean continent of *Ur* (consisting of the ancient Kaapvaal and Pilbara cratons, portions of India as well as Antarctica that coalesced approximately 3000 Ma) and an Archaean to early Proterozoic major continent of *Artica* (amalgamated parts of Siberia, Canada and Greenland), also commonly referred within earlier literature as *Laurentia* (Hoffman, 1991; Rogers, 1996; Robb, 2005).

The continued amalgamation of land masses in the Proterozoic formed what was known as the Atlantica at about 2000 Ma as well as the Baltica (Rogers, 1996; Robb, 2006). The new continent of *Nena* was formed as a result of the amalgamation of both the Arctica and the Baltica at approximately 1500 Ma, which was then followed by continuous amalgamation with the Mesoproterozoic until the believed consolidation of the supercontinent Rodinia (~1000 Ma) from the Ur, Atlantica and Nena continents (Dalziel *et* al., 2000; Robb, 2005).

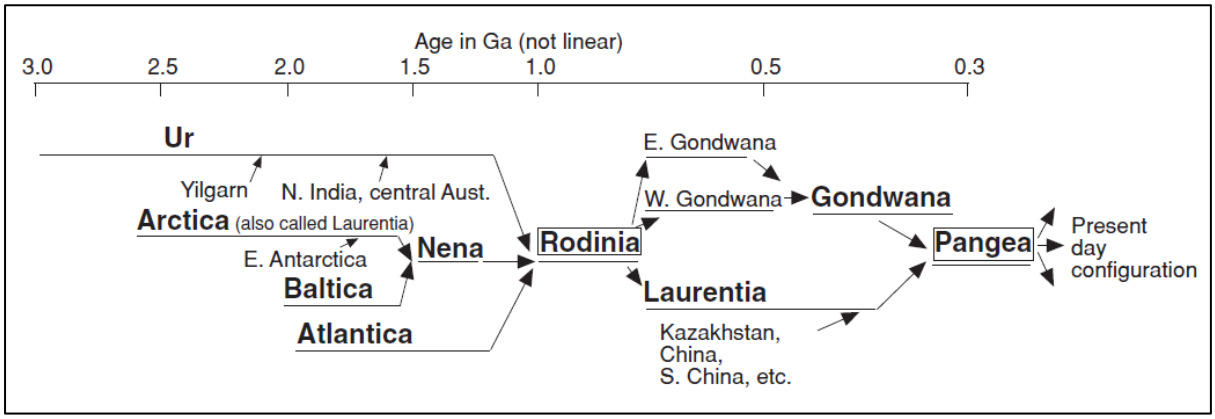

Figure 2.3. *A schematic diagram of the Rogers Model for the estimated timing of amalgamation, formation and breakup of major continental land masses between 3.0 and 0.3 Ga, and more specifically the evolution of Rodinia, the first supercontinent (After Robb, 2005).*

The pre-Bushveld tectonic setting and emplacement mechanics of the Bushveld Complex, the world's largest layered intrusion, into the Kaapvaal Craton is still poorly understood (Clarke *et al*., 2009). Highlighted by Clarke *et al*. (2009), the country rocks surrounding any form of intrusion are extremely useful with regards to information on emplacement history and tectonic processes, with the Bushveld Complex contact aureole having recorded the tectonic processes that occurred both during and after

its emplacement (Uken, 1999; Clarke *et al*., 2005). Host to the Bushveld Complex, the Kaapvaal Craton formed through the amalgamation and accretion of a mosaic of discrete major crustal blocks between 3.7 Ga and 2.7 Ga (De Wit *et al*., 1992; Armitage, 2011).

The aforementioned Archaean-aged Vaalbara major continent that existed and remained intact between 2.8 Ga and 1.8 Ga was composed of the Kaapvaal Craton and Pilbara Craton (Cheney, 1996; Zhao *et al*., 2002; de Kock *et al*., 2009; Letts *et al*., 2011). The Vaalbara continent assembly led to the formation of two major orogenic events, namely: the formation of the Limpopo Belt from the collision between the Kaapvaal Craton and the Zimbabwe Craton, and the formation of the Capricorn Orogen that resulted from the collision of the Pilbara and Yilgarn Cratons (van Kranendonk *et al*., 2002; Zeh *et al*., 2009; Letts *et al*., 2011). Both of these orogenic events, along with the other related orogenic events of roughly the same period is argued by Zhao *et al*. (2002), to have resulted in the formation of the Palaeoproterozoic Columbia supercontinent.

Controversy still remains with regards to the relation and origin of the Limpopo Belt to that of the adjacent Zimbabwe and Kaapvaal Cratons, the two main models proposing continent-continent collision between the two Cratons or the other origin proposal that involves non-plate tectonics (Gore *et al*., 2009). The models based on continent-continent collision are separated by the disagreement on the timing of collision and formation of the Limpopo Belt. McCourt and Armstrong (1998) produced an age range for the event of ~2.7 - 2.6 Ga, while Holzer *et al*. (1998) place the collision at ~2.0 Ga (Letts *et al*., 2011). A study done by Holzer *et al*. (1998) documented and recorded convergent tectonics between the two Cratons, interpreted as a high-grade collisional event within the Limpopo Belt that was later considered to rather be a reactivation of the Limpopo Belt during the Magondi Orogeny by Silver *et al*. (2004), Clarke *et al*. (2009) and Letts *et al*. (2011).

As a result of the regional convergent tectonics, the Kaapvaal Craton was subjected to a broadly NW-SE compression between ~2.05 Ga and ~2.0 Ga was in response to the collision between the two Cratons (Clarke *et al*., 2009). The stress field present at ~2.05 Ga allowed for the dilation of the ENE-trending TML and extensional tectonics within a back-arc tectonic setting, meaning that this proposed emplacement of the Bushveld Complex in a back-arc setting that represent extensional zones within an overall compressional regime (Clarke *et al*., 2009). This broadly syn-Bushveld NW-SE compressional tectonic regime and the suitably orientated TML parallel to the Limpopo Belt and subduction zone allowed for dilation of the TML, acting as a dyke-like feeder and facilitating the Bushveld Complex emplacement within a subduction-back-arc geodynamic setting.

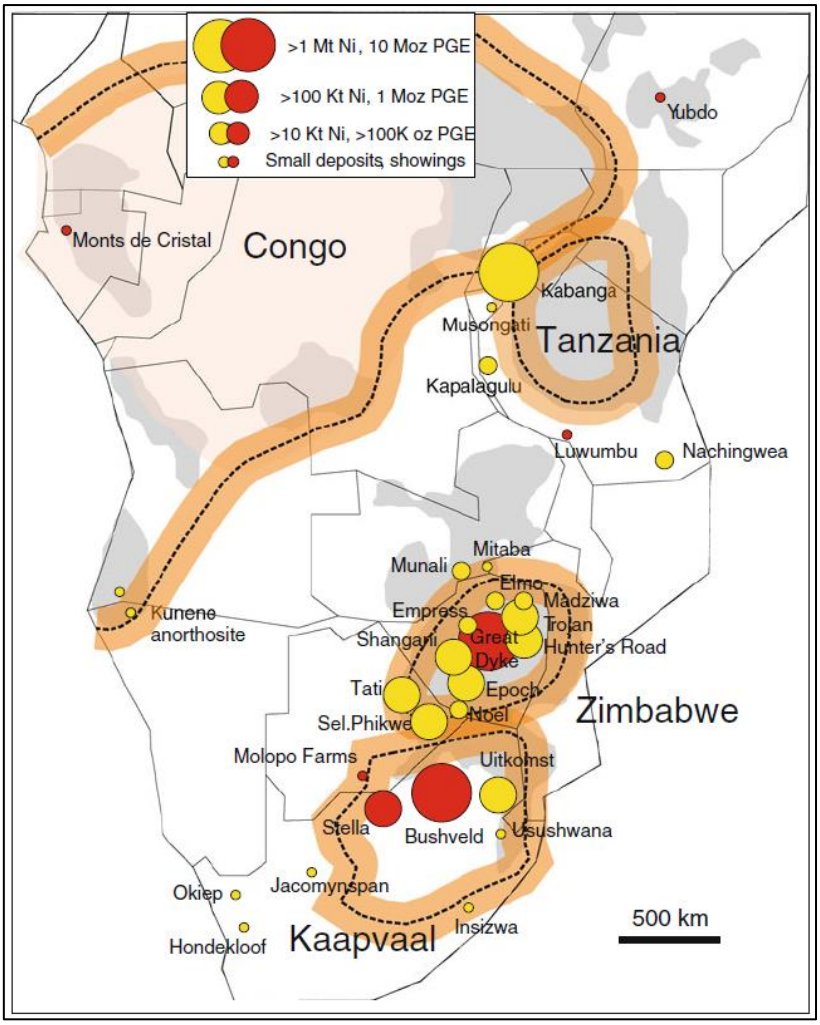

Figure 2.4. *The location of the Bushveld Complex PGE deposit within the Kaapvaal Craton, as well as the relation between the Kaapvaal and Zimbabwe Cratons (After Maier and Groves, 2011).*

Kamber (1995) was the first to argue that the formation of the Limpopo Belt was unlikely to have been the product of the proposed ~2.7 Ga to 2.6 Ga late Archaean continent-continent collision between the two cratons, with this being based on the prevalence of the 2.0 Ga tectonic events (Gore *et al*., 2009). Bleeker (2003) concurs with this argument, stating that on the basis of structure, timing of cratonisation and mafic dyke swarm emplacement, the Kaapvaal and Zimbabwe Cratons share no interactive history before ~2.0 Ga (Gore *et al*., 2009). Following this point, Bleeker (2003) asserts that the ~2.6 Ga Great Dyke does not cross the Limpopo Belt and is not present within the Kaapvaal Craton, meaning that two cratons are only likely to have collided close to 2.0 Ga (Mukasa *et al*., 1998; Gore *et al*., 2009).

All of the known globally significant PGE deposits have formed in association with stabilised cratons, with the majority occurring within the central sectors of the cratons (Maier and Groves, 2011). Such is the case with the Bushveld Complex that forms within the Kaapvaal Craton (*Figure 2.4.*), as well as the Great Dyke forming within the central region of Zimbabwe Craton further north. It is generally

accepted that following the stabilisation of the Kaapvaal Craton, the period ranging from the late Archaean to early Proterozoic within the Craton is characterised by the development of large volcano-sedimentary intracratonic basins (Kinnaird, 2005; Maier and Groves, 2011). These basins are regular with laterally continuous layering within, this being consistent with magma emplacement in a stable intracratonic environment (Kinnaird, 2005; Maier and Groves, 2011).

2.3. Age of the Bushveld Complex

A number of studies have attempted to precisely age date the volcanic rocks of the Complex – albeit these ages have been difficult to obtain as a result of subsequent metamorphism post-emplacement – with the majority obtaining ages close to that of 2060 Ma (Zeh *et al*., 2015). However, all of the studies yielded highly variable and significantly large uncertainties that scattered over more than 10 Ma period (Zeh *et al*., 2015). Previous age determinations of the Bushveld Complex rocks constrained using uranium-lead ID-TIMS (isotope dilution thermal ionisation mass spectrometry) and CA-ID-TIMS (chemical abrasion ID-TIMS) dating techniques on zircons, baddeleyite and titanite produced relatively more precise and typically older ages that ranged between 2058.9 ± 0.8 M and 2054.4 ± 1.3 Ma (Buick *et al*., 2001; Scoates and Friedman, 2008; Olsson *et al*., 2011, Zeh *et al*., 2015).

In comparison with Ar-Ar, Re-Os and Pt-Os age dating techniques that produced significantly younger and less precise ages between 2044 ± 3.0 Ma and 1995 ± 50 Ma (Schoenberg *et al*., 1999; Nomade *et al*., 2004; Reisberg *et al*., 2011; Coggon *et al*., 2012; Zeh *et al*., 2015). It was noted by Zeh *et al*. (2015) and Yudovskaya *et al*. (2013) that a few U-Pb SHRIMP (Sensitive High Resolution Ion Microprobe) ages showed an overlap with the CA-ID-TIMS and Ar-Ar ages, as well as a similar high degree of age date scatter.

The emplacement age of the Bushveld Complex was considered to have been relatively well constrained at 2060 Ma (± 3 Ma, Kruger *et al*., 1986; and ± 27 Ma, Walraven *et al*., 1990). This emplacement age was supported by the work of both Walraven (1997a) and Buick *et al*. (2001), with constrained ages of 2061 ± 2 Ma for the roof rocks of the Rooiberg Group and 2058.9 ± 0.8 Ma for the crystallisation and therefore minimum age of emplacement of the RLS in the eastern limb respectively (Smith *et al*., 2014). Together the ages provide a relatively precise time interval for the emplacement of the RLS. Significantly younger crystallisation ages of the Merensky Reef (2054.4 ± 1.3 Ma and 2055 ± 1.3 Ma) were then later constrained from high precision U-Pb zircon dating by Scoates and Friedmann (2008), similar to the minimum age of 2053.7 ± 3.2 Ma determined for the Platreef (Hutchinson *et al*., 2004). Olsson *et al*. (2010) also constrained a precise U-Pb baddeleyite age of 2057.7 ± 1.6 Ma for the Marginal Zone. These more recent crystallisation and cooling ages of the

Merensky Reef show a significant, younger age difference to that of the age determined by Buick *et al*. (2001).

Further study by Zeh *et al*. (2015) produced high precision U-Pb dates for the emplacement and crystallisation of the Rustenburg Layered Suite within the Bushveld Complex, supported by various petrological observations. This new and robust constraint of Bushveld Complex emplacement was obtained from eight zircon grains that were taken from nine mafic rocks of different RLS units (Zeh *et al*., 2015). The CA-ID-TIMS $^{207}Pb/^{206}Pb$ age dates obtained by Zeh *et al*. (2015) indicate that the crystallisation period of the Rustenburg Layered Suite (RLS) from the Marginal Zone (floor of the RLS) to the Upper Critical Zone and Main Zone (centre of the RLS) ranged over 1.02 ± 0.63 Ma, as opposed to the previously attained U-Pb ages that suggested a time interval between 3 Ma and 5 Ma for the crystallisation period of the Bushveld Complex rocks. The emplacement of the RLS magmas began at 2055.91 ± 0.26 Ma (Zeh *et al*., 2015), which is in agreement with the thermo-mechanical modelling of accretion and emplacement of the Bushveld Complex RLS in under 0.1 Ma and 0.5 Ma respectively (Cawthorn and Walraven, 1998). Despite the relatively old age of the large magmatic province, the Bushveld Complex is particularly well preserved as a result of having undergone minimal structural and metamorphic deformation after emplacement and solidification (Cawthorn *et al*., 2002).

2.4. The Transvaal Supergroup

The Bushveld Complex generally intruded into the Palaeoproterozoic supracrustal volcano-sedimentary rocks of the Transvaal Supergroup – comprising of a thick succession of volcanic and both chemical and clastic sedimentary rocks (Hall, 1932; van der Merwe, 1976; Ashwal *et al*., 2005). The Transvaal Supergroup forms a large volcano-sedimentary intracratonic basin on the Kaapvaal Craton. The Supergroup is a late-Archaean to early Proterozoic platform succession that contains two main unconformity-bound sequences of the lowermost Chuniespoort Group carbonate-BIF platform succession, followed by the volcano-sedimentary Pretoria Group (Eriksson *et* al., 1993; Eriksson and Reczko, 1995; Cheney, 1996; Moore *et al*., 2001). The approximately 15 km thick package ranges in age from the lowest contact between protobasinal rocks of the Wolkberg and Buffelsfontein Groups and Black Reef Sandstone Formation with an age of ca. 2658 ± 1 Ma, to the uppermost extent of the Pretoria Group dated at ca. 2050 Ma (Cheney, 1996; Moore *et al*., 2001; Zeh *et al*., 2016).

The Complex is almost entirely circumscribed by the Transvaal Basin into which it intruded, whereby the base of the Complex is represented by an unconformity between the underlying Pretoria Group and the overlying Rooiberg and Rustenburg Layered Suites (Cawthorn *et* al., 2006; Lenhardt and Eriksson, 2012). This separates the clastic sedimentary rocks of the Pretoria Group from the volcanic

rocks, which suggests considerable erosion of the overlying sedimentary rocks before the intrusion and eruption of the lavas (Cheney and Twist, 1992; Cawthorn *et* al., 2006; Lenhardt and Eriksson, 2012; Lomberg, 2012). The northern limb represents an extreme case of this erosion period prior to the eruption of lavas, with the Transvaal Supergroup being completely eroded and absent in the northern section of the limb. This leaves an unconformable contact between the base of the mafic-to-ultramafic rocks and the Archaean granitic-gneiss basement (White, 1994; Cawthorn *et al*., 2006). The exceptions where the Complex has not intruded along the unconformity formed between the Magaliesberg quartzites of the Pretoria Group and felsites of the overlying Rooiberg Group is in the above-mentioned northern limb, as well as in the eastern limb to the south of the Steelpoort fault where the Complex has transgressed upwards through more than ~2 km of the sedimentary package (Eales and Cawthorn, 1996; Cawthorn *et al*., 2006).

2.5. Magmatic Stratigraphy

The Bushveld Complex, as an entire entitity, refers to the combination of intricately-related intrusive components (the Rooiberg Group, the RLS, the Lebowa Granite Suite, the Rashoop Granophyre Suite, a series of marginal sills as well as varying satellite inrusions) within the greater Large Igneous Province. General literature, however, makes use of the term 'Bushveld' to typically refer to the entire package of mafic and ultramafic rocks that constitute the most voluminous preserved layered mafic intrusion in the world (Eales and Cawthorn, 1996; Cawthorn *et al*., 2006). This package of mafic and ultramafic rocks is known as the Rustenburg Layeyred Suite. The stratigraphic zones of the RLS include; the Marginal Zone, the Lower Zone, the Critical Zone, the Main Zone, and the Upper Zone, however not all of the Zones are present within the far western and Bethal limbs (Eales and Cawthorn, 1996; Cawthorn *et al*., 2006).

The Rustenburg Layered Suite is present within all of the five magmatic basins or limbs of the Complex, however not all are present within western and Bethal limbs. Lateral facies variations within the Suite sequence are common, with the only complete successions of the Suite being observed in the northern portions of the eastern and western limbs (Cawthorn *et al*., 2006; Smith *et al*., 2014). The following is a summary of the dominant and defining characteristics of the various zones, present within both the eastern and western limbs of the Complex (*Figure 2.5*.).

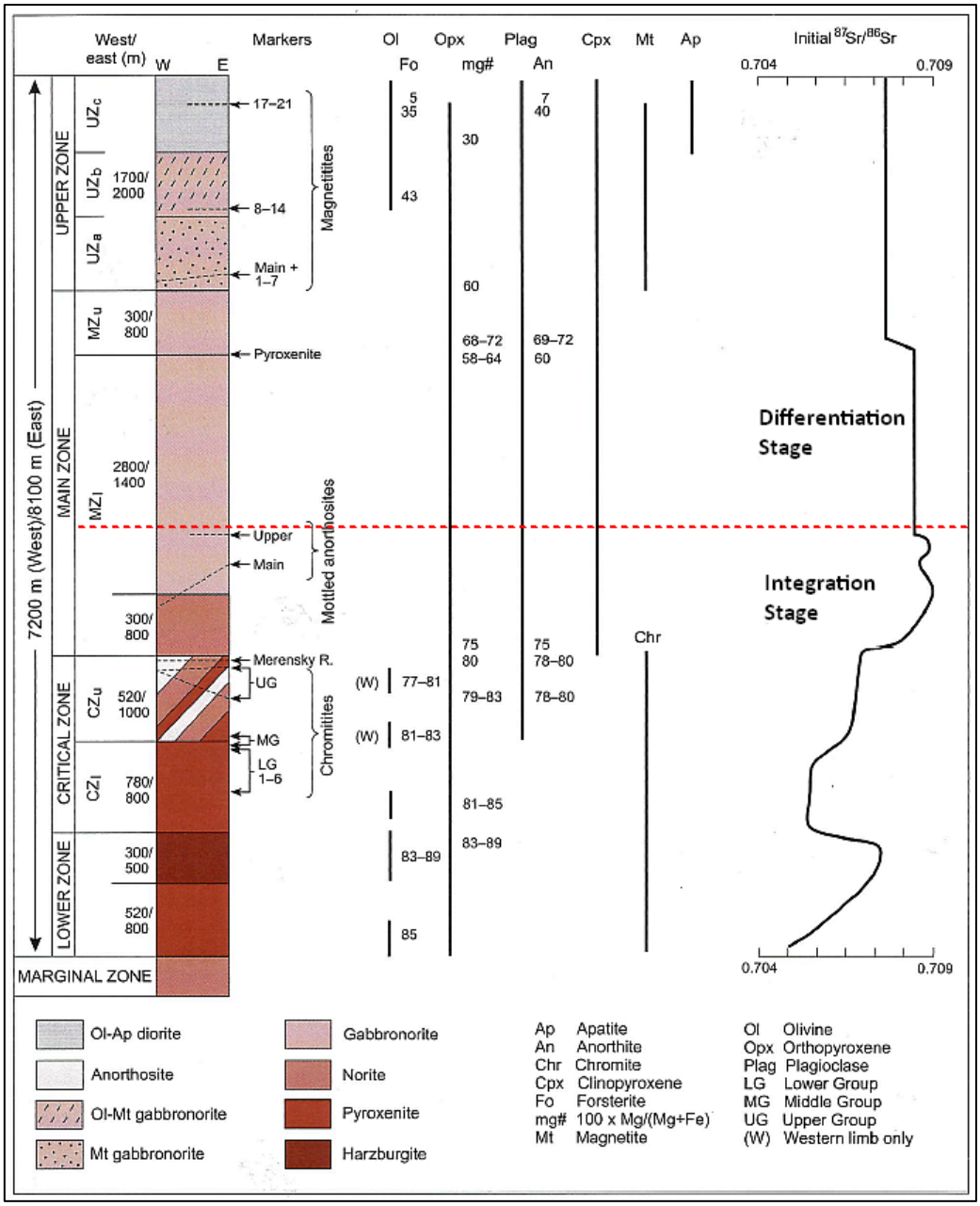

Figure 2.5. *A generalised stratigraphic succession through the RLS of the Bushveld Complex, highlighting the major subdivisions, dominant rock types, major marker horizons and appearance of the various cumulus phases throughout. Also shown are the major integration and differentiation evolutionary phases of the Complex discussed in section 1.2.1.2. (Adapted from Robb, 2005).*

2.5.1. The Marginal Zone (MZN)

The lowermost zone of the RLS is the Marginal Zone, situated along the basal contact of the Bushveld Complex. The zone is comprised of largely heterogeneous, medium-grained noritic rocks with minor proportions of pyroxenite that display no layering (Harmer and Sharpe, 1985; Eales and Cawthorn, 1996; Kinnaird *et al.*, 2002; Cawthorn *et al.*, 2006). The enigmatic and discontinuous succession that reaches a maximum thickness of ~800 m, encircles the majority of the Complex, but is not always present throughout (Engelbrecht, 1985; Kinnaird *et al.*, 2002; Cawthorn *et al.*, 2006). The zone reflects

the assimilation of surrounding country rock, with the presence of variable quantities of biotite, quartz, hornblende and clinopyroxene incorporated from the assimilation of shale (Cawthorn *et al*., 2006). Cawthorn *et al*. (2006) suggests that the MZN represents the relatively rapid crystallisation of variably contaminated and differentiated magmas in comparison to that of the voluminous, multiple injections of RLS magmas. The MZN is deemed not to be representative of a chilled margin to the entire Bushveld Complex, on the basis that the MZN formed from multiple magma injections (Cawthorn *et al*., 2006).

The recent discovery and identification of a basal ultramafic unit of magnesian pyroxenites, harzburgites and dunites situated below the Marginal Zone was made in the Clapham area of the eastern limb and in the northern limb by Wilson (2015) and Yudovskaya *et al*. (2013) respectively. The new Basal Ultramafic Sequence found below the MZN in the Clapham area of the eastern limb, is believed to have required a far more ultramafic parental magma than the 'B1' magma, commonly used to represent the parental magma of the Bushveld Complex (Yudovskaya *et al*., 2015; Wilson and Zeh, 2015).

2.5.2. The Lower Zone (LZ)

The ultramafic Lower Zone overlies the Marginal Zone and is the most limited with regards to its lateral extent relative to the other zones of the RLS (Eales and Cawthorn, 1996; Kinnaird, 2005). The LZ is best developed in the northern sections of both the eastern and western limbs as well as in the southernmost portion of the northern limb, with the thickness, distribution and overall development of the zone having largely been controlled by the basement topography and structure (Cameron, 1978; Kinnaird *et al*., 2005; Cawthorn *et al*., 2006). Local attenuations of the LZ, as well as propagation of the LZ into the overlying zones is the result of a variety of structural complexities that occur in the sedimentary footwall (Sharpe and Chadwick, 1982; Uken and Watkeys, 1997; Cawthorn *et al*., 2006).

The thickest and most well-developed sections of the LZ have been found within the Olifants River Trough in the eastern limb, near the Union Section Platinum Mine in the western limb, in the far western limb, as well as in the northern limb both to the south of Mokopane and on the Turfspruit property beneath the Platreef (Cameron, 1978; Hulbert and von Gruenewaldt, 1985; Eales and Cawthorn, 1996; Yudovskaya *et al*., 2013). It varies in thickness between 800 m and 1700 m, with the lowermost cumulate, ultramafic rocks of the LZ including dunites, harzburgites and pyroxenites (formerly referred to as 'bronzitites') (Cameron, 1978; Kinnaird *et al*., 2002; Cawthorn *et al*., 2006).

This zone of ultramafic rocks is further subdivided into three subzones, the Lower Pyroxenite, Harzburgite (middle) and Upper Pyroxenite Subzones, after the original four-fold subdivision proposed

by Cameron (1978) (South African Committee for Stratigraphy, 1980; Cawthorn *et al*., 2006). The LZ generally displays well developed cyclic units, containing nine dunite-harzburgite-pyroxenite cyclic units in the far western limb that have a thickness of up to 1050 m, as well as thirty-seven cyclic units within a 1700 m olivine-chromite-orthopyroxene succession (Engelbrecht, 1985; Hulbert and von Gruenewaldt, 1985; Cawthorn *et al*., 2006).

While it is agreed that the LZ transitions into the Critical Zone, with the CZ conformably overlying the LZ and there being no discernible break between the zones, the definition of upper boundary has been variably defined (Cameron, 1978; Cawthorn *et al*., 2006; McCreesh, 2016; Cronje, 2017). The boundary was initially defined as the level at which an increase of cumulus plagioclase in the pyroxenites from 3% to 8%, occurred (Cameron, 1978). Teigler and Eales (1996) argued that the definition lacked mineralogical and petrographical significance and consequently proposed the boundary be situated at the top of the uppermost, thick olivine-rich interval.

2.5.3. The Critical Zone (CZ)

The Critical Zone of the RLS, the most economically important zone within the Bushveld Complex, is host to vast reserves of chromite within the three stratigraphically delineated groups of the Lower (LG-1 to LG-7), Middle (MG-1 to MG-4) and Upper (UG-1 to UG-3) Group chromitite layers, as well as two of the world's largest platinum-bearing ore bodies, the Merensky Reef and UG2 Chromitite reef (Wagner, 1929; Cousins and Feringa, 1964; Eales, 1987; Hatton and von Gruenewaldt, 1987; Scoon and Teigler, 1994; Schürmann *et al*., 1998). The Critical Zone is characterised by spectacular layering of chromitite, pyroxenite, norite and anorthosite that ranges in scale from millimetres to metres throughout the zone, the ~1500 m thick CZ is divided into a Lower Critical Zone (C_LZ) and an Upper Critical Zone (C_UZ) (Cameron, 1980; Cameron, 1982; Kinnaird *et al*., 2005; Cawthorn *et al*., 2006).

The C_LZ consists of a succession of entirely ultramafic, orthopyroxenite cumulates with an interval of olivine-bearing cumulates one-third of the way up the ~700 to 800 m thick package (Kinnaird *et al*., 2005; Cawthorn *et al*., 2006). Almost all of the rocks within the C_LZ contain minor disseminated chromite, while the majority of chromite is hosted within up to seven feldspathic pyroxenite Lower Group chromitite layers and MG-1 and MG-2 of the Middle Group, all individually reaching up to 1 m in thickness and the thickest being the LG-6 chromitite layer (Kinnaird, 2005; Kinnaird *et al*., 2005; Cawthorn *et al*., 2006). The lowest four chromitite layers (LG-1 to LG-4) are distinguishable from the overlying chromitites in that they are associated with olivine while the other chromitites lack any olivine (Schürmann *et al*., 1998; Kinnaird, 2005).

The C_UZ of the CZ comprises of several cyclic successions (either partial or complete) composing of an ultramafic base of chromitite, harzburgite and pyroxenite cumulates through to considerably less mafic units of norite and anorthosite in the upward cyclic succession (Kinnaird *et al*., 2002; Kinnaird *et al*., 2005; Cawthorn *et al*., 2006). The transitional boundary between the two subzones and the base of the C_UZ is defined at the first appearance of cumulus plagioclase within the zone succession, with this occurrence typically being found at the base of the 1-3 m thick lowermost anorthositic layer of the RLS in the middle of the MG-1 to MG-4 Middle Group chromitite layers accompanied by a 1-2 mm chromitite stringer (Kinnaird, 2005; Kinnaird *et al*., 2005; Cawthorn *et al*., 2006; Maier *et al*., 2013). With the boundary straddling between the C_LZ and the C_UZ, the C_UZ hosts the two upper Middle Group chromitite layers of MG-3 and MG-4 which both lie above the first anorthosite layer as well as the three recognised Upper Group chromitite layers of UG-1 to UG-3 (Kinnaird, 2005; Kinnaird *et al*., 2005; Cawthorn *et al*., 2006).

Hulbert (1983) and Maier *et al*. (2008) mention that unlike in the eastern and western limbs, the northern limb displays C_UZ rocks in overlying harzburgites considered to be part of the LZ, insinuating that the C_LZ may be absent. Despite it being largely subjective, the subdivision of the characteristic magmatic cycles has resulted in nine cyclic units being recognised in the C_LZ, while eight cyclic units occur within the C_UZ (Cameron, 1982; Eales and Cawthorn, 1996; Kinnaird, 2005). These units display a similar upward progression from predominantly ultramafic cumulates through to more feldspathic rocks. The base of each cyclic unit has a sharp contact and is characterised by Fe enrichment reversal trends which have been interpreted by Kruger and Marsh (1982) and Eales and Cawthorn (1996), to be indicative of the process of magma replenishment.

The top two cycles of the C_UZ succession are referred to as the Merensky and Bastard Cyclic Units, they represent the thinnest of the cyclic units and define the transition from the CZ to the MZ (Cawthorn *et al*., 2006). PGE-mineralisation within the CZ is largely localised in the three layers of the Merensky Reef, the UG-2 chromitite and the Platreef (Cawthorn *et al*., 2006), however the Merensky reef is now typically regarded as interface between the CZ and MZ in literature. The PGE mineralisation within the CZ tends to be concentrated in the basal ultramafic portions of the cyclic units, as is the case with the feldspathic-pyroxenite-hosted Merensky Reef mineralisation and the UG-2 chromitite reef, with PGEs occurring interstitially amongst the chromitite cumulate grains (Cawthorn *et al*., 2006; Maier *et al*., 2013).

A definitive upper contact and boundary of the CZ is still largely contested, with the original boundary between the lower CZ and overlying MZ being placed at the top of a large pyroxene-oikocryst-bearing anorthosite at the top of the Bastard Cyclic Unit, referred to as the Giant Mottled Anorthosite (South

African Committee for Stratigraphy, 1980; Cawthorn *et al*., 2006). This distinctive layer that formed the basis for the boundary definition on petrological and mineralogical grounds has since been adapted as a result of the Rb-Sr isotopic data (Kruger and Marsh, 1982; Kruger, 1990). The major break in the Sr isotopic ratio, coupled with the rapid mineralogical transition from norite to gabbronorite above the Merensky Reef and a major unconformity at its base indicates the influx of new magma and has therefore isotopically defined the CZ-MZ boundary at the Merensky Cyclic Unit and relocated the Merensky Reef into the MZ from the CZ (Kruger and Marsh, 1982; Kruger, 1990; Kinnaird, 2005; Cawthorn *et al*., 2006).

2.5.4. The Main Zone (MZ)

The thickest zone in the layered suite, the Main Zone, forms close to half of the entire RLS with a thickness of greater than 3000 m. It comprises a succession of norites and gabbronorites (devoid of chromite and olivine) with small pyroxenite layers and rare layers of anorthosite (Molyneux, 1974; Mitchell, 1990; Nex *et al*., 1998; Kinnaird *et al*., 2005). It lacks any particularly spectacular layering or extreme lithological diversity when compared to that of the CZ, although the MZ does contain discontinuous but distinct packages of rocks that are modally layered and most likely to have resulted from a new influx of magma during the emplacement process (Molyneux, 1974; Mitchell, 1990; Nex *et al*., 1998, Nex *et al*., 2002; Cawthorn *et al*., 2006).

While Mitchell (1990) states that the thick MZ sequence begins with mainly norite in the basal portion, followed by largely gabbronorite in the intervening central portion of the zone underneath a mainly norite uppermost portion, a number of varying subdivisions of the zone have been proposed. The first proposed subdivision of von Gruenewaldt (1973) divided the MZ into three Subzones, namely: Subzone A, Subzone B and Subzone C, placing a 'Pyroxenite Marker' at the boundary between Subzones B and C. Nex *et al*. (1998) then further subdivided the MZ into five subzones (Subzones A to E) based on the pyroxene compositions and lithological variations observed.

After the suggestion of Mitchell (1990) that the original Subzones A and B from von Gruenewaldt (1973) be grouped together to represent a singular Lower Subzone, with Subzone C representing the Upper Subzone, Cawthorn *et al*. (2006) also subdivided the MZ into a relatively simple Lower Subzone composed of predominantly norite with lesser gabbronorite, and an Upper Subzone composed of almost entirely gabbronorite. Scoon and Mitchell (2012) went on to describe a similar two-fold subdivision of a gabbronorite-dominated Lower Main Zone that contains inverted pigeonite throughout and primary cumulus orthopyroxene reappearance at the Pyroxenite Marker, and an Upper Main Zone begins above the aforementioned Pyroxenite Marker.

The above-mentioned addition of a large volume of magma is supported by Sr isotopic data, whereby a strong change in the Sr isotope signature, coupled with a gradual reversal in all mineral compositions within the MZ rocks over a vertical distance of ~200 m occurs towards the top of the MZ, despite the boundary between the CZ and MZ being relatively ambiguous and difficult to define on mineralogical criteria alone (Sharpe, 1985; Cawthorn *et al*., 1991; Eales and Cawthorn, 1996; Cawthorn *et al*., 2006). The replacement of pigeonite for orthopyroxene and the reappearance of orthopyroxene at the base of the Pyroxenite Marker – observed at 2200 m and 3100 m above the base of the MZ in the west and east by Mitchell (1990) and von Gruenewald (1973) respectively – marks a significant influx of additional magma responsible for the development of the Upper Zone (Nex *et al*., 2002; Cawthorn *et al*., 2006). The Pyroxenite Marker was the initial placement of the proposed boundary between the MZ and the UZ, however, the boundary placement has subsequently been defined at the stratigraphic position at which the appearance of cumulus magnetite is first observed (Wagner and Brown, 1968; von Gruenewaldt, 1973, Molyneux, 1974; South African Committee for Stratigraphy, 1980).

2.5.5. The Upper Zone (UZ)

The intermittently layered and approximately 2000 m thick succession of the Upper Zone represents the most laterally extensive zone of the RLS (Eales and Cawthorn, 1996; Kruger, 2005; Cawthorn *et al*., 2006). Comprising gabbronorite, ferrogabbro, anorthosite and diorite, the plagioclase-rich UZ (with the majority of rocks within the zone containing more than fifty percent plagioclase) has traditionally been divided into three subdivisions based on the cumulate mineralogy, including: Subzone A, Subzone B and Subzone C (Eales and Cawthorn, 1996; South African Committee for Stratigraphy, 1980; Kinnaird *et al*., 2002). The rocks that dominate in the UZ succession range in composition from gabbronorite to anorthosite, whilst containing a few olivine-rich intervals as well as variable amounts of cumulus Fe-rich pyroxenites (South African Committee for Stratigraphy, 1980; Eales and Cawthorn, 1996).

In terms of the compositions of the three subzones, Subzone A which is situated at the base of the zone, comprises of largely magnetite-bearing gabbronorite and anorthosite (Eales and Cawthorn, 1996; Cawthorn *et al*., 2006). Subzone B is defined on the appearance of Fe-rich olivine in the succession, with the subzone consisting of olivine-magnetite gabbronorite, anorthosite, and troctolite (Eales and Cawthorn, 1996; Cawthorn *et al*., 2006). The base of overlying Subzone C is marked at the first appearance of cumulus apatite, with the subzone containing olivine-apatite diorite and anorthosite (Eales and Cawthorn, 1996; Cawthorn *et al*., 2006). As noted by Cawthorn *et al*. (2006), this mineralogical evolution and sequence observed in the eastern limb is also present within the

western, northern and southern limbs of the Complex (van der Merwe, 1976; Buchanan, 1977; Cawthorn *et al*., 1991; Cawthorn *et al*., 2006).

The UZ contains approximately 8% magnetite by volume with ilmenite exceeding the abundance of magnetite towards the top of the zone, however, it is the presence of 25 magnetite layers throughout the zone that are the most characteristic feature (Reynolds, 1985; Eales and Cawthorn, 1996; Cawthorn *et al*., 2006). The magnetite layers range in thickness from a few centimetres to 2 m, with the thickest layer being recorded at 6 m (Molyneux, 1974; Eales and Cawthorn, 1996; Cawthorn *et al*., 2006). The magnetite layers are generally clustered into four groups, Subzone A hosts eleven magnetite layers in two groups – three thin layers near the base of the zone, a 2 m thick layer referred to as the Main Magnetite Layer approximately 130 m above the base and seven other magnetite layers above –, while the other two subzones host seven magnetite layers in each group (Eales and Cawthorn, 1996; Cawthorn *et al*., 2006).

Chapter Three

Geology of the Northern Limb of the Bushveld Complex

3.1. Introduction

The northern limb of the Bushveld Complex, located in the Limpopo Province of South Africa, has a sinuous north-south trending and west-southwest dipping outcrop that extends along a strike length of approximately 110 km and varies in thickness between 4 km and 15 km (*Figure 3.1.*). The limb covers an estimated total areal extent of 7275 km^2 based on early geophysical work, the limb stretches from the southern Zebediela Fault that lies to the south of Mokopane – where Phanerozoic Karoo sediments from the upper Transvaal Supergroup are juxtaposed on top of the mafic layered rocks of the Complex – extending to the northern Melinda Fault that forms part of the larger Palala Shear Zone, where the limb is mostly covered by younger Waterberg sediments (van der Merwe, 1976; Kinnaird *et al*., 2005; Kinnaird *et al*., 2017).

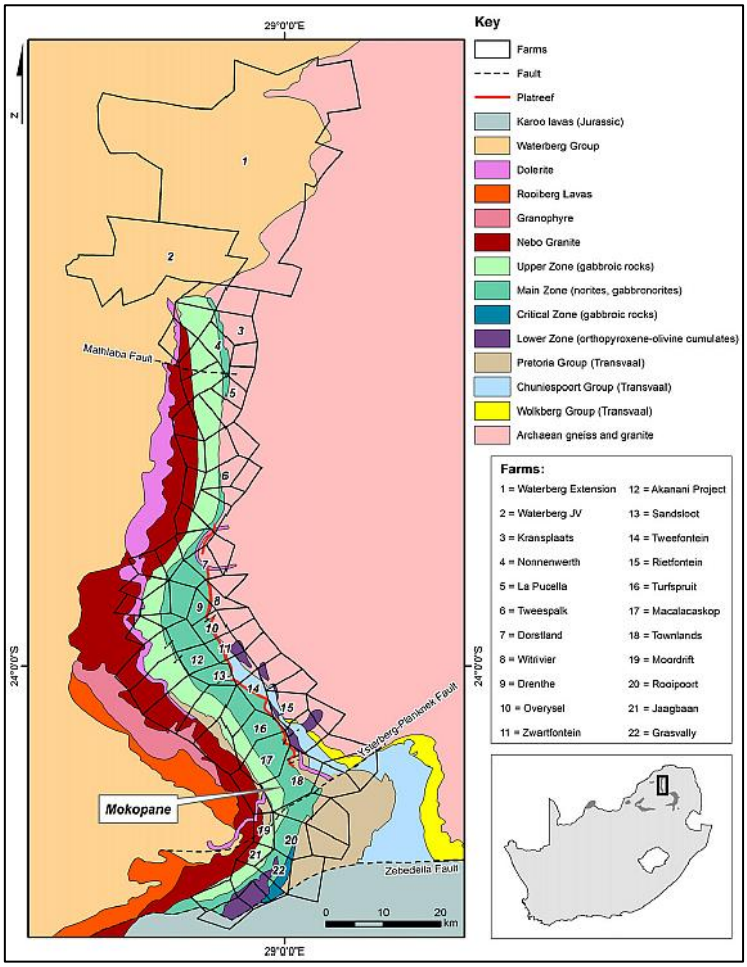

Figure 3.1. *A geological map of the northern limb of the Bushveld Complex, showing the geology of the northern limb as well as the locations and boundaries of farm properties therein (After van der Merwe, 1976).*

The Villa Nora segment is a ~320 km^2 outcrop exposure of layered mafic rocks that was considered to be part of total areal extent of northern limb, as a single compartment formed by a suggested feeder to the west of Mokopane (Cawthorn and Lee, 1998; Cawthorn and Webb, 2001; Kinnaird *et al*., 2005; Armitage, 2011). However, on the basis of subsequent aeromagnetic and gravity data, it has been suggested that the exposed northern limb – of which the Villa Nora segment is included – forms part of a far larger ~160 x ~125 km basin (Finn *et al*., 2015; Cronje, 2017).

Previously referred to as the Mokopane or Potgietersrus Limb, the northern limb is separated from the rest of the Bushveld Complex by the aforementioned Thabazimbi-Murchison Lineament, a 25 km wide craton-scale structure that extends in an east-northeast west-southwest direction for more than 500 km (Good and de Wit, 1997; McDonald *et al*., 1999; McDonald and Holwell, 2011; Smith *et al*., 2014; Kinnaird *et al*., 2017; Huthmann *et al*, 2018). This lineament is an active pre-Bushveld collisional suture zone between the Pietersberg Block and Kaapvaal Shield terranes, that developed at approximately 2960 Ma as a result of collision between the two terranes during the Meso-Archaean period, undergoing repeated reactivation until about 145 Ma within the Cretaceous (Good and de Wit, 1997; McDonald *et al*., 1999; McDonald and Holwell, 2011; Smith *et al.*, 2014; Kinnaird *et al*., 2017; Huthmann *et al*, 2018). As mentioned by van der Merwe (2008), the Zebediela Fault as well as the Ysterberg-Planknek Fault both represent near surface expressions of the TML, with the northern limb being truncated by the NE trending Zebediela Fault in the south and separating it from the eastern and western limbs. Despite not being well understood, Kinnaird *et al*. (2005) suggested that the TML may have acted as a feeder during the emplacement of Bushveld Complex magmas, serving as a fairly important structural control on its intrusion and formation.

Silver *et al*. (2004) and McDonald and Holwell (2011), both make reference to the formation of the Limpopo Orogenic Belt (between ~2700 Ma and ~2600 Ma), followed by shear zone reactivation within the Limpopo Belt during the Magondi Orogeny (~2000 Ma) leading to the emplacement of magmas along the axis of the TML. Kruger (2005), proposed that TML acted as either temporary or permanent barrier to the movement of the Bushveld Complex magmas northwards, allowing for the northern limb to develop separately to the main complex as a result of restricted magma flow to the north, at least up until the period of Main Zone emplacement (McDonald *et al.*, 2005; Cronje, 2017). van der Merwe (1978) also suggested that the triple intersection point of three major tectonic lineaments to the west of Mokopane was a major controlling factor on the emplacement of the northern limb.

3.2. Magmatic Stratigraphy

While the stratigraphic correlation between the northern limb and the eastern and western limbs of the Bushveld Complex – to the north and south across the TML respectively – remains contentious, for the most part the stratigraphic succession of the northern limb shows broad similarities to the rest of the complex (van der Merwe, 1976; Ashwal *et al.*, McDonald *et al*., 2005; Kinnaird and Nex, 2015; Huthmann *et al*., 2018). The five stratigraphic subdivisions of the Bushveld Complex are arguably all recognised within the northern limb, but only to the south of the Ysterberg-Planknek fault (van der Merwe, 1976; Woods, 2012; Huthmann *et al*., 2018). Despite not strictly correlating and having a number of distinct differences to that of the eastern and western limbs, there are a few widely accepted relationships between the magmatic stratigraphy of the northern limb and the rest of the complex, as summarized in *Figure 3.2.* below (van der Merwe, 1976; McDonald *et al*., 2005; Yudovskaya *et al*., 2013).

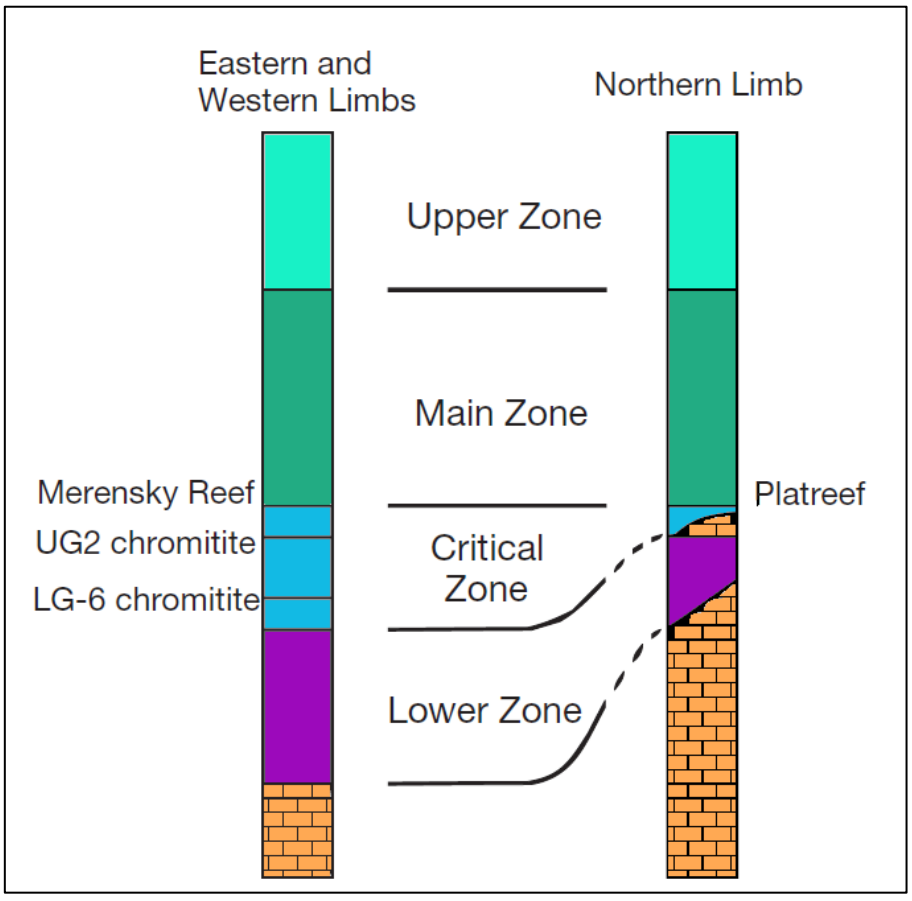

Figure 3.2. *A schematic illustration of the stratigraphic columns of the Rustenburg Layered Suite in the northern limb relative to the Western and Eastern Limbs of the Bushveld Complex. The illustration shows the inferred correlation between the Merensky Reef in the Eastern and Western Limbs and the Platreef in the northern limb (Adapted from McDonald and Holwell, 2005).*

The complex stratigraphy of the RLS is characterised by the subdivision into several different units that are separated and demarcated by various markers. This allows for the correlation between the

different limbs. The northern limb however, lacks a few of these common markers that are consistent throughout the rest of the complex and – although having a multitude of commonalities – has a distinctly different stratigraphy in relation to the rest of the Complex (van der Merwe, 1976; McDonald *et al*., 2005; McCreesh, 2016). The detailed stratigraphic elements of the northern limb differ with that of the eastern and western limbs, with the northern limb being subdivided into four principal zones of the Lower Zone, Critical Zone, Main Zone and Upper Zone.

There are two specifically distinct and characteristic features of the northern limb, the first being the presence of the aforementioned Platreef, an economically significant magmatic body hosting world-class PGE and Ni-Cu mineralisation that is unique to the northern limb (Kinnaird and Nex, 2015; Cronje, 2017). The second characteristic feature is the pronounced transgression of the northern limb mafic succession northwards, through the Palaeoproterozoic Transvaal Supergroup, from the TML at the southern extent of the limb (Sharman-Harris *et al*., 2005; van der Merwe, 2008; Smith *et al.*, 2014). This transgressive nature of the northern limb stratigraphy, shows the change in footwall units in a northerly direction from interbedded quartzites and shales of the Magaliesberg Formation to the shales and quartzites of the Timeball Hill Formation, both part the Lower Pretoria Group, followed by the shales of the Duitschland Formation and banded iron Penge Formation of the Chuniespoort Group, onto the Malmani subgroup dolomites and finally the Archean basement granites and gneisses (van der Merwe, 1976; Sharman-Harris *et al*., 2005; Holwell and McDonald, 2006; Woods, 2012; Smith *et al.*, 2014).

The mafic succession of the northern limb deviates from the typical convention of the RLS stratigraphy to the south of the TML, and while it has been largely agreed upon in literature that all five stratigraphic subdivisions are present, the limb is divided into the four principal zones of the LZ, CZ (Platreef or GNPA member), MZ and UZ (*Figure 3.3.*) (McDonald *et al*., 2005; Woods, 2012; Smith *et al.*, 2014). The Marginal Zone, consisting of predominantly norites is typically poorly exposed throughout the northern limb, with the only few outcrops of noritic to gabbroic rocks ranging in width between a few centimetres and a few tens of metres (van Der Merwe, 1976; McCreesh, 2016).

The Lower Zone component in the northern limb comprises pyroxenites and harzburgites, with layers of chromitites within an unusually thick sequence greater than 1600 m (generally varies between 800 m and 1600 m), producing more than 37 cyclic units in the zone (van der Merwe, 1976; Hulbert and von Gruenewaldt, 1985; Smith *et al.*, 2014). The LZ was originally thought to only occur as satellite bodies situated within the sedimentary country rock to the north of Mokopane, however, the LZ has also developed as a continuous cumulate sequence beneath the Platreef that is approximately 800 m in thickness, southwards of Ysterberg-Planknek fault (van der Merwe, 1976; Hulbert and von

Gruenewaldt, 1982; Kinnaird and Yudovskaya, 2010; Yudovskaya *et al*., 2013). Olivine and orthopyroxene in LZ have higher *magnesium number* values and have chromitite layers with higher Cr_2O_3 contents than the rest of the complex (van der Merwe, 1976; McDonald *et al*., 2005).

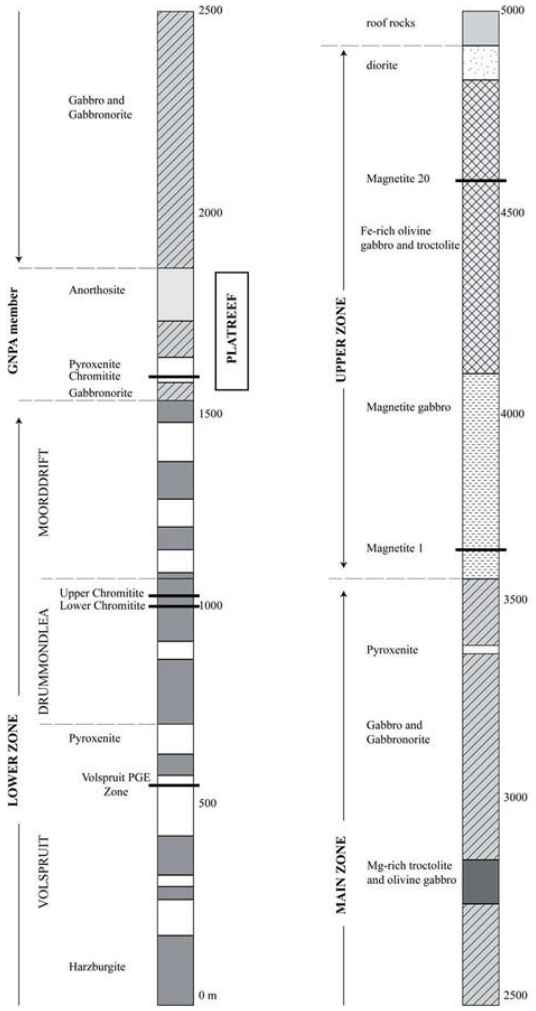

Figure 3.3. *The general stratigraphy of the northern limb of the Bushveld Complex (After McDonald et al., 2005 and Smith et al., 2014).*

The LZ of the northern limb is considered to be unique when compared with the LZ throughout the rest of the complex, as a result of its relatively extreme thickness as well as its greater chromite ore quality in the two main chromitite seams that outcrop over a strike length of ~500 m (van der Merwe, 1976; Hulbert and von Gruenewaldt, 1982; Smith *et al.*, 2014) south of the TML. Hulbert (1983) proposed and defined three subzones within the LZ of the northern limb, these being: the Volspruit pyroxenite, the Drummonlea harzburgite chromitite and the Moordrift Harzburgite pyroxenite. As stated by Hulbert and von Gruenewaldt (1982), there is currently no known stratiform PGE mineralization within the LZ in the rest of the Bushveld Complex besides for the PGE sulphide horizon which occurs in the Volspruit Subzone in the LZ of the northern limb south of the TML (Armitage, 2011).

The eastern and western limb CZ stratigraphic equivalent in the northern limb is considered to be the Platreef and what is referred to as the Grasvally Norite-Pyroxenite-Anorthosite (GNPA) Member, with the ~350 thick GNPA sequence forming between the Ysterberg-Planknek fault and the Zebediela fault (GNPA) (Hulbert, 1983; McDonald *et al*., 2005; Maier *et al*., 2008; Smith *et al.*, 2014). Despite not showing cyclic layering typical of the Bushveld CZ, as well as containing only two chromitite horizons that are discontinuous in nature, the Platreef is still believed to analogous – in terms of silicate geochemistry, stratigraphic position relative to the MZ and the presence of PGE mineralisation in the upper GNPA – to the CZ of the eastern and western limbs (van der Merwe, 1978; Kruger, 2005; Maier *et al*., 2008; Armitage, 2011; Grobler *et al*., 2018). However, the correlation between the Merensky Reef and UG2 chromitite of the CZ in eastern and western limbs, and the Platreef and GNPA member in the northern limb is still disputed (van der Merwe, 1978; McDonald *et al*., 2005; Yudovskaya et al.,2018; Grobler *et al*., 2018).

The MZ in the northern limb and the rest of the Bushveld show large differences, with the western and eastern limbs having a distinct, although discontinuous, pyroxenite marker, while the northern limb also displays a pyroxenite marker in areas, although it is far less distinct and disagreed upon in literature (van der Merwe, 1976). The northern limb MZ has a fairly consistent thickness of ~2200 m throughout, which contrasts with the eastern and western limbs that have highly variable thicknesses ranging between 2500 m and 4000 m (van der Merwe, 1976; Nex *et al*., 1998; Kinnaird *et al*., 2005). Another observed difference is the lack of a troctolite unit in the MZ of the Bushveld, whereas a troctolite unit is seen above the Platreef in the northern limb (van der Merwe, 1976).

The northern limb MZ is dominated by homogenous gabbronorites, gabbros and norites, with up to seven interlayered anorthosite layers as well as four pyroxenite layers, and a single 110 m thick troctolite layer that lies ~1100 m above the Platreef and represents the only reliable marker horizon (Smith *et al.*, 2014). A number of PGE-enriched zones have been identified within the MZ of the northern limb, in contrast to the MZ in the eastern and western limbs that have been proven to be barren of PGE (Maier and Barnes, 2010; McDonald and Harmer, 2011; Holwell *et al*., 2013; Smith *et al.*, 2014).

The UZ of the northern limb consists of a succession of cyclic units of magnetite, magnetite-gabbro, gabbro and anorthosite up to a thickness of 1500 m (van der Merwe, 1976; Smith *et al*., 2014). As in the rest of the Bushveld, the contact between the UZ and MZ of the northern limb is defined by the appearance of cumulus magnetite and apatite, with the northern limb UZ comparing with the Bushveld UZ in terms of stratigraphy and the twenty distinct magnetite seams traced throughout (van

der Merwe, 1976). Ashwal *et al*. (2005) later defined the UZ-MZ boundary on the basis of the abrupt and sharp change in magmatic susceptibility between the two zones.

3.3. The Platreef

The Platreef (sensu stricto) in the northern limb of the Bushveld Complex, as proposed and defined by Kinnaird and McDonald (2005), is a pyroxenite-dominated, lithologically variable package of mafic to ultramafic units that are enriched and irregularly mineralised with PGEs and Ni-Cu base metal sulphides (Kinnaird *et al*., 2005; McDonald and Holwell, 2011; McDonald *et al*., 2017). The package of mafic and ultramafic units is situated between the Transvaal Supergroup metasedimentary footwall in the south or an Archaean granite gneiss basement in the north, and overlying gabbros and gabbronorites of the MZ (Kinnaird *et al*., 2005; McDonald and Holwell, 2011; McDonald *et al*., 2017). These units are observed towards the base of the RLS, with some portion of Marginal and Lower Zones beneath (Kinnaird *et al*., 2005; McDonald and Holwell, 2011; McDonald *et al*., 2017).

This definition of the Platreef however, fails to account for the PGE-Ni-Cu mineralisation that occurs to the south of Mokopane, such as mineralisation associated with calcsilicate xenoliths within the Main Zone gabbronorite, and the Cu-rich PGE mineralisation present within the Aurora Project (Kinnaird *et al*., 2005; McDonald and Holwell, 2011). On the basis of this definition, the Platreef is essentially characterised as a stratigraphically significant PGE and base metal magmatic mineralisation, thereby regarding any PGE mineralisation within evidently older or younger Bushveld Complex rocks in the northern limb as not forming part of the defined "Platreef" (McDonald and Holwell, 2011). This statement is supported by Kinnaird *et al*. (2005), mentioning that the mineralisation in the northern limb unaccounted for in the definition to date, is referred to as "Platreef-style" mineralisation that is not within the sensu stricto Platreef rocks.

The Platreef is a 10 to 400 m thick package of largely pyroxenitic lithologic units that contain PGE and Ni-Cu sulphide mineralisation, developed along a generally northward strike to the north of Mokopane (*Figure 3.4.*) (McDonald *et al*., 2017). Pyroxenitic units make up the predominant rock type present in the Platreef, although overall it is heterogeneous in nature and includes peridotites, cycles of norites, and anorthosites from the middle of the stratigraphy, upwards (Kinnaird, 2005; Kinnaird *et* al., 2005). According to Kinnaird *et al*. (2005), the package of Platreef rocks comprises of an upward succession of dunite, serpentinised peridotite, feldspathic pyroxenite – considered to be the dominant rock type of the package –, melanorite, leuconorite and finally anorthosite.

The orebody of the Platreef displays irregular PGE, Ni and Cu mineralisation over a strike length of ~30 km, with the central sector between the Tweefontein and Overysel farms associated with the highest

and most consistent grades (McDonald and Holwell, 2011; Smith *et al.*, 2014). The Platreef strike is offset by a several faults that are predominantly north-south in orientation and steeply dipping. The secondary set of faults dip between 50˚ and 70˚, striking in east-north-east or east-south-east directions and cross-cutting the north-south set (Kinnaird *et al*., 2005; McDonald and Holwell, 2011). Further investigation of the Platreef in its entirety has resulted in it now being regarded as having formed as a series of intrusions that have sporadically been separated by screens of country rocks along the length of its strike (Kinnaird, 2005).

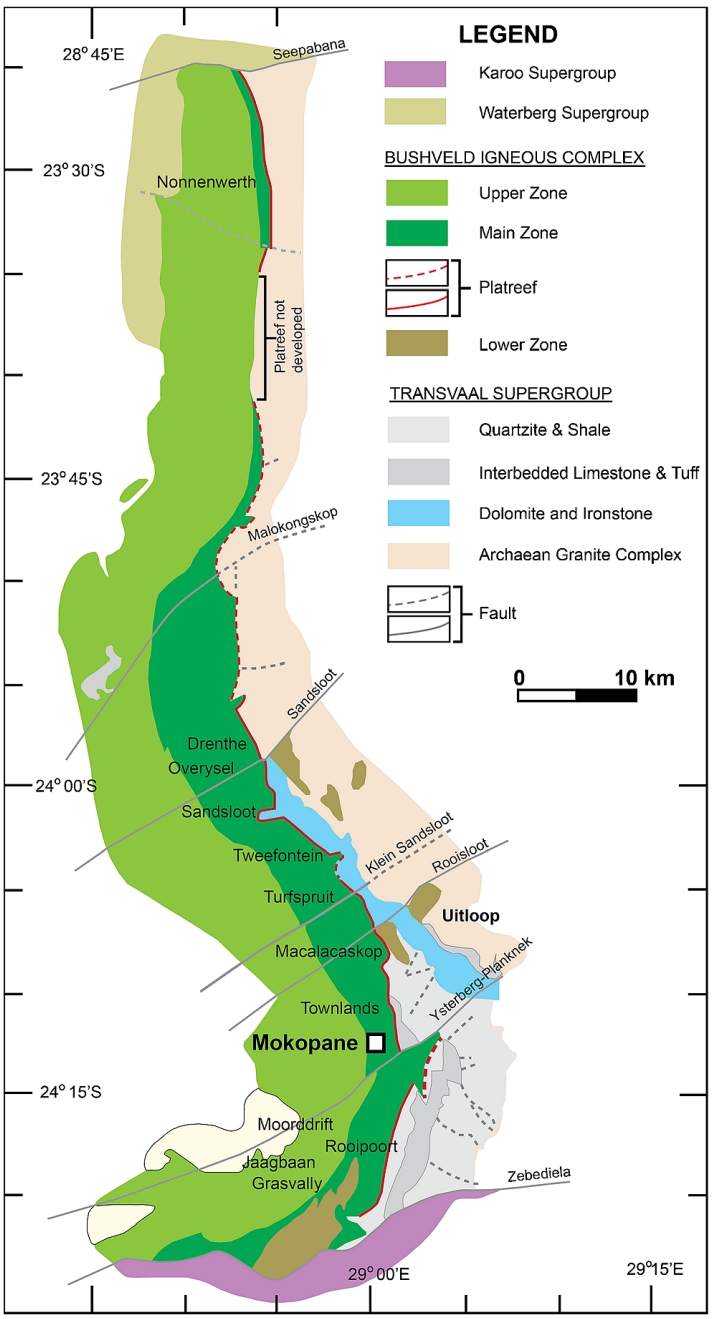

Figure 3.4. *A geological map of the of the northern limb of the Bushveld Complex, highlighting Platreef development by the red line and the ~10 km sector south of Nonnenwerth where Platreef mineralisation has not developed (Adapted from Grobler et al., 2018).*

All Platreef rocks consist of varying proportions of orthopyroxene, clinopyroxene, olivine and plagioclase, each ranging between less than 10% and over 90%, which results in a diverse combination of rock types as highlighted by Kinnaird *et al*. (2005) and further outlined by Yudovskaya and Kinnaird (2010). The major rock type of the Platreef is medium- to coarse-grained feldspathic pyroxenite which consists of 30% to 70% cumulus orthopyroxene, 10% to 30% intercumulus plagioclase, and as much as 20% post-cumulus clinopyroxene by volume with minor quartz, phlogopite and other accessory phases (Yudovskaya and Kinnaird, 2010; Andrews, 2015). According to the Streckeisen (1976), the upper limit of 10% plagioclase by volume separates the pyroxenes from the norites and gabbronorites in the stratigraphy, with the major pyroxenite variations present in the Platreef seen in the grain sizes of the orthopyroxenes and the volume of interstitial plagioclase (Nex *et al*., 2006). Although, the feldspathic harzburgite and olivine pyroxene (containing between 5% and 70% olivine) may have plagioclase contents as high as 10% to 15% (Yudovskaya and Kinnaird, 2010).

As a unique feature to the northern limb, the Platreef has often been considered to be the PGE-rich northern equivalent of the Critical Zone seen in the rest of Complex (Kinnaird, 2005; McDonald *et al*., 2005). This correlation with the Merensky Reef and UG2 chromitite of the CZ originally proposed by Wager (1929), was considered on the basis of the stratigraphic position between the LZ and MZ lithologies (McCreesh, 2016). However, this suggestion is still highly debated with the Platreef varying significantly in terms of lithology, mineral textures, mineral chemistries, and the geochemistry of both the rare earth elements and PGEs (McDonald *et* al., 2005; Kinnaird, 2005). The Platreef also differs from the Merensky Reef and UG2 units based on its overall package thickness, which ranges between 400 m and 800 m, in contrast to the 1 - 2 km thickness of the Merensky Reef (Kinnaird, 2005). In addition, the Platreef displays typically lower PGE grades, higher Ni contents and a Pt to Pd ratio close the value of 1 (Kinnaird, 2005). The Platreef generally shows lower and highly variable grades of PGE mineralisation, with PGE grades averaging between 1 and 2 g/t in areas where there is granite or silica-rich metasedimentary footwall with some intersection presenting grades of over 10 g/t, while PGE grades of the Platreef where the footwall is Malmani Dolomite typically exceed 4 g/t (Kinnaird *et al*., 2005; Kinnaird, 2005).

Previous literature on the Platreef predominantly regarded the unit as a single body, however the work of White (1983) and Barton *et al.* (1986) suggested the subdivision of the pyroxenitic units into three main reefs – although as noted by Nex and Kinnaird (2004), this subdivision is not applicable along the entire Platreef strike length – (McCreesh, 2016). More recent studies have confirmed that the Platreef is not a single body, but rather a number of different tabular-shaped bodies that formed as a result of the broadly horizontal sill-like emplacement of the Platreef magma into the Transvaal Supergroup (Kinnaird, 2005; Armitage, 2011). The local variations in the orientation and thicknesses

of reefs A, B and C were caused by the pre-existing country rock structures, with the tabular-like units displaying changes in orientation from south to north (Armitage, 2011; Smith *et al.*, 2014). The Platreef has a north-northwesterly strike in the south, changing to a north-west-north and eventually due north orientation further north, with the dip angle changing from between 15° and 27° in a generally southwest direction to angles between 45° and 10° in a westerly direction respectively (Kinnaird, 2005; van der Merwe, 2008; Smith *et al.*, 2014). As mentioned, the northern limb has variable footwall lithologies along its strike, with the lithologies becoming successively older northwards (Kinnaird, 2005). The overall geometry of the Platreef is deemed to have been largely controlled by the irregular floor topography above which it was emplaced (Kinnaird *et al*., 2005; Yudovskaya and Kinnaird, 2010; Armitage, 2011).

3.4. The Aurora Project

The Aurora Project was operated by Pan Palladium Limited (PPD) in the northern sector of the northern limb of the Bushveld Complex. The project area consisted of seven farms that cover a 20 km strike of Platreef style mineralisation (McDonald *et al*., 2017; Harmer *et al*., 2017). The project was established in the year 2002, initially comprising of the four farms of Nonnenwerth, Altona, La Pucella and Kransplaats, with the farms of Schauffhausen, Non Plus Ultra and Luge having been added to the project in 2005 (Harmer *et al*., 2017). An ownership change occurred in the year of 2010, whereby Sylvania Resources Limited (SLV) acquired the PPD assets, which included the Aurora Project (Harmer *et al*., 2017).

Previous studies on the Aurora Project area have suggested that the area represents a far-northern facies of the Platreef that lies along the margin of the Complex, however, this has subsequently been disproven with the Aurora rocks and mineralisation being both chemically and mineralogically distinct from that of the Platreef (McDonald *et al*., 2017; Harmer *et al*., 2017). Harmer *et al*. (2017) states that the mineralisation at Aurora has a lower Pt to Pd ratio, a lower IPGE, a lower Ni/Cu ratio and a significantly higher Au content than present in the Platreef. It is also stated that the lithology of the host rocks differs from that of the Platreef, with the host rocks being leuco- to mela-gabbronorites and consisting of cumulus plagioclase, orthopyroxene and inverted pigeonite, with the overall mineralisation being hosted within the upper Main Zone and not the Critical Zone (Harmer *et al*., 2017; McDonald *et al*., 2017). McDonald *et al*. (2017) suggest that the Aurora Project represents a marginal facies of the Main Zone above the Troctolite Marker, rather than an unlikely simple strike extension of the Platreef (Huthmann *et al*., 2017).

The base metal sulphide mineralisation at Aurora is both Au- and Cu-rich, being hosted predominantly within the leucocratic rocks of the Upper Main Zone (McDonald *et al*., 2017). In terms of the

stratigraphy of the Aurora Project, the rocks are subdivided into four different units, the first being Unit 1 which consists of orthopyroxenites, websterites and melagabbronorites that overlie the granitoid gneissic basement (McDonald *et al*., 2017; Harmer *et al*., 2017). Unit 2 is comprised of gabbronorites and leuco-gabbronorites, with the pigeonite gabbronorites of Unit 3 overlying these Unit 2 rocks (McDonald *et al*., 2017; Harmer *et al*., 2017). The uppermost Unit 4 comprises of ferro-gabbros with cumulus magnetite (Harmer *et al*., 2017). The PGE-Ni-Cu-Au mineralisation of the Aurora Project is different from that of the mineralisation observed in the stratiform reefs of the Critical Zone and the Platreef, with the most important observation being that the mineralisation is not concentrated within melanocratic units which commonly characterise the PGE and base metal mineralisation throughout the Platreef and Critical Zone, but rather within leucocratic units with the presence of inverted pigeonite and orthopyroxenites (McDonald *et al*., 2017).

3.5. The Waterberg Project

The Waterberg Project is a project operating within the northern limb of the Bushveld Complex, north of the town of Mokopane by Platinum Group Metals (PTM) from the year of 2011 (Kinnaird *et al*., 2012; Lombard, 2012; McCreesh, 2016). Previous literature interpreted the northern limb of the Bushveld to have terminated at the Hout River Shear Zone (HRSZ), which was believed to have been the northern-most extent of the limb (Huthmann *et al*., 2016; McCreesh, 2016). Further exploration of the area led to the discovery of northern limb Bushveld rocks below a thick succession of Proterozoic Waterberg sediments, and therefore the project looked to target the potential PGM and base metals (Cu and Ni) within this previously unknown extension of the northern limb (Kinnaird *et al*., 2012; Kinnaird *et al*., 2017; Lombard, 2012).

The project itself is part of a larger group of exploration projects operated by PTM from 2010 onwards and is located approximately 70 km to the north of Mokopane (Huthmann *et al*., 2016; Lombard, 2012). As mentioned by Kinnaird *et al*. (2017), the discovered succession of ultramafic-mafic rocks extends ~24 km to the north of the HRSZ, typically 1 km thick and dipping at 34˚ to 38˚ to the west. The succession is a basal ultramafic sequence comprised of a lower-orthopyroxenite and upper-harzburgite, which overlies an Archaean granite gneiss basement. This sequence is succeeded by a troctolite-gabbronorite-anorthosite sequence and then Upper Zone rocks with red bed sedimentary rocks of the Waterberg covering the Bushveld rocks (Kinnaird *et al*., 2017; McCreesh, 2016).

In terms of the mineralisation identified within the Waterberg Project, there are two defined intervals of PGE-Cu-Ni-Au mineralisation, a lower F zone and upper T zone (Kinnaird *et al*., 2017; Lombard, 2012). The PGEs and base metals are hosted within gabbros, anorthosites, pyroxenites, troctolites and norites (Lombard, 2012). The T zone, occurring within a lithologically varied sequence near to the

boundary between the Upper Zone and the lower troctolite-gabbronorite-anorthosite sequence and only occurring in the southern region of the project, varies in thickness between ~30 m and ~60 m (Kinnaird *et al*., 2017). In contrast, the F Zone occurs across a broader region of the project, extending 17 km along strike and hosting disseminated sulphides with accessory chromite within the sequence of pyroxenite and harzburgite ultramafics (Kinnaird *et al*., 2017; Lombard, 2012; McCreesh *et al*., 2018). The mineralisation occurs as a typically ~10 m interval in the central portion, with the zone thickening to approximately 60 m and increasing in grade in what is known as the "Super F Zone" (Kinnaird *et al*., 2017; Lombard, 2012; McCreesh *et al*., 2018).

3.6. Mineralisation in the Northern Limb

The northern limb of the Bushveld Complex contains a diverse range of Ni-Cu-PGE, Cr, Fe-V and Sn mineralisation types and styles, with these mineralisation types varying in size and scale between world-class and subeconomic deposits (Kinnaird and McDonald, 2018). The majority of economic geology literature since the early 2000s primarily focused on PGE, Ni and Cu mineralisation associated with the Platreef, with older literature having predominantly concentrated on Bushveld granite Sn mineralisation (Kinnaird and McDonald, 2018). Mineralisation in the northern limb is notably not exclusive to the Platreef with other observed PGE-Ni-Cu mineralisation not strictly falling within the Platreef (ss) definition. These various types of mineralisation in the northern limb are considered to be separate from that of the Platreef on the basis of their differing host lithologies as well as their stratigraphic position within the RLS (Kinnaird *et al*., 2005; McDonald and Holwell, 2011).

The working definition of the Platreef proposed by Kinnaird *et al*. (2005) explicitly excludes PGE-Ni-Cu mineralisation present to the south of Mokopane, the Aurora Project and the Waterberg Project in particular (Kinnaird *et al*., 2005; McDonald and Holwell, 2011). The following descriptions for the various styles of mineralisation is presented in stratigraphic sequence for the different geographical locations throughout the northern limb (*Figure 3.5*).

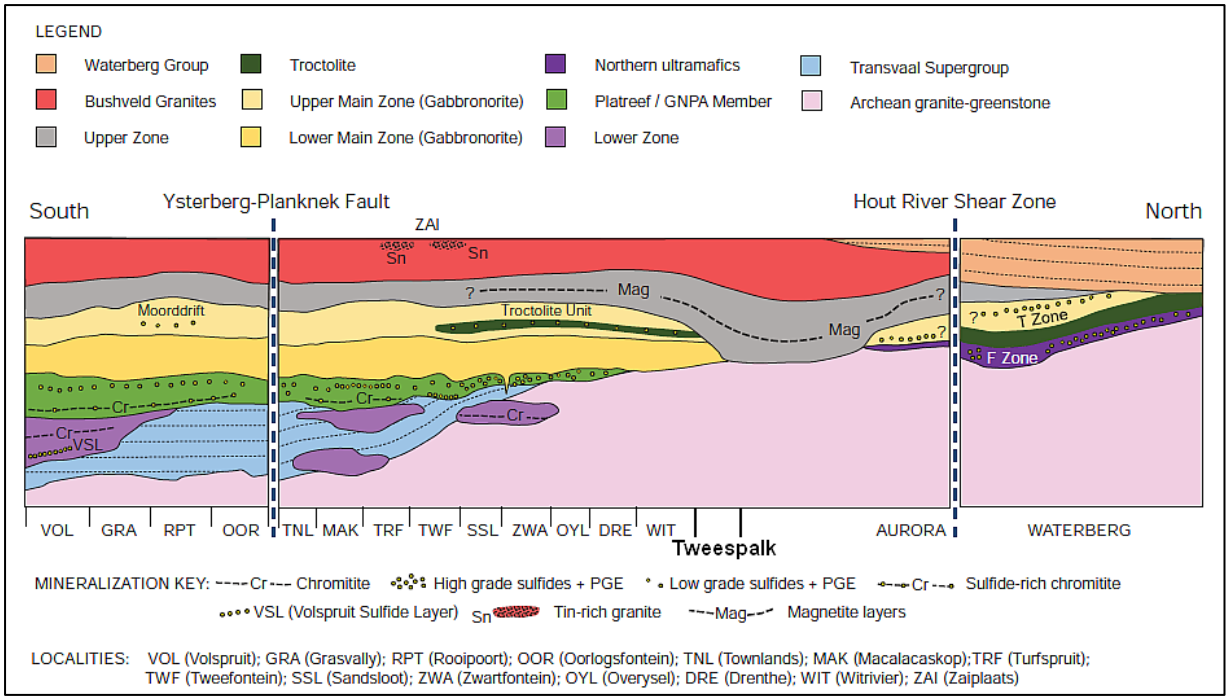

Figure 3.5. *A schematic south-north cross-section of the northern limb showing the complex geographic and stratigraphic relationships between the various farm and deposit localities, with the Tweespalk farm location specifically illustrated to the north of Witrivier (Adapted from Kinnaird and McDonald, 2018).*

3.6.1. Lower Zone Mineralisation

3.6.1.1. South of the Ysterberg-Planknek fault

The Lower Zone ultramafic sequence of the northern limb comprises three major subzones, they are the orthopyroxene and olivine-orthopyroxene cumulates of the Volspruit subzone, the olivine and olivine-chromite dominating cumulates of the Drummondlea subzone, and Moordrift subzone which consists of approximately equally proportioned orthopyroxene and olivine-chromite cumulates as previously discussed (Hulbert, 1983; Hulbert and von Gruenewaldt, 1985; Kinnaird and McDonald, 2018). South of the Ysterberg-Planknek fault, the LZ attains a minimum thickness of ~1600 m, with the base of the zone having not been intersected (Hulbert, 1983; van der Merwe, 2008; Kinnaird and McDonald, 2018).

The Volspruit subzone which contains the Volspruit sulphide zone, an orthopyroxene-chromite cumulate with disseminated base metal sulphides, represents the only known significant stratiform PGE mineralisation in the LZ of the entire Bushveld Complex and is the earliest stratigraphic magmatic sulphide mineralisation present in the northern limb (Tanner *et al*., 2017; Kinnaird and McDonald, 2018). The mineralisation is hosted within a typically harzburgitic sequence, the economic mineralisation is separated between the Volspruit North and Volspruit South deposits, with the former containing roughly two-thirds of the combined minable ore (Venmyn-Rand, 2010; Kinnaird and

McDonald, 2018). The platinum group metals are predominantly Pt and Pd tellurides and bismuthides, whilst the base metal sulphide mineralogy is dominated by pyrrhotite, pentlandite, chalcopyrite and cubanite (Kinnaird and McDonald, 2018). The deposits show an increase in sulphide content and layer thickening downdip towards the west of the intrusion margin (Kinnaird and McDonald, 2018).

Two prominent chromitites are present in the Drummondlea subzone, with these being the only developed chromitites of significance in the LZ of the Bushveld and have contain the highest Cr/Fe ratios in the entire Complex to date (Hulbert and von Gruenewaldt, 1985; (Kinnaird and McDonald, 2018).

3.6.1.2. North of the Ysterberg-Planknek fault

The LZ to the north of the Ysterberg-Planknek fault was originally considered to have only developed as satellite bodies that intruded into the Archaean granite gneiss basement, however subsequent drilling through the Platreef on the Sandsloot and Turfspruit farms discovered <800 m thick sequences of LZ rocks that display a chilled contact between the Transvaal Supergroup and Archaean granite gneiss rocks (van der Merwe, 2008; Yudovskaya *et al*., 2013; Kinnaird and McDonald, 2018). Fingers of LZ rocks appear to link the sub-Platreef intrusions with the isolated satellite bodies within the granite gneiss to the east, as a result of the LZ not being uniformly distributed (Yudovskaya *et al*., 2013). The LZ north of the Ysterberg-Planknek fault generally lacks any economic sulphide mineralisation within the harzburgite-pyroxenite cycles, with these cycles also containing sporadic Cr/Fe chromitites that do not reach an economic thicknesses (Kinnaird and McDonald, 2018).

3.6.2. Platreef Mineralisation

The Platreef has conventionally been discussed with specific reference to the farm on which it occurs, however the subdivision of the Platreef into sectors by Kinnaird *et al*. (2005) allows for the geographical grouping of individual farms into zones of Platreef that display specifically shared characteristics north of the Ysterberg-Planknek fault (Kinnaird and McDonald, 2018). These aforementioned sectors include a southern sector, central sector and northern sector, while the GNPA is included as a result of it forming at a similar stratigraphic position to the south of the Ysterberg-Planknek fault.

3.6.2.1. GNPA member south of the Ysterberg-Planknek fault

The Grasvally Norite-Pyroxenite-Anorthosite member is located at a similar stratigraphic position to the Platreef and is underlain by both ultramafic cumulates of the LZ and the Magaliesberg Quartzite Formation with the MZ gabbronorites sitting above it (Hulbert, 1983; Smith *et al.*, 2014; Kinnaird and

McDonald, 2018). Striking in a north-easterly direction for 30 km, the 400 m to 800 m thick layered succession comprises a variably textured succession of gabbronorites, norites, anorthosites, pyroxenites as well as PGE-bearing chromitite (Smith *et al.*, 2014). De Klerk (2005) subdivided the succession into the three stratigraphic units, the Lower Mafic Unit (LMF, the Lower Gabbronorite Unit (LGN), and the Mottled Anorthosite Unit (MANO), of which the LMF and MANO are the two major units separated by the fine- to medium-grained gabbronorites of the LGN with variable chilled zones, gradational and sheared contacts observed between the three units (Smith *et al.*, 2014; Kinnaird and McDonald, 2018).

The PGE and BMS mineralisation within the GNPA developed as wide, irregular zones throughout the LMF and MANO units, however this mineralisation is not lithologically bounded (Smith *et al.*, 2014). Seven PGE- and BMS-bearing horizons were identified on the Grasvally and Rooipoort farms, as well as thin PGE-bearing chromitites that developed within the basal LMF (Smith *et al.*, 2014). The GNPA member is characterised by a Pt/Pd ratios of less than 1 as a result of being Pd-rich, with the orthopyroxene-clinopyroxene cumulate dominated LMF carrying PGE mineralisation grades of 1.15 ppm (2PGE + Au) over 1.3 m, reaching up to 5 ppm at sulphide enriched intersections (Smith *et al.*, 2014; Kinnaird and McDonald, 2018). The MANO is dominated by anorthosites and norites and contains zones of disseminated sulphide mineralisation at an average grade of 1.34 ppm (2PGE + Au) over 1.8 m (Smith *et al.*, 2014; Kinnaird and McDonald, 2018). The chromitites within the GNPA host significant and consistent PGE concentrations of around 4 ppm throughout the region (Smith *et al.*, 2014).

3.6.2.2. Southern Sector (Ysterberg-Planknek to Turfspruit)

The southern sector of the Platreef package that occurs on the Townlands, Macalacaskop and Turfspruit farms, is made up of a number of different sills that display contact-metamorphosed metasedimentary rock screens or rafts at the Timeball Hill Formation and Duitschland Formation contacts (Kinnaird, 2005; Manyeruke *et al*., 2005; Kinnaird and McDonald, 2018). The Platreef comprises three separate sills on the Townlands farm – of which the medium-grained and heterogeneous olivine-bearing feldspathic pyroxenite with a thickness of ~35 m carries the highest grade – each separated by hornfels (Manyeruke *et al*., 2005; Kinnaird and McDonald, 2018).

The subdivided Platreef extends northwards onto and through the Macalacaskop farm where the basal Platreef is composed of serpentinised harzburgite, serpentinised pyroxenite, feldspathic pyroxenite and parapyroxenite with some country rock xenoliths (Kinnaird and McDonald, 2018). The middle and upper Platreef sills in the sector are dominated by medium-grained pyroxenite-norite and

coarse-grained orthopyroxenite respectively (Kinnaird and McDonald, 2018). Mineralisation in this section of the southern sector is bottom loaded, with the variable but typically 150 m thick package concentrating PGE in the basal pyroxenites (Kinnaird, 2005). The relatively significant grades of mineralisation are observed in the structural basin, whilst a weaker zone of mineralisation occurs higher up in the succession in pyroxenites and norites (Kinnaird and Nex, 2015; Kinnaird and McDonald, 2018).

The Platreef on the Turfspruit farm has been interpreted by Kinnaird (2005) to have separated into four sill-like intrusions that dip between 40° and 60°. The basal sill is composed of a heterogeneous rock type package, followed by porphyrictic feldspathic orthopyroxenite with intercumulus sulphides and coarse-grained feldspathic orthopyroxenite of the lower and upper middle sill, with the top sill being a fine-grained dark pyroxenite that contains oikocrysts of clinopyroxene (Kinnaird and McDonald, 2018). The PGE mineralisation is also bottom loaded in the basal sill or in the footwall, with elevated PGE grades in the middle and upper Platreef where the there is a minor concentration of sulphides (Kinnaird and McDonald, 2018). Towards the north of the Turfspruit basin, the Platreef flattens out at a depth of ~600 m, with this locally subhorizontal layered and thickened section forming what is known as the Flatreef (Kekana and Broughton, 2011; Kekana, 2014; Grobler *et al*., 2018).

The Flatreef is also associated with the appearance of zones of anorthosite and norite, as well as chromitites (Kinnaird and McDonald, 2018). The Flatreef is divided into two packages, an upper anorthosite-norite-pyroxenite package and a lower unit comprising of a series of cycles ranging from anorthosite-leuconorite-norite to feldspathic pyroxenite and harzburgite (Yudovskaya *et al*., 2017). The very unusual thickness and grade of the mineralised interval of the Flatreef has resulted in increased attention and subsequent underground mine development, with indicated resources of 346 MT at a grade of 3.77 g/t (3PGE + Au) and 0.16% Cu and 0.32% Ni in the southern sector (Kinnaird and McDonald, 2018). Some boreholes in the area have intersected over 90 m of mineralisation with up to 4.5 ppm of PGEs (Kinnaird and McDonald, 2018).

3.6.2.3. Central Sector (Tweefontein to Zwartfontein)

The Platreef sequence in the southern portion of the Tweefontein farm of the central sector, ranges in thickness between 100 m and 220 m and consists of varied textured pyroxenites, parapyroxenites, serpentinites and micronorites (Kinnaird and McDonald, 2018). This sequence of Platreef in this region hosts massive to semi-massive sulphides that are net-textured and/or blebby in nature, with this sulphide mineralisation generally occurring within the basal Platreef unit (Nex, 2005; Kinnaird and McDonald, 2018). This basal sulphide-rich mineralisation has a grade of 5 g/t (3PGE + Au), containing

1.41 Moz of combined PGEs and 0.54% Cu and 0.65% Ni for a total inferred resource of approximately 5 Mt which stands as a significant potential resource in the future (Kinnaird and McDonald, 2018).

Further north on the Tweefontein farm, the threefold Platreef division comprises a felspathic pyroxenite and melanorite interlayered package, feldspathic harzburgite and norite included with serpentinite layers, ironstone or hornfels rafts and granitic veins (McCutcheon, 2012; Kinnaird and McDonald, 2018). In contrast to mineralisation further south in the sector, the highest PGE grades are present in the upper Platreef unit in the homogeneous pyroxenite, with the highest grades associated with the chromitite layer that lies approximately 20 m below the MZ (Yudovskaya and Kinnaird, 2010; Kinnaird and McDonald, 2018).

Dolomites of the Malmani Group on the Sandsloot and Zwartfontein farms were intruded by the Platreef, causing their conversion to metamorphic clinopyroxenites and calc-silicate hornfels that are possibly serpentinised with strong mineralisation (Wagner, 1929; Armitage *et al*., 2002; Holwell *et al*., 2006). Generally, the mineralisation on the Sandsloot farm is top loaded and in the form of fine-grained but visible interstitial sulphides (Kinnaird and McDonald, 2018). As discussed, the highest PGE grades occur specifically in the chromitiferous zone that lies near the base of the uppermost pyroxenite unit with grades of PGE also extending into the calc-silicate floor for tens of metres (Kinnaird and Nex, 2015; Kinnaird and McDonald, 2018). PGE mineralisation on the Zwartfontein farm occurs throughout, however the greatest concentration occurs near to the contact with the MZ within the upper portion of the package (Grobler *et al*., 2018; Kinnaird and McDonald, 2018).

Mineralisation in the Akanani project which lies downdip of Zwartfontein, occurs within the 80 m to 300 m thick Platreef package (Kinnaird and McDonald, 2018). This package is subdivided into four units (P1 to P4), averaging grades of 4 g/t to 6 g/t (3PGE + Au) in the feldspathic pyroxenite/ harzburgite of P2 (Kinnaird and McDonald, 2018). Once again, the highest grades of PGE mineralisation are associated with discontinuous and basal P2 chromitite stringers or within narrow intervals of chromitite at the top of P2, with PGE grades ranging between 25 g/t and 30 g/t (Kinnaird and McDonald, 2018).

3.6.2.4. Northern Sector (Zwartfontein to Witrivier)

The northern sector extends northwards from the centre of the Zwartfontein farm through to Witrivier where the northern limb succession no longer lies on rocks of the Transvaal Supergroup but rather sits directly on the Archaean granitic gneiss basement (Kinnaird and McDonald, 2018). To the north of the Witrivier farm the Platreef disappears with the cumulates of the MZ and UZ resting successively against the granite gneiss floor (Kinnaird and McDonald, 2018). The presence of dolomite-dominated

calc-silicate rafts within the Platreef and this subsequent disappearance of the Platreef were the basis for the argument made by McDonald and Holwell (2011) that the unconformity between the Transvaal Supergroup sediments and Archaean basement was exploited by the Platreef itself (Kinnaird and McDonald, 2018). It was proposed that the dolomite to the north of Zwartfontein acted as the roof to the Platreef above the granite basement, until its disappearance further north (Kinnaird and McDonald, 2018).

The PGE mineralisation at Overysel (formerly known as PPRust North) is not obviously top loaded like at Sandsloot, but rather occurs throughout the Platreef in this section with zones of pyroxenite containing chromitite xenoliths and discontinuous chromitites hosting the majority of PGE mineralisation at the bottom and top of the Platreef (Holwell and McDonald, 2006; Yudovskaya and Kinnaird, 2010; Kinnaird and McDonald, 2018). Relatively PGE-rich sulphides have also been observed in the granite gneiss floor at the Overysel farm (Kinnaird and McDonald, 2018). Once again, a threefold subdivision of the Platreef is observed on the Drenthe farm, hosting several subparallel PGE-mineralised horizons throughout as well as a subzone of mineralisation around the hanging-wall dolomite xenoliths (Kinnaird and McDonald, 2018). The main PGE mineralisation in the sector forms over a 30 m interval at 1.26 g/t to the south of the sector and within multiple mineralised intervals in the northern section, however the overall PGE grades of the sector are lower than the central sector (Kinnaird and McDonald, 2018).

3.6.3. Main Zone Mineralisation

It has recently been shown that gabbronorite-dominated Main Zone cumulates of the northern limb may be highly prospective for PGE-rich mineralisation unlike that of the Main Zone of the eastern and western Bushveld (Kinnaird *et al*., 2017; McDonald *et al*., 2017; Kinnaird and McDonald, 2018). Along with the gabbronorites, the MZ of the northern limb contains minor proportions of norites and pyroxenites towards the base of the zone as well as an increasing upward proportion of anorthosite throughout the succession (van der Merwe, 1976; Ashwal *et al*., 2005). A unique feature of the northern limb MZ is the presence of 100 m to 200 m thick and ~30 km long troctolite unit in the middle of the zone, which is later transgressed by magnetite-bearing gabbros or regional faults (Kinnaird and McDonald, 2018). This unit is unique in that the MZ of the eastern and western limbs lack this presence of olivine-bearing rocks, with the troctolite forming a regional stratigraphic marker (Kinnaird and McDonald, 2018). On the other hand, the distinctive Pyroxenite Marker that is present in the eastern and western limbs seems to be absent in the northern limb (Ashwal *et al*., 2005; Tanner *et al*., 2014).

A chilled and erosional contact between the lower MZ and underlying Platreef recognised by Holwell and Jordaan (2006), demonstrates that MZ magma emplacement significantly post-dated the intrusion of the Platreef (the Platreef was largely solidified) and therefore resulted in the restriction of metal contribution to the Platreef by the MZ magma (McDonald *et al*., 2017; Kinnaird and McDonald, 2018). This observation and the lack of the Pyroxenite Marker suggests that during MZ and UZ intrusion the northern limb may have been isolated from the rest of the complex with the chalcophile element budget therefore concentrating elsewhere with the northern limb MZ (McDonald and Holwell, 2011; Kinnaird and McDonald, 2018). This is supported by the discoveries of PGE mineralisation in the MZ at Aurora project, and within the likely MZ affinity present at the Waterberg project north of the HRSZ (Kinnaird and McDonald, 2018).

Mineralisation of relatively low-grade PGE concentration is defined at the basal and top extents of the troctolite unit, with up to five mineralised units containing fine-grained and disseminated sulphides have been identified (Viljoen, 2016; Kinnaird and McDonald, 2018). The highest grade observed between is 3.68 g/t (2PGE + Au), with the zone of the unit having an average 1.15 g/t (2PGE + Au) grade over 3.23 m (Viljoen, 2016; Kinnaird and McDonald, 2018).

3.6.4. Upper Zone Mineralisation

The UZ of the northern limb comprises predominantly magnetite-gabbro, gabbro, magnetite-bearing ferrodiorites, anorthosite and up to 20 layers of magnetitite that have been identified across the northern limb (Kinnaird and McDonald, 2018). In addition, as many as five zones of disseminated magnetite are recognised (Kinnaird and McDonald, 2018). The magnetite layers in the UZ of the northern limb are of significant economic importance as they potentially contain exploitable grades of Fe, Ti and V, with these possibly economic layers extending along a north-south strike for approximately 5.5 km (Viljoen, 2016; Kinnaird and McDonald, 2018).

Chapter Four

Local Geology and Core Logging

4.1. Introduction

The Tweespalk property located just north of the centre of the northern limb was privately owned prior to the year of 2002, with the records and reports of previous exploration in the area being relatively non-existent and the exploration information being largely restricted to a regional Pietersburg 2328 geological map produced by the South African Council for Geoscience at a scale of 1:250 000 that covered the Tweespalk area (PTM Annual Report, 2004). This initial geological map showed the contact between the complex footwall and the Mapela gabbronorite traversing through the Tweespalk property for a strike length ~3.5 km, which sparked interest for exploration of the area on the basis that near this contact to the south of the property, Platreef-style mineralisation was observed (van der Merwe, 1976; PTM Annual Report, 2004, Visser and McWha, 2005).

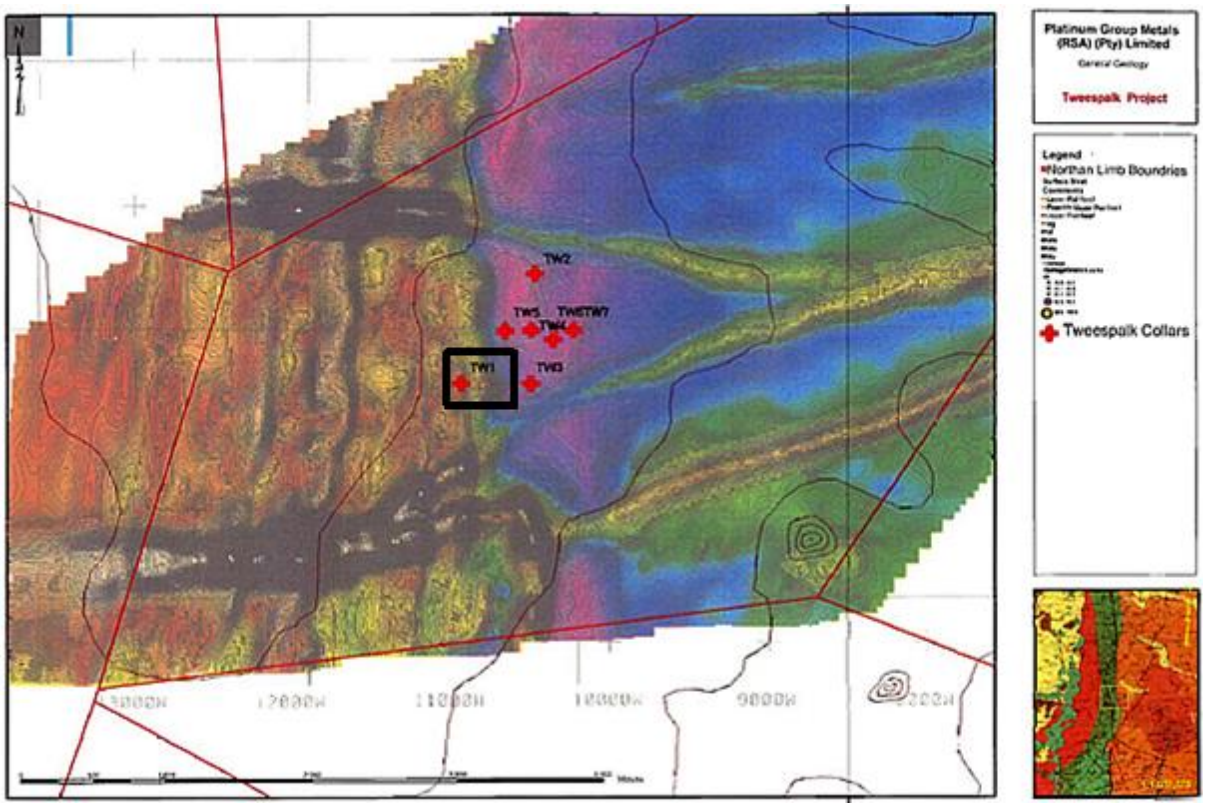

Figure 4.1. *Locations of seven of the nine borehole collars drilled on the Tweespalk farm with borehole TW1 highlighted by the black rectangle. The generalised surface geology of the area is also shown, with the purple and blue colours representing the Upper and Main Zones respectively (Adapted from Visser and McWha, 2005).*

In 2002, PTM carried out a limited program of soil sampling, mapping and high resolution airborne magnetic and radiometric surveys of the property (*Figure 4.1.*), with the soil sample surveys identifying anomalous platinum, palladium, nickel and copper values that confirmed the presence of PGE mineralisation associated with the lower Bushveld contact (PTM Annual Report, 2004; Furness, 2004). The interpretation of the geophysical survey data highlighted the basal contact of the Bushveld Complex along with the overlying Upper Zone and Main Zone contacts, that correlated well with the geochemical soil survey results (PTM Annual Report, 2004).

4.2. Core Logging Features

In order to investigate the local geology of the Tweespalk area, a core logging programme was carried out at the PTM Marken core yard north of Mokopane, Limpopo. The core of borehole TW1 was logged and appropriate core samples were collected in order to determine the general stratigraphy of the area. The traditional core logging techniques that were used on the Tweespalk exploration core, formed the basis for the identification and description of the different rock types, modal mineralogy, nature of contacts, grain sizes, intervals of mineralisation, as well as various textural and alteration features present in the core. In addition, the minerals, textures, and features observed in the core was used for stratigraphic comparison and correlation with other well-known stratigraphies of different areas in the northern limb as well as the Waterberg project further to the north.

4.2.1. Rock Classification

The northern limb of the Bushveld Complex has a considerably more diverse range of rock types present than that of the other limbs. This large variation of rock types is predominantly the result of significant interaction with the wide range of footwall lithologies transgressed by the mafic succession of the northern limb, and the subsequent contamination of the intruding magma. The majority of the primary magmatic rocks of the northern limb contain plagioclase, orthopyroxene and clinopyroxene in varied proportions. However, there are a few cases in which lithologies that have undergone some form of metamorphic alteration do not confirm to this shared characteristic.

The primary classification of the igneous rocks in this study are based on the Classification and Nomenclature Recommendations of the IUGS Subcomission on the Systematics of Igneous Rocks, with plutonic and volcanic rocks first being classified according to their proportion of mafic minerals present (Streckeisen, 1976; Le Bas and Streckeisen, 1991; Le Maitre *et al*., 2020). If the proportion of mafic minerals in the rock is less than 90%, then modal mineral contents of its felsic minerals are plotted on the QAPF double triangle (*Figure 4.2. A)* (Streckeisen, 1976; Le Bas and Streckeisen, 1991; Le Maitre *et al*., 2020). The Bushveld rock types that typically fall within the diorite-gabbro-anorthosite

field at the plagioclase apex of the QAPF diagram (*Figure 4.2. A*), are classified further according to their relative abundances of plagioclase, orthopyroxene, clinopyroxene and olivine (Le Maitre *et al*., 2020). These gabbroic rocks (*sensu lato*) that fall within the highlighted field of *Figure 4.2. A*, are subdivided further by the two mafic ternary diagrams respectively (*Figure 4.2. B and C*).

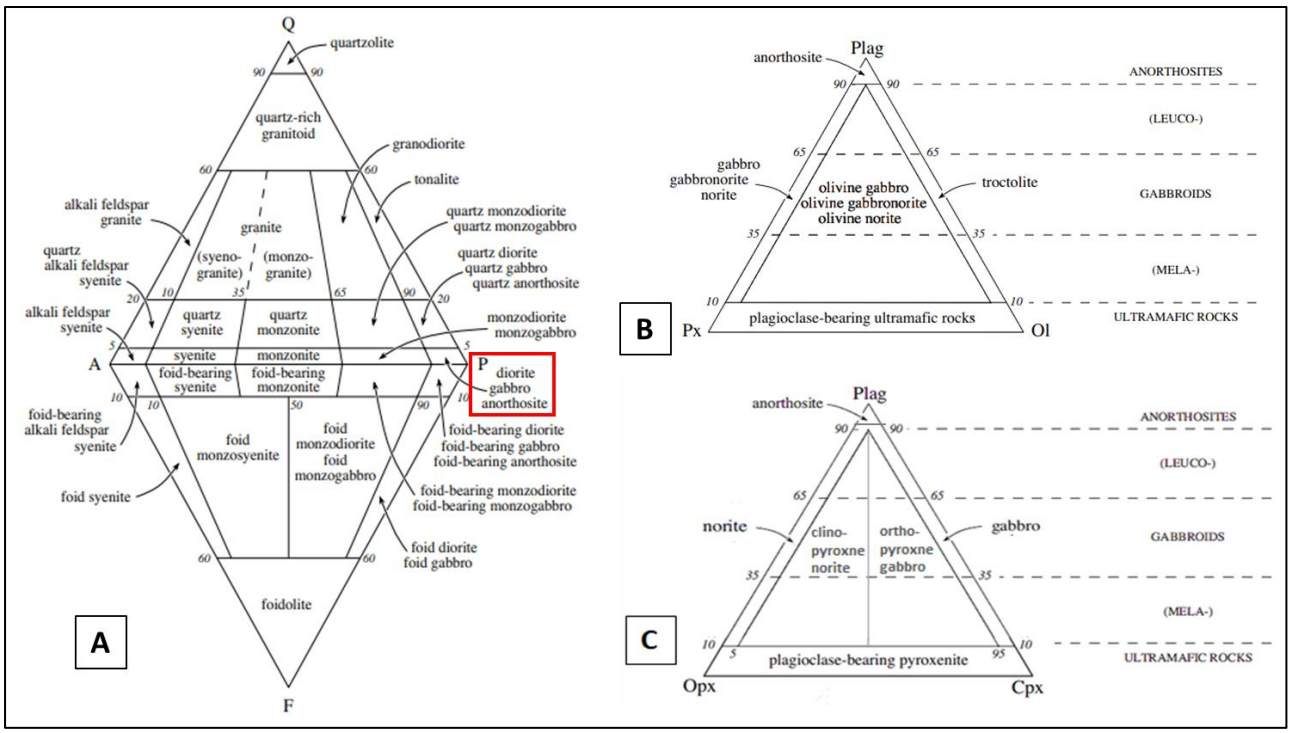

Figure 4.2. A) *The QAPF double triangle modal classification diagram for plutonic rocks (based on Streckeisen (1976)).* ***B)*** *Modal classification Plag-Px-Ol ternary diagram of Gabbroic rocks* ***C)*** *Modal classification Plag-Opx-Cpx ternary diagram of Gabbroic rocks. (Adapted from Le Maitre et al., 2002).*

4.2.2. Mineralisation

The initial drilling programme of the exploration project commenced on the 14th of October 2003. This led to the discovery of platinum and palladium mineralisation in hole TW1, producing assay results of 1.09 g/t (2PGE + Au) over 6.68 m from a 27.99 m reef intersection section at a depth of 642 m, including a 4.04 m reef intersection grading at 4.40 g/t (*2PGE + Au)* from the Bushveld sequence (Furness, 2004; Visser and McWha, 2005). The mineralisation was located near to, but not at the base of Bushveld Complex sequence, with the borehole TW1 also intersecting two zones of lower grade mineralisation, a 6.07 m interval returning 0.5 g/t (2PGE + Au) and 0.12% (Cu + Ni), and a 5.31 m interval yielding 0.36 g/t (2PGE + Au) and 0.09% (Cu + Ni) (Furness, 2004; Visser and McWha, 2005). Extension of the drilling programme resulted in six more diamond drill holes being drilled, along strike, both up and down dip of TW1, totalling 2667.97 m in length drilled (*Table 4.1.*) (Furness, 2004; Visser and McWha, 2005). Two more boreholes were drilled (TW8 and TW9), however the drilling

information and assay results from these particular boreholes were not released by PTM and have therefore not been included in the tables below.

Table 4.1. *Collar co-ordinates, orientations and the number of samples taken for each the boreholes drilled on the Tweespalk farm (Adapted from Visser and McWha, 2005).*

BHID	From (m)	To (m)	Latitude (S)	Latitude (E)	Dip	Samples
TW1	0,00	702,60	23˚ 42' 11.7"	28˚ 53' 34.8"	90	880
TW2	0,00	307,54	23˚ 41' 48.0"	28˚ 53' 50.3"	90	351
TW3	0,00	333,37	23˚ 42' 12.3"	28˚ 53' 49.2"	90	436
TW4	0,00	470,08	23˚ 42' 0.07"	28˚ 53' 49.9"	90	594
TW5	0,00	551,23	23˚ 42' 0.04"	28˚ 53' 44.2"	90	650
TW6	0,00	257,00	23˚ 42' 0.07"	28˚ 53' 55.7"	90	267
TW7	0,00	46,15	23˚ 41' 59.9"	28˚ 53' 58.9"	90	*
	Total	2667,97				3178

** Not sampled.*

The first phase of drilling at Tweespalk led to the confirmation of the presence of a traditional Bushveld layered sequence with the possibility of this sequence hosting economic PGE and base metal mineralisation (PTM Annual Report, 2004; Visser and McWha, 2005). Upper Zone rocks underlying the western portion of the property and granitic gneiss underlying the eastern portion of the property confirmed a dip of the layered rocks between 25˚ and 40˚ and a thickening of the entire sequence towards the west (PTM Annual Report, 2004; Visser and McWha, 2005). As mentioned by Furness (2004), the assay results for Cu and Ni correlated with the identified zones of PGM mineralisation. However, exploration work on the property was downscaled towards the end of July in 2004, having produced assay results from the 9 drill holes that were not of any economic significance at the time of exploration (PTM Annual Report, 2004; Visser and McWha, 2005). It is highlighted that there is potential for higher grade intercepts within the deeper portion of the Complex further to the west of the property, but no further exploration has been recommended for the project as a result of the significant depth at which this mineralisation is likely to occur (PTM Annual Report, 2004; Furness, 2004; Visser and McWha, 2005). A summary of the specific mineralised intersections observed in the Tweespalk boreholes is shown in *Table 4.2.*

Table 4.2. *Specific mineralised intersections from the Tweespalk boreholes (Adapted from Visser and McWha, 2005).*

BHID	Unit	Interval Length (m)	Top of Intercept (m)	Reef	Pt (g/t)	Pd (g/t)	Au (g/t)	2PGE + Au (g/t)	Interval Type
TW1	Zone 2	27,99	542,80	Platreef	0,36	0,70	0,03	1,09	Total Unit
TW1	Zone 2	4,04	645,90	Platreef	1,56	2,74	0,09	4,40	Selective Cut
TW1	Zone 4	24,00	599,90	Platreef	0,07	0,10	0,10	0,27	Total Unit
TW1	Zone 4	7,65	616,25	Platreef	0,13	0,18	0,18	0,49	Selective Cut
TW1	Zone 6	25,45	542,37	Platreef	0,04	0,15	0,07	0,26	Total Unit
TW1	Zone 6	8,72	542,37	Platreef	0,08	0,22	0,01	0,31	Selective Cut
TW2	Zone 2	4,13	206,93	Platreef	0,04	0,05	0,01	0,10	Total Unit
TW2	Zone 4	5,57	191,16	Platreef	0,03	0,07	0,00	0,10	Total Unit
TW2	Zone 6	16,60	154,40	Platreef	0,07	0,13	0,01	0,21	Total Unit
TW3	Insignificant Values								
TW4	No Mineralisation								
TW5	No Mineralisation								
TW6	No Mineralisation								
TW7	No Mineralisation								

4.2.3. Mineralogy

The lithologies present in the TW1 core from the Tweespalk area show mineral assemblages and textures similar to that of the rocks present in the rest of the northern limb, and are predominantly representative of UZ and possibly MZ rocks of the northern limb Bushveld stratigraphy. There are a few key identifiable minerals and features present in the core that are of great importance to this study, with these minerals and features being used to help identify notable stratigraphic markers and aiding in stratigraphic correlation with the rest of the northern limb stratigraphy. These identifiable minerals that have been specifically noted in the core logs are magnetite and olivine.

4.2.4. General stratigraphy of the Tweespalk area

The depths in the stratigraphic logs of this study are purely a reflection of the actual depth in metres in the borehole and are not a reflection of the true thickness of the stratigraphic units and features, as a result of the borehole beings drilled vertically. A detailed core log of TW1 can be found in Appendix 1.

4.2.4.1. The Footwall (Granite Gneiss)

The footwall rocks of the Tweespalk area are intersected at a depth of 696 m towards the base of the TW1 core, with a sharp contact between the Archaean granite gneiss basement and overlying MZ gabbronorite rocks (*Figure 4.3. A and B*). The basement Archaean granite gneiss in this region is widespread and comprises of a wide spectrum of granites and gneisses that vary in composition and

type (Robb *et al*., 2006). The regional Archaean basement consists of tonalitic gneisses (Hout River gneisses) and heterogenous potassic granites (Utrecht granite) that show variable textures from fine-grained to pegmatoidal, and colours ranging between milky white and pinkish red (Cawthorn *et al*., 1985; Robb *et al*., 2006). The granite gneiss at Tweespalk predominantly comprises quartz and altered feldspars. One sample (TW1-40) of the footwall rock was taken from the TW1 core for thin sectioning and geochemical analysis.

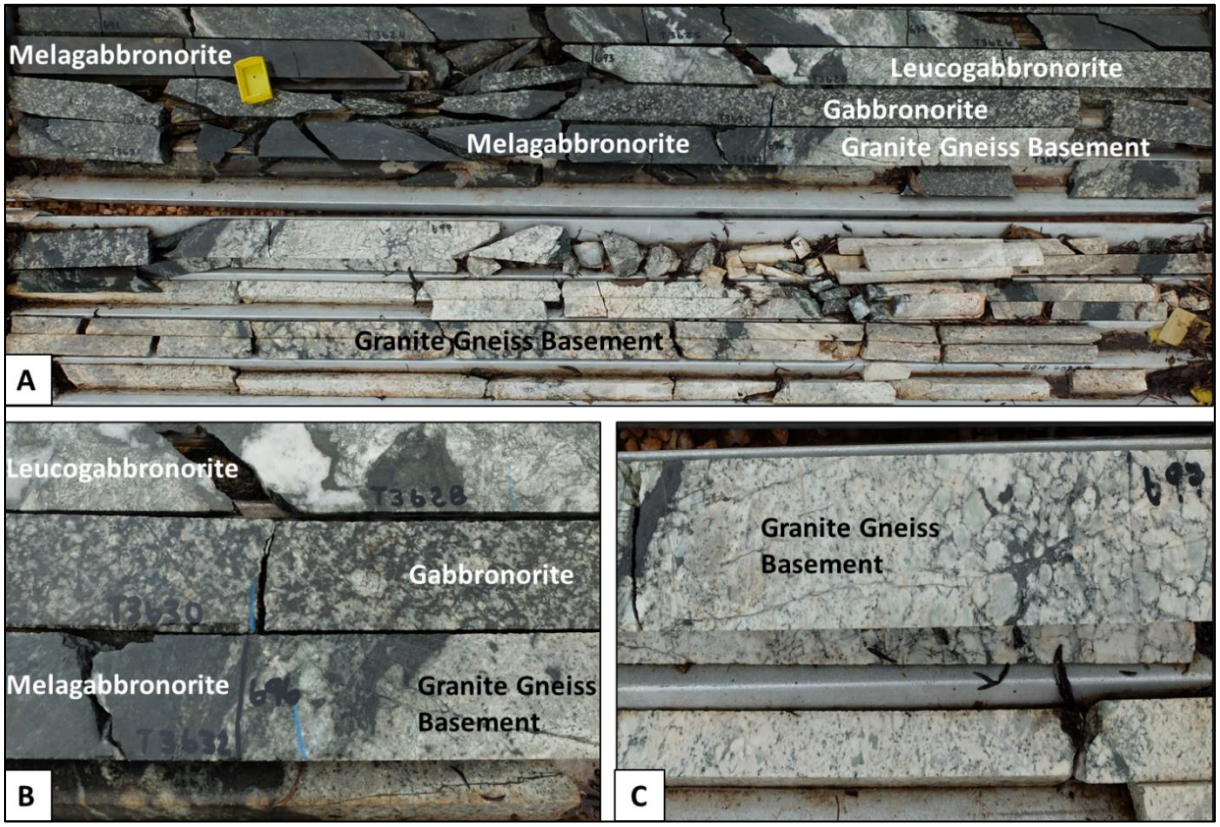

Figure 4.3. *Photos of the Tweespalk core TW1 showing* ***A)*** *Main Zone Gabbronorites overlying the Granite Gneiss Basement.* ***B)*** *A sharp contact between Melagabbronorite and the Granite Gneiss Basement.* ***C)*** *The leucocratic Granite Gneiss Basement rock.*

4.2.4.2. Main Zone

Overlying the footwall granite gneiss in the Tweespalk borehole are rock types that typically constitute MZ stratigraphy in the northern limb. The MZ at Tweespalk is composed of homogenous gabbronorites, olivine-bearing gabbronorites, pyroxenites, anorthosites and norites with minor and more atypical feldspathic harzburgite and feldspathic pyroxenite units (*Figure 4.4.*). The anorthosite at 644.50 m has either been tectonised or represents a plagioclase-rich vein.

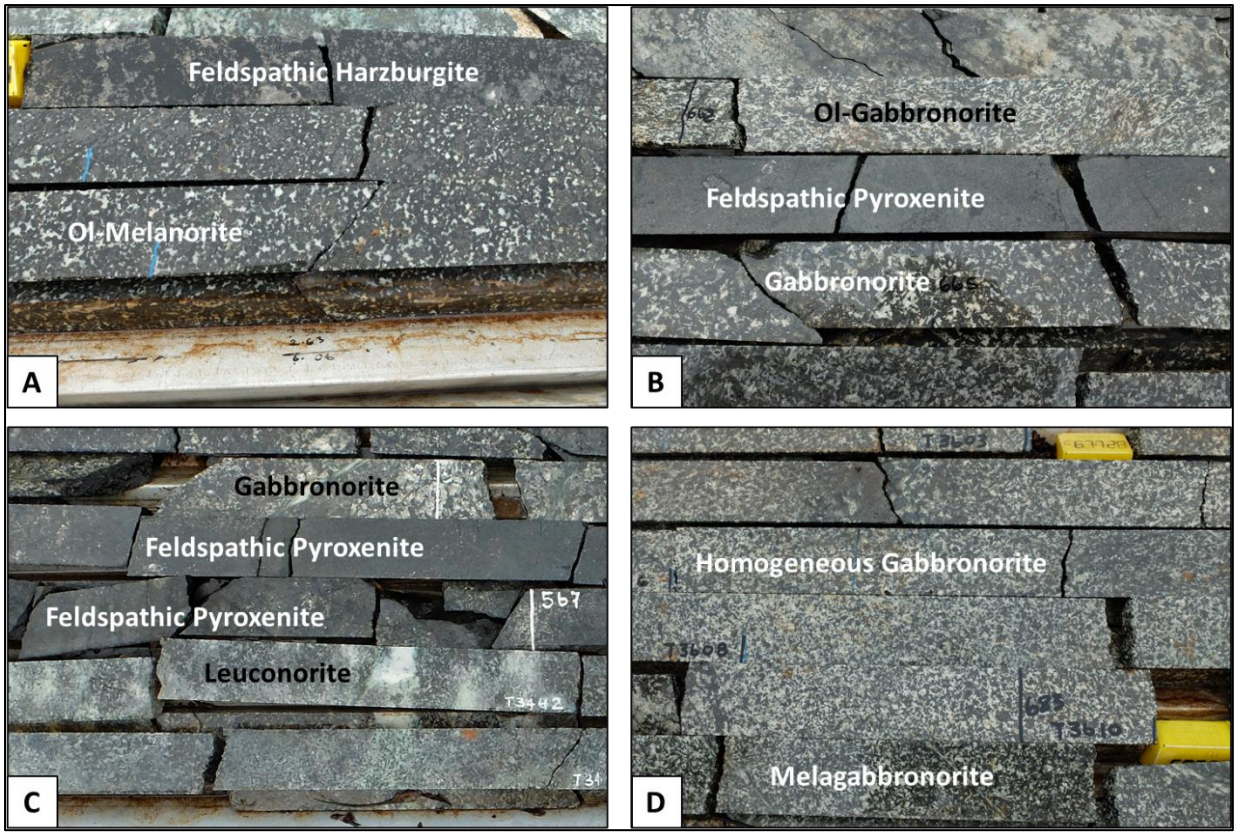

Figure 4.4. *Main Zone rock types observed in the Tweespalk core of TW1.* ***A)*** *A fine-grained Feldspathic Harzburgite that transitions into Olivine-bearing Melanorite* ***B)*** *A section of Olivine-bearing Gabbronorite, Feldspathic Pyroxenite and Gabbronorite* ***C)*** *A range of MZ rock types from Gabbronorite, to Feldspathic Pyroxenite, to a patchy textured Leuconorite.* ***D)*** *A homogeneous Gabbronorite towards Melanorite.*

As is the case generally throughout the northern limb, the MZ at Tweespalk lacks a distinctive pyroxenite marker that is prominent and characteristic of the MZ in the eastern and western limbs. The extensive and well-known troctolite unit which typically lies above the Platreef and serves as a reliable regional stratigraphic marker for the centre of MZ in the northern limb is absent from the TW1 borehole. This absence of any troctolite within the TW1 core suggests that MZ rocks that are present are representative of the upper portions of typical MZ stratigraphy in the northern limb.

4.2.4.3. Upper Zone

The northern limb Upper Zone rocks overlie this thin MZ succession, with the UZ in the Tweespalk core predominantly comprising of gabbros, magnetite gabbros, gabbronorites, individual magnetitite layers or stringers, and anorthosites (*Figure 4.5.*). In comparison with the UZ stratigraphies of the northern limb and the rest of the Bushveld Complex, the UZ at Tweespalk is a generally plagioclase-rich zone throughout as is evident in the abundance of anorthosite units, typically more leucocratic gabbroic units, scattered granitic veining and some pegmatoids. The zone also presents a number of olivine-rich intervals along with rare pyroxenite units.

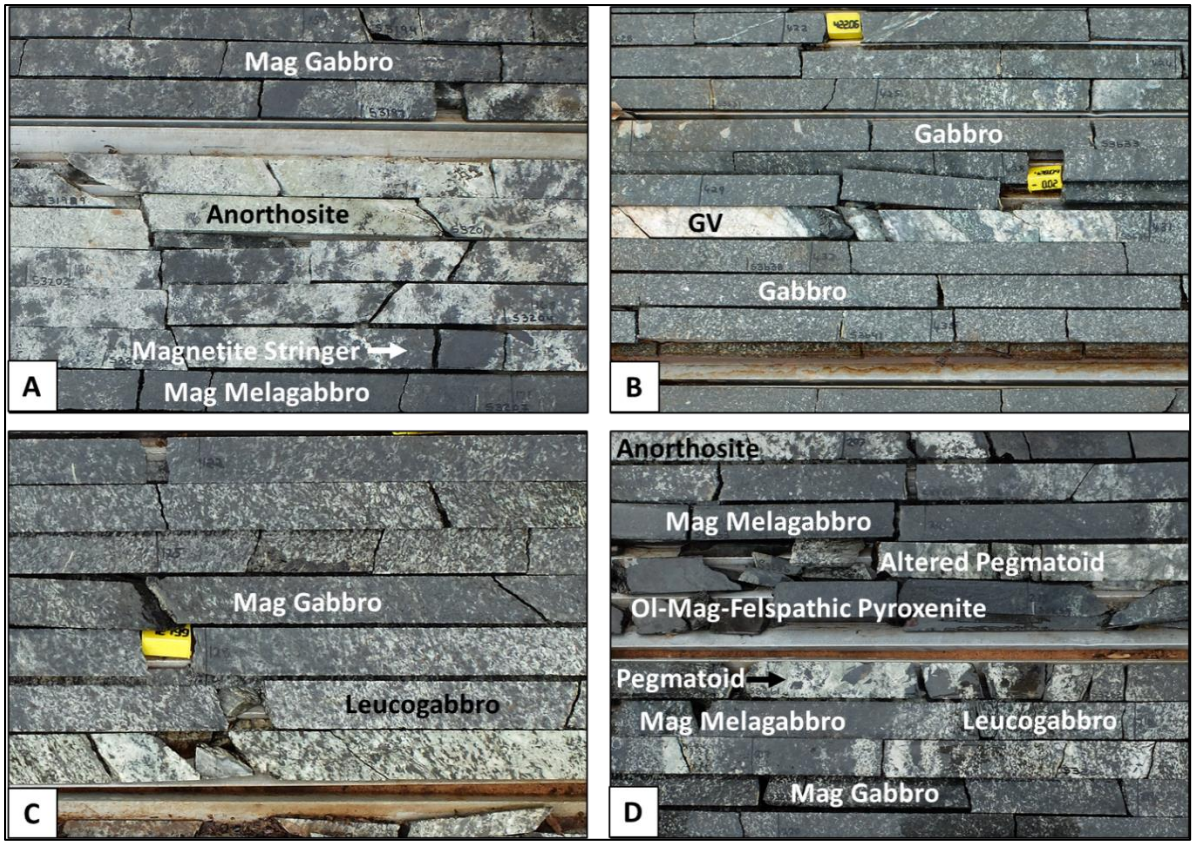

Figure 4.5. *Upper Zone rock types observed in the Tweespalk core of TW1.* ***A)*** *Magnetite Gabbro and Anorthosite with magnetite patches or oikocrysts.* ***B)*** *Normal Gabbro with the presence of Granitic Veining.* ***C)*** *Magnetite Gabbro towards magnetite-bearing Leucogabbro.* ***D)*** *A range of UZ rock types including Anorthosite, Magnetite Gabbro, Olivine- and Magnetite-bearing Feldspathic Pyroxenite, as well as a pegmatoid and altered pegmatoid.*

A prominent and diagnostic feature of the UZ in the northern limb is the presence of cumulus magnetite. This appearance of cumulus magnetite in the Tweespalk core marks the boundary between the UZ and MZ. However, small proportions of magnetite have often been seen in MZ units within various northern limb stratigraphies, which makes the placement of this stratigraphic boundary difficult and generally less easy to define.

Magnetite is abundant throughout various units of the Tweespalk stratigraphy from the first appearance of cumulus magnetite at a depth of 596.3 m through to a depth of 28 m where the magmatic stratigraphy at Tweespalk ceases. A sequence of gabbronorites and norites that extends from 596.3 m to 456.1 m represents the first portion of magnetite-bearing units in the stratigraphy. An ~203.4 m (456.1 m to 252.7 m) sequence of homogeneous gabbros and grantic veining then continues, with this sequence containing significantly lower proportions of cumulus magnetite that typically form as sporadically dispersed magnetite patches within various units. The upper portion of the Tweespalk stratigraphy from a depth of 252.7 m through to 28 m contains significant volumes of magnetite predominantly within gabbros (10% to 25% in volume), as individual 2-3 cm layers and stringers, as well as within anorthosites to a lesser extent.

The appearance of olivine is first observed within a gabbronorite unit at a depth of 663 m, from there the sequence of feldspathic harzburgites and gabbronorites display variable olivine contents until a depth of 541.2 m. The olivine content from this depth upwards through the stratigraphy remains extremely low, until its noted reappearance within a package of pyroxenite, feldspathic pyroxenite and magnetite gabbro between 214 m and 210.3 m. The olivine present within this package higher up in the stratigraphy is not fresh and has been serpentinised.

4.2.4.4. Sedimentary Cover

The magmatic stratigraphy at the Tweespalk property is covered by a thin succession of sediments and weathered Bushveld material which lies at the top of the TW1 core. This cover is comprised of Quaternary Karoo Supergroup sediments in the form of unconsolidated alluvium and weathered sedimentary units, as well as a small portion of highly weathered gabbro (*Figure 4.6.*). This succession is generally very thin, only extending from a depth of 28 m to the surface in the TW1 core and a mere 7 m in TW8 core. A notable difference to the typical succession observed throughout most of the northern limb, is the lack of Bushveld Granite Suite and granophyre volcanic units that are usually present above the Bushveld mafic/ultramafic succession (SACS, 1980; Eales and Cawthorn, 1996; Kinnaird *et al*., 2002; McCreesh, 2016).



Figure 4.6. *Unconsolidated alluvium and weathered sedimentary cover, as well as highly weathered gabbro overlying Magnetite Gabbro of the Upper Zone in core TW1.*

4.3. Local Geology

The geology at Tweespalk when compared with the rest of the Bushveld Complex and northern limb specifically, shows significant similarities. While these mafic and ultramafic rocks observed within the TW1 core can be broadly correlated with the Upper and Main Zones of the northern limb and are representative of a typical upper Bushveld stratigraphy, there are some notable differences and unique features. A definitive subdivision of the two zones is difficult to confirm having only studied

the core of a single borehole from the area, with further petrographic and geochemical analysis required to fully understand the relationships and features present.

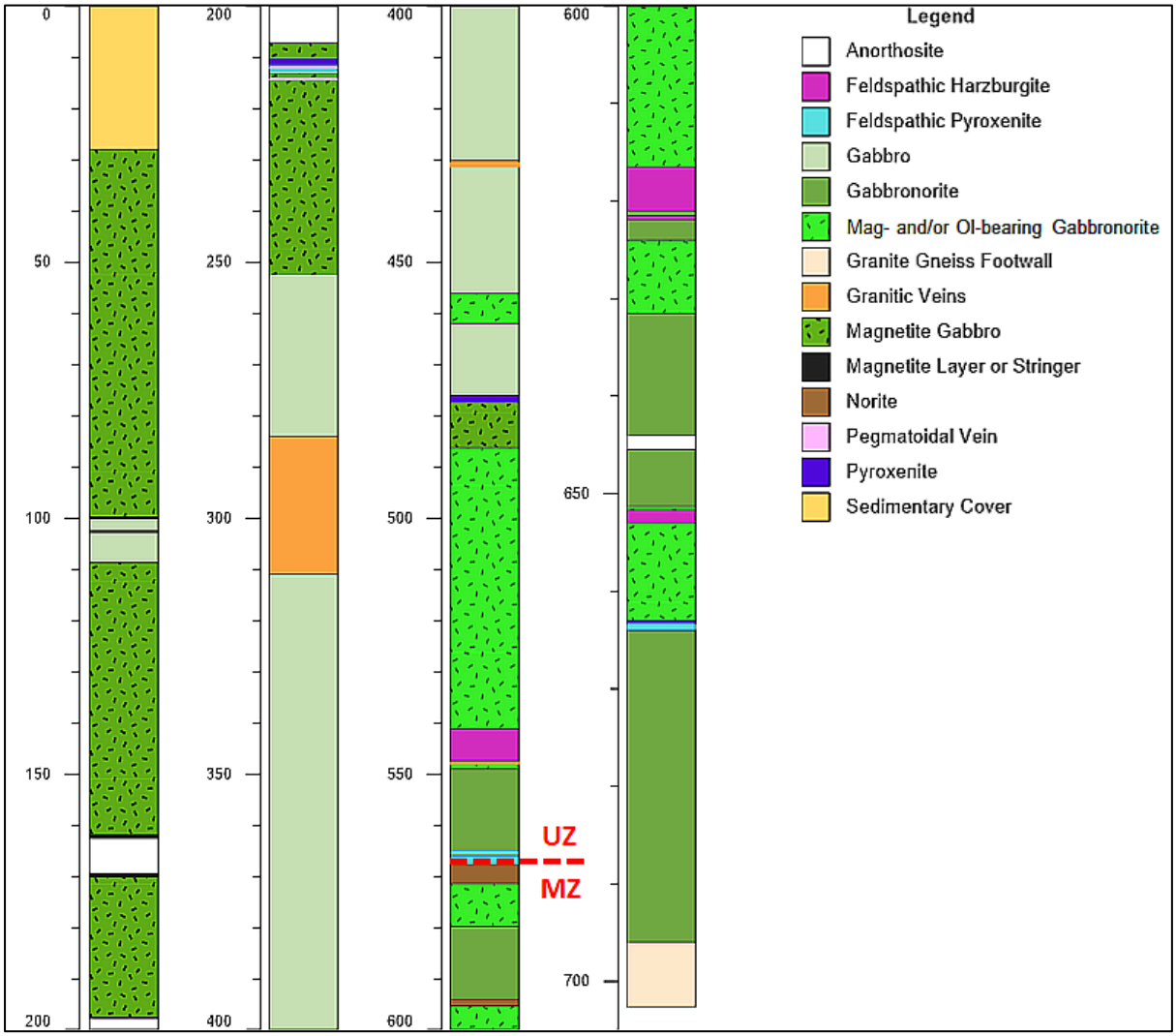

Figure 4.7. *Full stratigraphic log of borehole TW1 from Tweespalk, showing the different lithologies observed at various depths.*

Gabbronorites, norites and feldspathic harzburgites are the prominent rock types observed towards the base of the Tweespalk stratigraphy. The majority of the MZ stratigraphy at Tweespalk however, comprises medium- to coarse-grained gabbronorites that generally become less homogeneous with decreasing depth and contain variable olivine contents. Gabbronorites within the Main Zone of the Bushveld Complex are typically devoid of any olivine, with olivine usually only present within the Upper Zone (UZ_b and UZ_c, and not within UZ_z which lies directly above the Main Zone), in parts of the Lower Critical Zone and in the Lower Zone. Therefore, the presence of olivine within the gabbronorites situated towards the base of the Tweespalk RLS stratigraphy is unique with respect to the rest of the Bushveld Complex, and is an important factor to note within the context of this study.

The stratigraphy of the MZ at Tweespalk is relatively thin when compared to the thick portions of MZ observed in boreholes further south in northern limb. Although present, the limited ~128.2 m thick package of MZ rocks at Tweespalk makes it difficult to identify any notable features that typically characterize the Bushveld MZ. For example, the absence of any troctolite unit or marker – which is normally indicative of a more central section of MZ in the northern limb – suggests that only small portion of upper MZ stratigraphy is present at Tweespalk.

The definitive placement of the of the UZ-MZ boundary proved to be a challenge, although a relatively accurate estimate of this boundary can be inferred based on observations made in the core, together with magnetic susceptibility survey data of McCreesh (2016). McCreesh (2016) noted that the UZ-MZ boundary produced by increased magnetic susceptibility readings from the Waterberg exploration area, was usually around 100 m below the first significant appearance of magnetite. The first significant volume of cumulus magnetite in TW1 is observed at 541.2 m, with a few units below this containing magnetite but in very low proportions. At a depth of 566.1 m, a succession dominated by norites and gabbronorites ends, with these units characterising typical MZ rocks (Cawthorn *et al*., 2006). Therefore, the placement of the UZ-MZ boundary in the Tweespalk area at end of the last norite (566.1 m) which lies ~24.9 m below the first significant volume of cumulus magnetite seems the most appropriate.

The Upper Zone at Tweespalk makes up the thickest portion of the TW1 magmatic stratigraphy and is characterised by its high proportion of cumulus magnetite throughout the gabbro, anorthosite and minor pyroxenite units. Magnetite-bearing units observed in the core extend from a magnetite-bearing melagabbronorite at a depth of 596.3 m through to magnetite-rich gabbros with interlayered magnetite-bearing anorthosites, magnetite layers and stringers at the top of the succession. The magnetite content throughout the TW1 profile generally increases with decreasing depth. Also present in the Upper Zone stratigraphy are late-stage granitic and pegmatoidal veins that crosscut the mafic stratigraphy. Olivine first appears within the Tweespalk stratigraphy at a depth of 663 m, where it is found to be most abundant within a sequence of feldspathic harzburgites, feldspathic pyroxenites and gabbronorites until a depth of 541.2 m. This package of olivine-bearing units represents the first of the UZ rocks and a transition from the underlying MZ rocks. Olivine-bearing units are not particularly common throughout UZ stratigraphy at Tweespalk, and occurs towards the UZ-MZ transition as well as within a thin portion of pyroxenites and a magnetite gabbro between 210.3 m and 214 m.

The specific subdivision of the Upper Zone into subzones A, B and C according to Cawthorn *et al*. (2006) is difficult to accurately define, however the general succession of UZ can be broadly correlated with the mineralogical evolution and sequence seen elsewhere in the Bushveld (*Table 2.1.*). The first

appearance of cumulus magnetite within gabbronorites at a depth of 596.3 m marks the start of Subzone A at the base of the UZ. This zone extends until the appearance of Fe-rich olivine in gabbros and gabbronorites that are also typically magnetite-bearing, this suggests that Subzone B begins at a depth of 214 m. However, this Fe-rich olivine package reaches only ~4 m in thickness with magnetite gabbros and anorthosites without olivine continuing until the top of the magmatic stratigraphy. The lack of apatite in the UZ rocks above Subzone's A and B indicates that Subzone C may be absent from the stratigraphy, possibly a result of post-emplacement erosion.

The thin succession of unconsolidated alluvium and weathered sedimentary units of the Karoo Supergroup and highly weathered portions of mafic Bushveld rocks mark the top of the TW1 stratigraphy (*Figure 4.7.*). This is the first prominent difference observed in the magmatic succession at Tweespalk, with the area lacking the typical hanging wall comprising of granitic or volcanic units common in the southern and central sectors of the northern limb and elsewhere in the Bushveld (SACS, 1980; Eales and Cawthorn, 1996; Kinnaird *et al.*, 2002; McCreesh, 2016). The relationship between the Upper Zone Bushveld rocks and overlying sedimentary succession suggests that the Bushveld magmas may have intruded into an unknown succession of rocks before erosion and Karoo sediment deposition. The cover succession may represent a volcanoclastic unit.

The RLS stratigraphy at Tweespalk has some unique differences to that of stratigraphy in the rest of the northern limb, but in general the overall differences are very slight. The most apparent difference is in the limited thickness of a magmatic succession at Tweespalk when compared to the average thickness of the Bushveld stratigraphy south of the farm. North of the Tweespalk, the magmatic succession thicknesses are relatively similar. Other specific features and observations in this chapter will be studied further in *Chapters 5* and *6* to follow.

Chapter Five

Petrography

5.1. Introduction

The thin sections and core samples analysed in this section were selected from the length of the TW1 borehole core. The detailed petrographic studies carried out on the thin sections predominantly made used use of transmitted light, with the majority of minerals being transparent, however reflected light was used for the confirmation and identification of opaque minerals such as magnetite and the minor proportion of sulphides observed. Petrographical descriptions made in this study are based on the internationally accepted classification schemes that are defined by the modal percentages of minerals as well as the cumulus and intercumulus phases present. The thin sections serve a number of purposes in this study, namely: the confirmation of rock types identified during core logging, the confirmation of the appearance and/or disappearance of indicator minerals used for stratigraphic correlation with the rest of the northern limb stratigraphy as well as for specific stratigraphic markers, the identification of unknown or unclear features seen in the core samples, and for the description of alteration and textural features.

5.2. Methodology and Analytical Techniques

5.2.1. Sample Selection

The selection of the forty samples used in this study were obtained from the borehole TW1, drilled by Platinum Group Metals (PTM) on the Tweespalk farm. Relevant samples of each lithology were taken and specific sampling of rock types hosting visible sulphide mineralisation was carried out. Mineralisation has been observed within the gabbronorites of borehole TW1 and the early assay results from PTM showed the borehole to contain relatively significant grades of PGE mineralisation. However, this mineralisation is largely absent in any of the other boreholes drilled, with the assay results indicating very little to no PGE grades.

5.2.2. Sample preparation for polished thin sections

The polished section preparation process began with the selection of the forty specific drill core samples from the length of the TW1 borehole at the PTM Marken core yard in Mokopane, Limpopo. The thin sections were prepared as polished thin sections for optical microscopy. The forty core samples labelled TW1-1 through to TW1-40 were slabbed into small, flat sections of rock (approximately 30 mm by 50 mm) using the large cut-off diamond-tipped rock saw in the University

of the Witwatersrand Geosciences thin section laboratory. The slabbed samples were then coarsely ground using an automatic grinder and a silicon carbide grit powder with water. Thereafter, the samples were mounted on glass and cut down further by a thin sectioning machine to 30 microns in thickness and to the standard size specifications of 27 x 46 mm and finally polished. All of this preparation was done by the laboratory technicians and supervised by the head laboratory technician.

5.2.3. Petrography

The petrography for the study was carried out using the *Olympus BX41* microscope in the University of the Witwatersrand Geology Department ore microscopy room. Attached to the microscope is the Olympus SC50 which was used to take photomicrographs that were then later processed and enhanced using the *Olympus Stream Basic* software.

5.3. Petrologic Features

5.3.1. Gabbro

Gabbro was sampled from depths of 339.7 m, 389.9 m, and 468 m and is represented by samples TW1-17, -18 and -19 respectively. These gabbro samples are typically medium- to coarse-grained and have a predominant equigranular to subophitic texture. In terms of their compositions, the gabbros comprise plagioclase, clinopyroxene, orthopyroxene, and minor biotite as well as rare grains of magnetite. Samples TW1-17 and TW1-18 have modal plagioclase abundances of between 40% and 50%, 20-30% clinopyroxene, orthopyroxene ranging between 15% and 20 % and less than ≤1% magnetite (*Figure 5.1.*). The clinopyroxene grains have an average size of between 0.5 mm and 1 mm, while the orthopyroxene grains are typically larger and average 2 mm in size with a few individual grains reaching up to 4 mm. A number of the orthopyroxene grains contains minor inclusions of plagioclase and clinopyroxene. The volumes of magnetite in these samples are not sufficient enough for them to be classified as magnetite gabbro.

Sample TW1-19 is coarse-grained, significantly more leucocratic and contains a higher proportion of plagioclase which makes up approximately 70% of the modal abundance. This classifies the gabbro as a leucogabbro, with the sample displaying an irregular texture in the form of patches or blotches of pyroxenes and magnetite in the plagioclase-dominated cumulus rock.

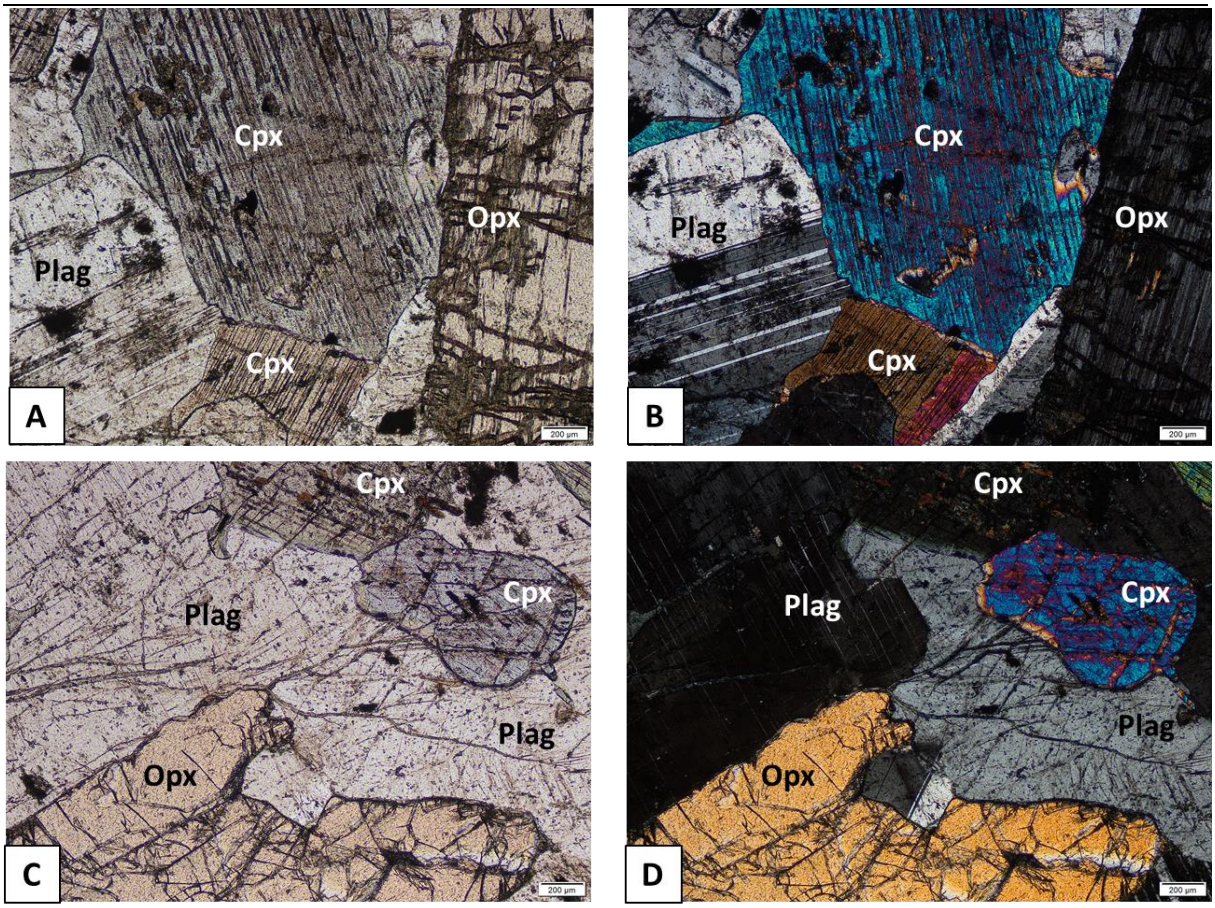

Figure 5.1. *The photomicrographs **A)** and **B)** display a medium-grained gabbro from TW1-17 (339.8 m), showing two large grains of clinopyroxene and orthopyroxene surrounded by plagioclase grains and smaller clinopyroxene grains (PPL and XPL). Photomicrographs **C)** and **D)** show a slightly more leucocratic gabbro of TW1-18 (390 m), showing coarse grains of orthopyroxene and plagioclase with medium-grained clinopyroxene grains (PPL and XPL).*

5.3.2. Magnetite Gabbro

Magnetite-rich gabbro units are present in the TW1 core samples from a depth of 252.7 m to a depth of 28 m at the top of the magmatic stratigraphy. These magnetite-bearing gabbros which make up a large portion of the sampled core are generally medium- to coarse-grained with variable but high proportions of magnetite throughout (*Figure 5.2.*). While these samples are very similar to the normal gabbro samples mentioned above in terms of minerals present, the significant proportions of magnetite markedly affect the modal abundances seen in the gabbros. Between the 12 magnetite gabbro samples the proportions of magnetite range from 10% to a maximum of 40%, whilst the relative proportions of plagioclase, clinopyroxene and orthopyroxene remain similar to the normal gabbros but with significantly lower contents overall. The modal abundances of plagioclase throughout the magnetite gabbros are between 30% and 40%, however some samples such as TW1-6, TW1-9 and TW1-16 are plagioclase-rich (proportions of up to 60%) and contain predominantly clinopyroxene (20% to 30%) as the major pyroxene mineral with low proportions of orthopyroxene (10% to 20%). The magnetite gabbros generally display an inequigranular texture with the majority of

mineral grains displaying a subhedral to anhedral shape. Sporadic sulphide specks or blebs are observed in association with magnetite throughout the samples, however their volumes are very low.

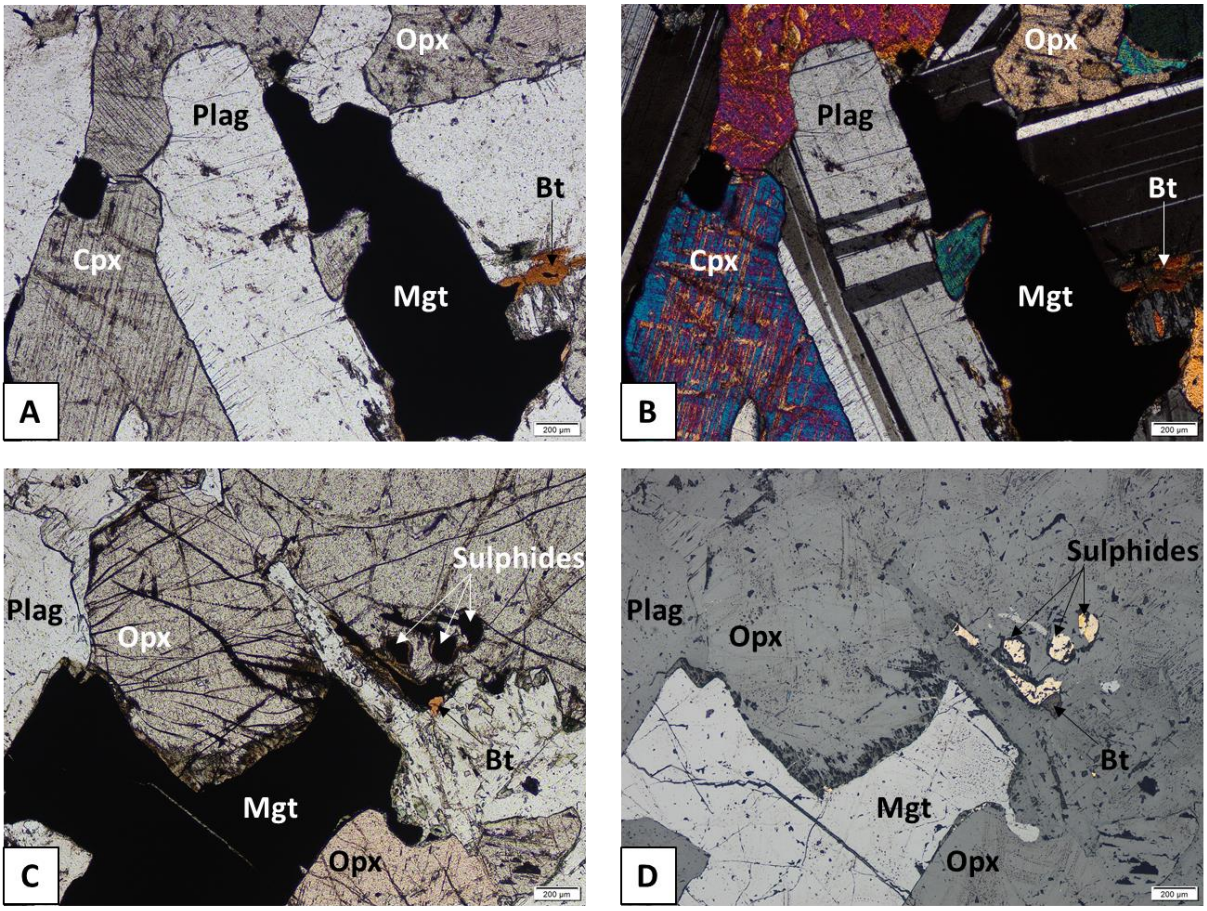

Figure 5.2. *The photomicrographs **A)** and **B)** shows plagioclase, clinopyroxene and orthopyroxene grains with intercumulus magnetite and minor biotite in a typical magnetite gabbro sample from TW1-1 (30.2 m) (PPL and XPL). Photomicrographs **C)** and **D)** also show the magnetite gabbro from TW1-1 (30.2 m), but the sample displays a small volume of disseminated sulphides with biotite and other accessory minerals forming around the sulphide grains as well as at the boundary between orthopyroxene and magnetite grains (PPL and reflected light).*

5.3.3. Gabbronorite

Gabbronorite is the dominant lithology of the Main Zone at Tweespalk and is also prevalent towards the lower extent of Upper Zone. Gabbronorite samples from the lower Upper Zone differ from the largely homogeneous Main Zone gabbronorites near the base of the TW1 borehole. Samples TW1-21, TW1-26 and TW1-29 that are situated at depths of 489.4 m, 584.1 m, and 614.4 m respectively, and are classified as leucogabbronorites as a result of their relatively high plagioclase contents. The samples are medium- to predominantly coarse-grained with the exception of TW1-26 which is very coarse-grained to pegmatoidal. The samples are composed of clinopyroxene, plagioclase, orthopyroxene as well as minor pigeonite and accessory biotite and chlorite (*Figure 5.3. A and B*). Once again clinopyroxene is the dominant pyroxene present within the leucogabbronorites ranging between 30% and 40% with grain sizes of 1-5 mm and as large as 8 mm in the pegmatoidal sample.

Plagioclase proportions in the leucogabbronorites vary between 60% and 70% with a slightly smaller average grain size of 0.5 mm to 1.5 mm. A few speckles of magnetite are observed in TW1-26 but it is otherwise absent.

Samples TW1-31 to TW1-38 that are situated towards the base of the Tweespalk magmatic stratigraphy are all generally equigranular medium-grained and homogeneous gabbronorites (*Figure 5.3. C and D*). These samples consist of an average mineralogy of: 50% to 60% plagioclase, 35% to 40% clinopyroxene, 5% to 10% orthopyroxene, <1% magnetite and scattered sulphides throughout. The plagioclase grains are generally euhedral in shape and range between 0.5 mm and 1.5 mm in size. Orthopyroxene grains typically form as anhedral and coarser-grained oikocrysts (1 mm to 3 mm) that host a number of inclusions of plagioclase, biotite and other accessory minerals. Clinopyroxene grains are far more prominent throughout the sections but also display a largely anhedral shape with an average grain size of 0.5 mm to 1 mm. Sample TW1-39 deviates from the rest of the gabbronorite samples in that it is fine-grained (0.1 mm to 0.5 mm) and its plagioclase content is considerably lower than the other normal gabbronorites (<15%), which makes it a melagabbronorite. Pyroxene is the most abundant mineral present in the sample, with well-rounded grains and the presence of a relatively increased volume of cumulus magnetite (*Figure 5.3. E and F*). Common throughout the portion of homogenous gabbronorites towards the base of the TW1 core, is the increase in volume of scattered sulphides. These volumes are still relatively low but are representative of a greater mineralised interval relative to the rest of the TW1 core.

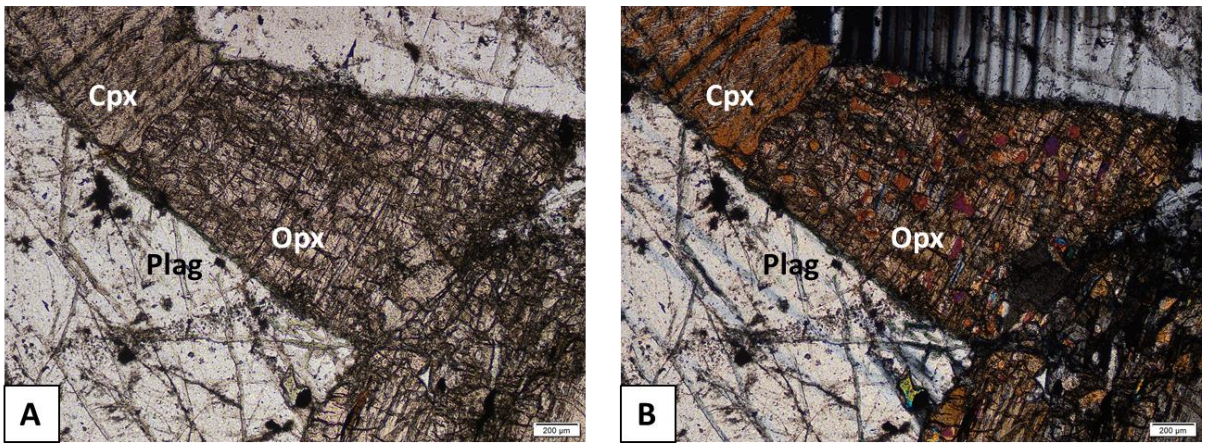

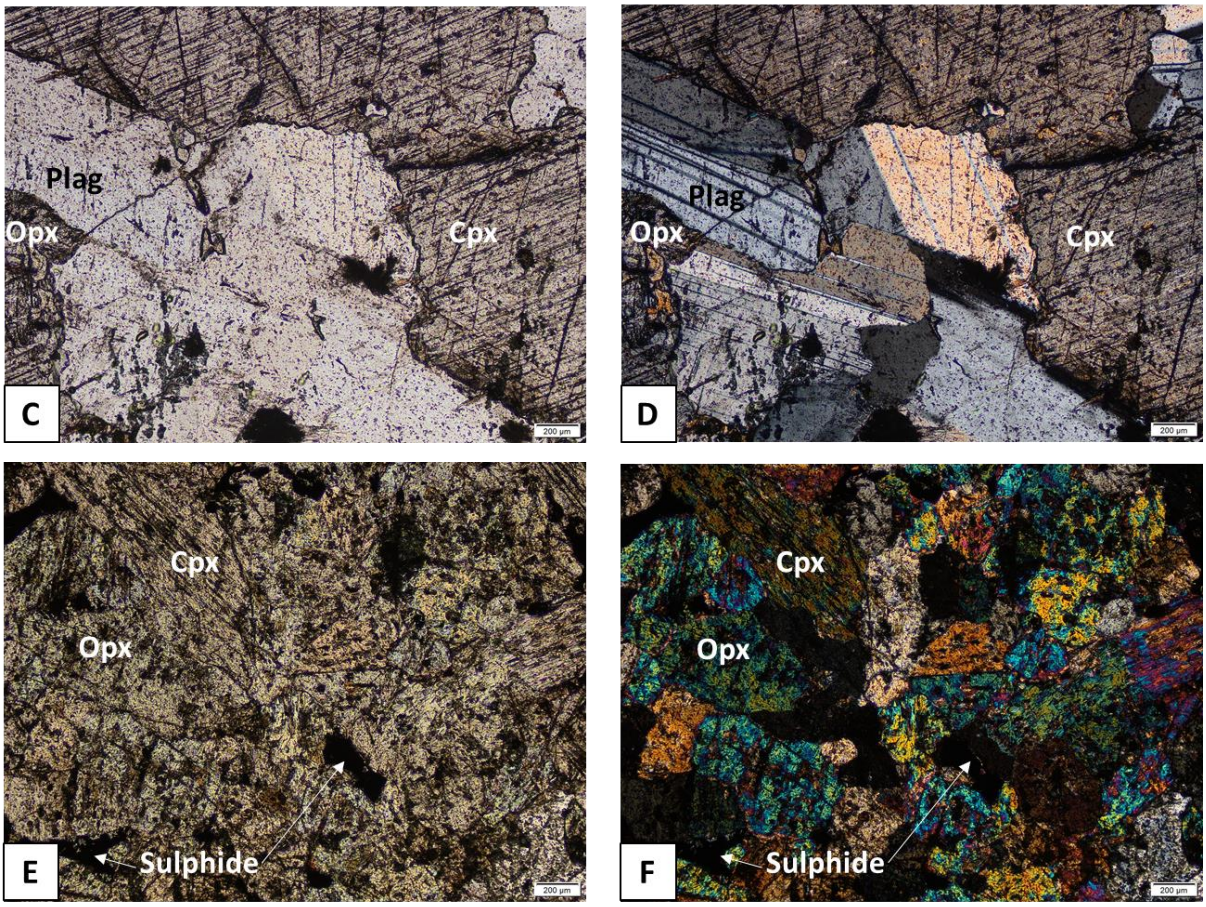

Figure 5 3. *Photomicrographs **A)** and **B)** of TW1-26 (584.3 m) exhibit a coarse-grained to pegmatoidal leucogabbronorite, with a large orthopyroxene grain that hosts inclusions of finer-grained orthopyroxene, surrounded by large grains of plagioclase (PPL and XPL). Photomicrographs **C)** and **D)** show a more typical gabbronorite sample of TW1-31 (627.6 m) that is generally more equigranular with large proportions of clinopyroxene and plagioclase with lesser orthopyroxene (PPL and XPL). Photomicrographs **E)** and **F)** are representative of the largely homogeneous gabbronorites observed towards the base of the succession, displaying a largely equigranular texture with limited plagioclase and speckles of sulphides throughout the TW1-39 (686.1 m) sample (PPL and XPL).*

5.3.4. Magnetite- and/or Olivine-bearing Gabbronorite

The gabbronorite samples that contain magnetite, olivine or a combination of the two are: TW1-25, TW1-27 and TW1-28. Sample TW1-25 is a magnetite-bearing leucogabbronorite, while sample TW1-27 is classified as both an olivine- and magnetite-bearing melagabbronorite (*Figure 5.4. A and B*), and TW1-28 is a homogeneous olivine-bearing gabbronorite (*Figure 5.4. A and B*). The medium-grained leucogabbronorite of TW1-25 has a modal mineralogy of 70% plagioclase, 20% clinopyroxene, 7% orthopyroxene and 3% magnetite. The melagabbronorite has a varied texture with some sections exhibiting fine-grained and interlocking orthopyroxenes, plagioclases and clinopyroxenes, while other areas are generally medium- to coarse-grained.

Despite TW1-27 being described as olivine- and magnetite-bearing in the core, the presence of both minerals observed within the thin section was very rare. Magnetite in TW1-27 accounts for less than

1% of the volume and is seen in the form of extremely fine grains, while olivine is largely non-existent throughout the section. As a result, this sample can neither be described as olivine- or magnetite-bearing upon closer petrographical analysis. A section of the TW1-27 sample shows a unique feature of a distinct replacement and alteration texture of the fine-grained and rounded orthopyroxene and clinopyroxene grains. TW1-28 is similar to TW1-25 in that it is dominated by plagioclase and clinopyroxene, and despite being fine-grained and homogeneous is predominantly leucocratic like the TW1-25 sample. The high proportion of plagioclase (~60% to 70%) changes the classification of this sample to a leucogabbronorite, but unlike TW1-25 the sample lacks any magnetite.

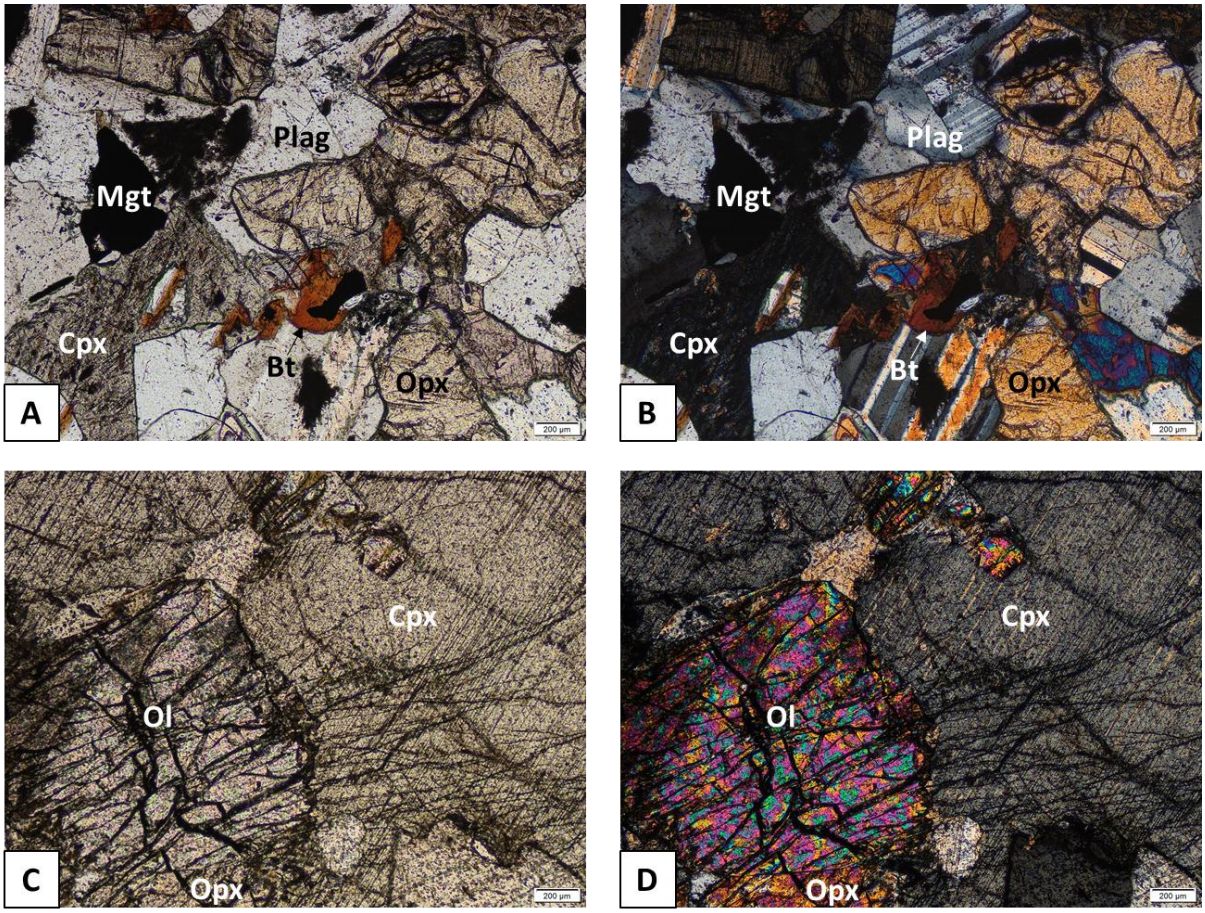

Figure 5.4. *Photomicrographs* ***A)*** *and* ***B)*** *show the melagabbronorite sample of TW1-27 (595.5 m) which contains small grains of cumulus magnetite amongst the plagioclase, orthopyroxene, clinopyroxene and biotite (PPL and XPL). Photomicrographs* ***C)*** *and* ***D)*** *are images of the olivine-bearing and homogeneous gabbronorite sample TW1-28 (603.3 m) (PPL and XPL).*

5.3.5. Anorthosite

Samples TW1-8 and TW1-11 within the Upper Zone sequence at Tweespalk classify as anorthosite. These samples are dominated by lath-shaped plagioclase (>90% modal percentage) with up to 8% intercumulus magnetite and minor abundances of biotite, orthopyroxene and chlorite (*Figure 5.5.*). The plagioclase grains are predominantly euhedral in shape and display polysynthetic twinning. The

average grain size of the white to dirty-white plagioclase grains is 4 mm, while the orthopyroxene grains average 1 mm in diameter. The intercumulus magnetite grains are completely anhedral in shape and vary considerably in size as an intercumulate between the plagioclase grains. The anorthosite samples are largely homogeneous and lack any specific mottled or patchy texture. Chlorite and biotite grains are generally situated at the grain boundaries of plagioclase and magnetite.

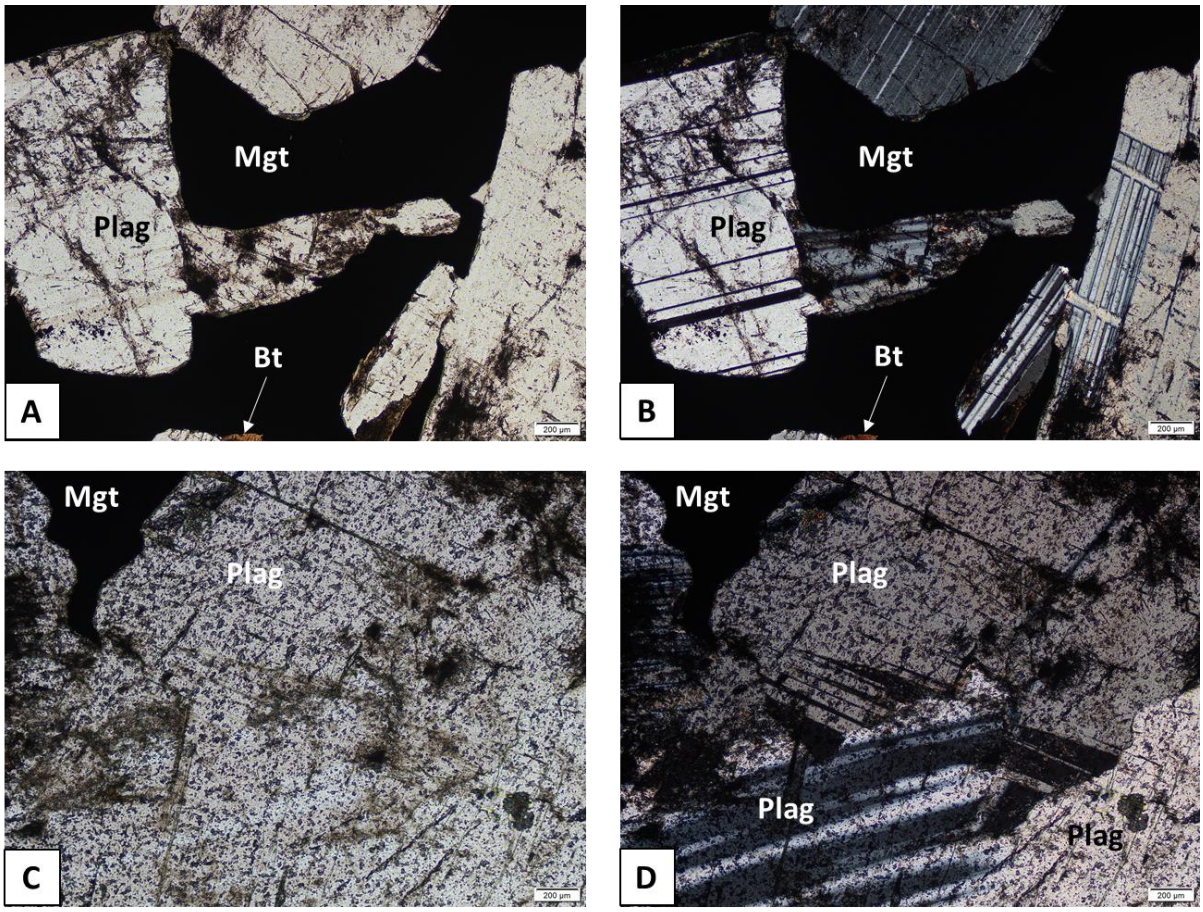

Figure 5.5. *Photomicrographs **A)** and **B)** show a medium-grained magnetite-rich anorthosite of TW1-8 (166.5 m) with largely euhedral cumulus plagioclase grains and anhedral intercumulus magnetite grains with minor biotite at the grain boundaries (PPL and XPL). Photomicrographs **C)** and **D)** show a more typical anorthosite of TW1-11 (206.6 m), largely dominated by medium-grained plagioclase with some intercumulus magnetite (PPL and XPL).*

5.3.6. Feldspathic Harzburgite

Only one feldspathic harzburgite was sampled from the TW1 core, this being TW1-22 from a depth of 544 m. This sample is medium-grained (0.5 mm to 1.5 mm), olivine-bearing and comprises predominantly cumulus orthopyroxene (~50%) and olivine (~20%), lesser amounts of post-cumulus clinopyroxene (~10%) and intercumulus plagioclase (~20%), as well as small volumes of other accessory minerals (*Figure 5.6.*). Relative to the other olivine-bearing samples examined, this feldspathic harzburgite is olivine-rich and hosts a small fraction of sulphides that are very fine-grained and scattered throughout.

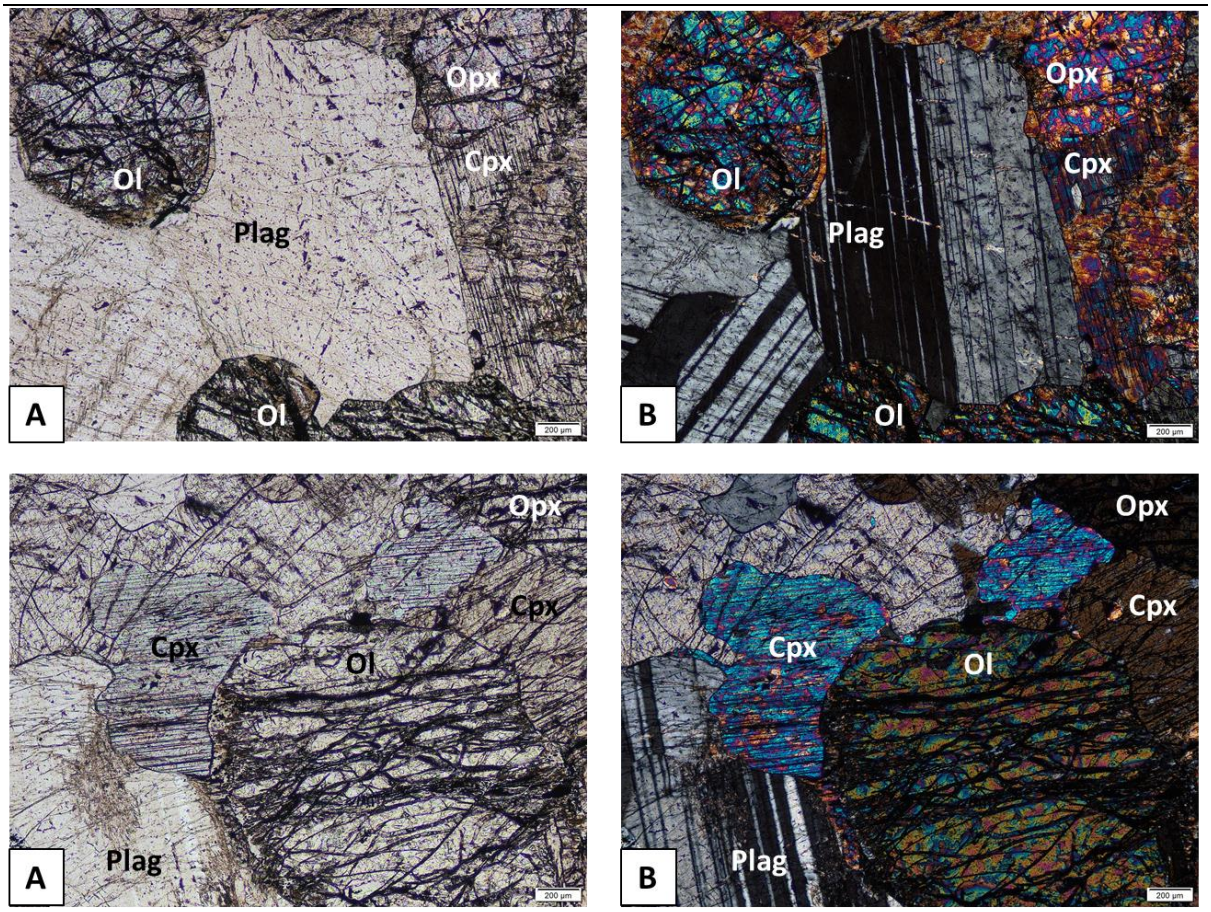

Figure 5.6. *Photomicrographs **A), B), C)** and **D)** show the olivine-bearing feldspathic harzburgite sample TW1-22 (544.2 m), which comprises largely of medium-grained orthopyroxene, olivine and plagioclase with lesser clinopyroxene (PPL and XPL).*

5.3.7. Pyroxenite/Feldspathic Pyroxenite

The pyroxene and feldspathic pyroxenite samples of TW1-12, -13, -20 and -23 exhibit the highest degree of variability and alteration amongst all of the classified lithologies, as such they are each described individually. Sample TW1-12 is classified as an olivine-bearing pyroxenite that has undergone alteration. The average mineralogy of the sample is 40-50% olivine, 30-40% plagioclase and ~5% magnetite. The coarse-grained and olivine-rich pyroxenite has been altered, where half of the olivine in the thin section occurs as fresh, light yellow to light pink olivine grains (averaging 1-2 mm in size), while the other half of the thin section comprises of altered, pale green olivine grains that host a substantial volume of magnetite (*Figure 5.7. A and B*). Plagioclase is very coarse-grained and has formed as 2-6 mm intercumulus grains. There are also relict olivine grains that have undergone significant alteration and produced iddingsite. This alteration is also highly evident in the serpentine and chlorite veining present within the thin sections, indicating the occurrence of fluid interaction.

An olivine- and magnetite-bearing feldspathic pyroxenite is observed in TW1-13 (*Figure 5.7. E and F*). The sample is once again highly altered but also extremely magnetite rich. The magnetite grains are

typically large and average between 2 mm and 6 mm in size, but small (<1 mm) grains are scattered throughout. Reaction rims of predominantly quartz surround the magnetite grain boundaries, with some of the grains enclosing small sulphide minerals. The generally coarse-grained (averaging 2-3 mm) olivine grains within the sample are highly altered and show serpentinite-dominated reaction rims with some chlorite, in some cases the cracks of the olivine grains have been infilled with magnetite. The average mineralogy of the sample is ~50% magnetite, ~40% olivine, ~5-10% clinopyroxene and <5% plagioclase. The majority of the section has been altered, but there is a small section that has been less affected.

Sample TW1-20 is classified as a pyroxenite that has been altered, although it is far more representative of the typical pyroxenite mineral proportions, despite having undergone alteration and brecciation. The sample exhibits clear zones of brecciation and the augite grains in particular show evidence of shearing along their cleavage. There is a small patch of intercumulus magnetite (0.5-1 mm) present in the section with small grains of biotite forming around them.

Sample TW1-23 was classified in the core logging as either a feldspathic pyroxenite or melanorite. The term feldspathic pyroxenite is used in nomenclature for the Bushveld to distinguish a pyroxene-rich rock with interstitial feldspar, from a norite, where both pyroxene and feldspar are cumulus. In TW1-23, the rock contains an abundance of both cumulus plagioclase and pyroxene, which indicates that it should be termed a norite (*Figure 5.7. C and D*). The section is dominated by plagioclase (~60%) which is fine- to medium-grained (0.5-1 mm) and lacking a euhedral shape seen in the other samples. It is also an olivine-bearing unit with a lower content of between 10% and 15%. These olivine grains also show slight alteration and host fine-grained magnetite within. Clinopyroxene accounts for approximately 15% of the sample volume, while orthopyroxene makes up the remaining 10%. Hornblende is present but in low proportions amongst the plagioclase, orthopyroxene and clinopyroxene.

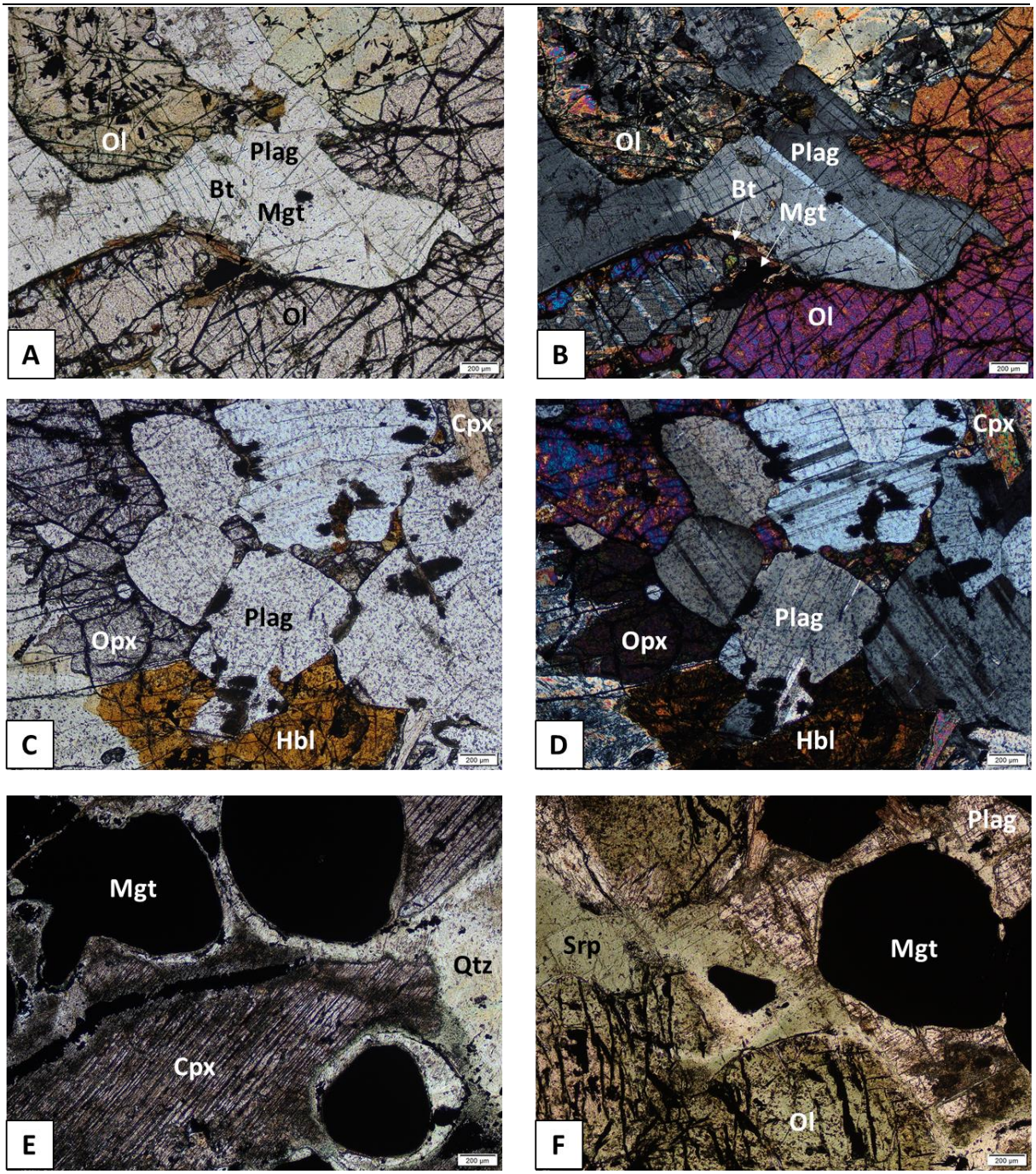

Figure 5.7. *Photomicrographs **A)** and **B)** show the coarse-grained and olivine-rich pyroxenite of TW1-12 (210.5 m) that has undergone moderate alteration (PPL and XPL). Photomicrographs **C)** and **D)** show sample TW1-23 (567.5 m) which is reclassified as a norite on the basis of both cumulus plagioclase and pyroxenes being present (PPL and XPL). Photomicrographs **E)** and **F)** show the highly altered feldspathic pyroxenite of TW1-13 (212.8 m) which shows quartz reaction rims around the rounded magnetite grains as well as altered olivine grains in association with chlorite (PPL and PPL).*

5.3.8. Norite

In *Chapter 4*, both of the samples TW1-24 and TW1-30 were classified as norites in the core logging. This initial classification is incorrect for both, as TW1-24 is an anorthosite based on its very high plagioclase content and TW1-30 is classified as a coarse-grained melagabbronorite, based on its high

content of clinopyroxene (similar volume to orthopyroxene). Based on these observations, no norite unit from TW1 was sampled after further petrographic analysis.

Sample TW1-30 comes from a section of core at a depth of 618.2 m that has been logged as feldspathic harzburgite and transitions towards melanorite. From petrographic study of the thin section, it appears that the sample was taken from the olivine-bearing melanorite member rather than the feldspathic harzburgite. This classification is made on the basis of the high proportion of clinopyroxene relative to orthopyroxene and the occurrence of plagioclase seen in the core and thin section. The norite has a similar texture to that of the gabbronorites aside from it being generally coarser-grained and having a more significant proportion of olivine (*Figure 5.8. A, B, C and D*). As mentioned, the sample is rather coarse-grained ranging from 2-5 mm with an inequigranular texture. In terms of the proportions of minerals in the rock, clinopyroxene makes up ~40%, while orthopyroxene accounts for ~30% and olivine makes up ~20%, with lesser volumes of chlorite, biotite and magnetite. The olivine grains often display reaction rims and the fractures within some of the olivine grains have been infilled with secondary magnetite.

Between the depths of 567.8 m and 571.4 m, the unit was logged as being magnetite-bearing leuconorite towards anorthosite with an overall mottled texture. Upon investigation of the TW1-24 thin section, the rock type should be classified as anorthosite as opposed to leucocratic norite based on plagioclase content. Further it cannot be described as being magnetite-bearing as suggested from the core logging, as it contains almost no magnetite (*Figure 5.8. E and F*). The plagioclase content of the sample is extremely high (>90%), however when compared to anorthosite samples of TW1-8 and TW1-11, the grain size is significantly smaller and is fine- to medium-grained. Another noticeable difference between the two types of anorthosites besides the lack of magnetite, is the presence of fine-grained intercumulus clinopyroxene grains (~8%) in TW1-24, which is not observed in the other anorthosite samples. A small (<1 mm) grantic vein is also present within the sample.

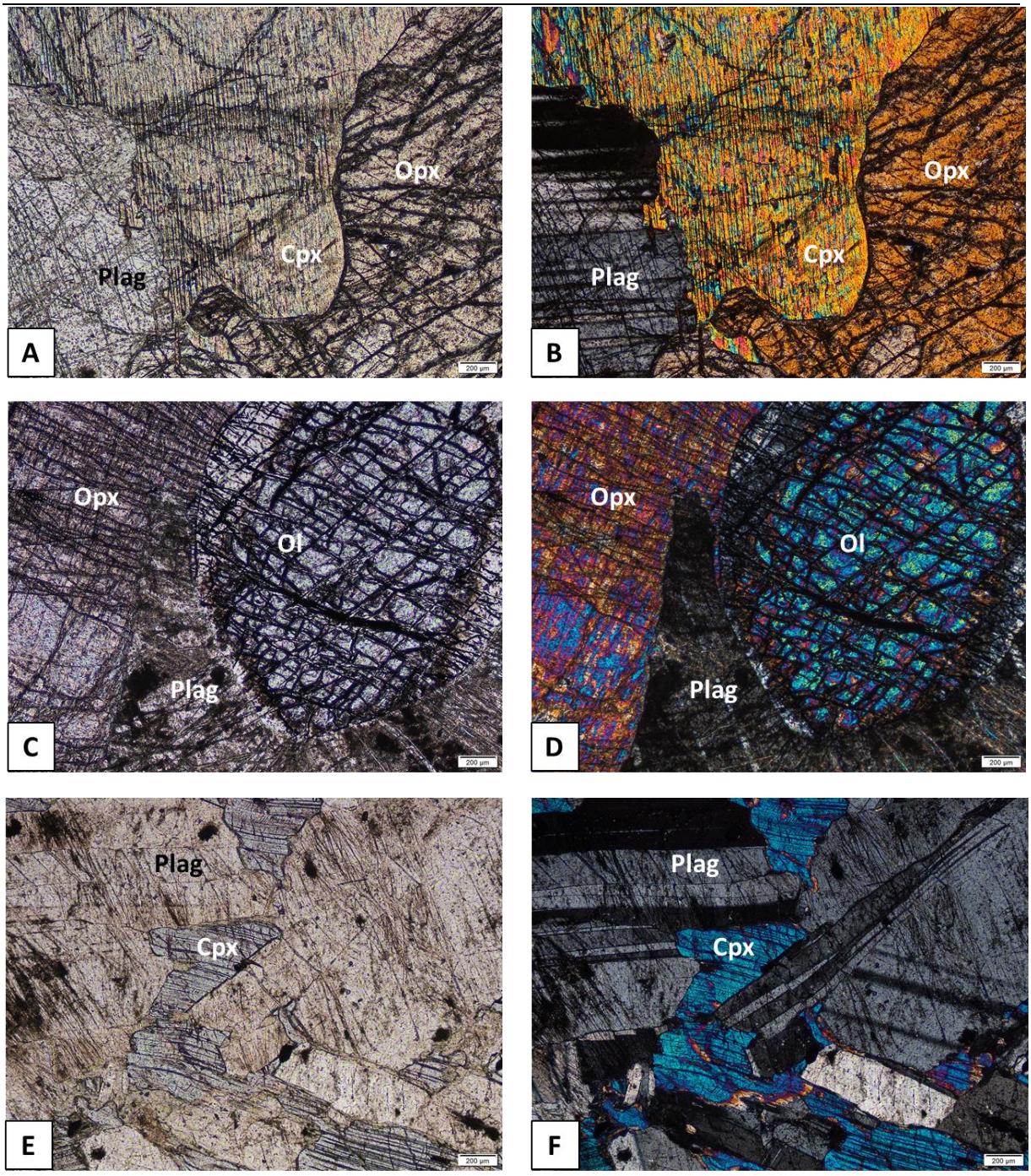

Figure 5.8. *Photomicrographs **A), B), C)** and **D)** are all images of sample TW1-30 (618.2 m) which is a melagabbronorite, generally containing a higher proportion of clinopyroxene to orthopyroxene, and olivine-bearing (PPL and XPL). **E)** and **F)** show sample TW1-24 (568.1 m) which contains high proportions of plagioclase and clinopyroxene, is reclassified as an anorthosite from a leuconorite.*

5.3.9. Granite Gneiss (Footwall)

The interlocking texture of fine- to medium-grained quartz and completely altered feldspars in the Archaean granite gneiss sample TW1-40 taken from a depth of 698.5 m is not part of the RLS and is therefore indicative of the end of the observed magmatic stratigraphy in the TW1 borehole (*Figure 5.9.*). The overall milky-white to grey granite gneiss is the footwall to the Tweespalk stratigraphy.

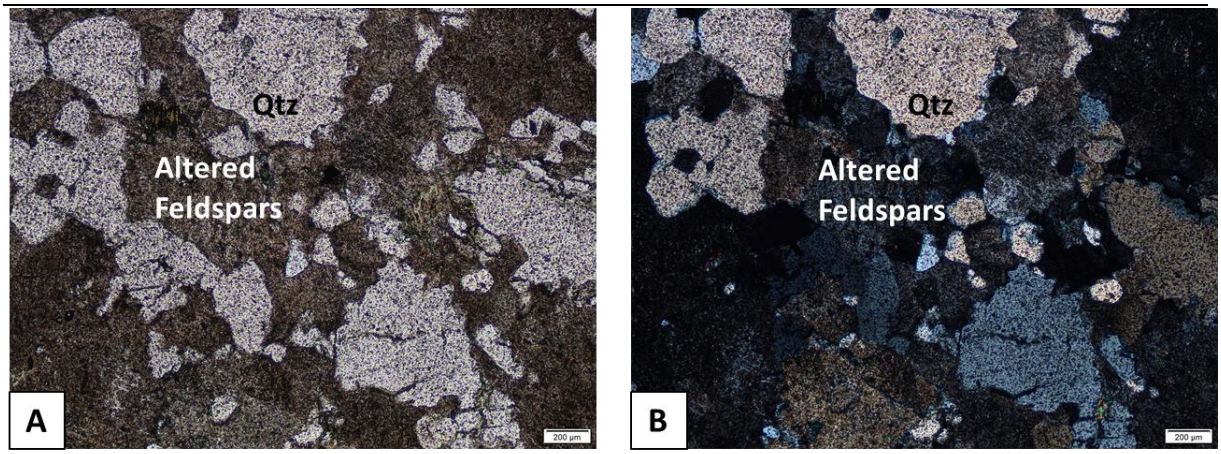

Figure 5.9. *Photomicrographs **A)** and **B)** show fine- to medium-grained quartz and altered feldspars in an interlocking texture of the granite gneiss sample TW1-40 (698.6 m) (PPL and XPL).*

The petrographic study of the TW1 samples helped to further improve the accuracy of the assigned nomenclature from core logging, noting a few disparities between the field names and the rock nomenclature from microscopy documented in this section. Samples TW1-24 and TW1-30, both classified as norites in the core where reclassified as an anorthosite and melagabbronorite respectively. The lack of any olivine grains and very limited magnetite content in TW1-27, requires the change to a normal gabbronorite that is not olivine- or magnetite-bearing. In terms of the overall proportions of the identified rock types within the Tweespalk stratigraphy, gabbro and magnetite-bearing gabbro make up bulk of the succession. Gabbronorite and magnetite- or olivine-bearing are the next most common rock type in the stratigraphy. Anorthosites, feldspathic harzburgites and the granitic veining share similar overall proportions at Tweespalk, with pyroxenites, feldspathic pyroxenites and norites making up the smallest proportions of rock types observed. The changes in the names of the TW1-24 and -30 samples from core logging-based norites to an anorthosite and melagabbronoite based on microscopic analysis, had no significant impact on the whole borehole log of the study. The whole rock geochemical study carried out in the following chapter, looks to provide further analysis of the sample geochemistry to get a better understanding the sample mineralogy as well as the geochemical profile of the Tweespalk stratigraphy.

Chapter Six

Whole Rock Geochemistry

6.1. Introduction

Whole rock geochemistry analyses were performed on the forty samples collected from borehole TW1 to further investigate the stratigraphy of the area outlined in *Chapter 4* and supported by petrographical analyses in *Chapter 5*. This chapter looks to highlight the variation of a multitude of geochemical features throughout the length of the borehole, investigating various compositional breaks, transitions, and trends of the lithologies within the stratigraphic succession. The whole rock geochemistry was also carried out in order to determine whether the stratigraphy at Tweespalk resulted from one or more pulses of magma and the effect of the Archaean granite gneiss footwall on the emplacement of the Bushveld magma.

6.2. Whole Rock Geochemistry

The whole rock geochemical analyses were carried out in order to provide further elemental data for the major and minor oxides as well as the trace element concentrations (*Table 6.1.*). The sample preparation and geochemical analyses of the forty samples elemental majors, minors and trace elements was undertaken at *Earth Laboratory* in the Bernard Price Building at the University of the Witwatersrand. Both of the major oxides and trace element compositions for whole rock geochemistry were analysed using an X-ray Fluorescence Spectrometry machine with the bulk major oxide compositions being determined using the fused disk method, while the concentration of a full suite trace elements was determined using a pressed pellet method.

Table 6.1. *A list of the TW1 samples with their respective depths and lithologies.*

Sample ID	Depth From (m)	Depth To (m)	Lithology
TW1-1	30.0	30.2	Magnetite-Gabbro
TW1-2	42.8	43.1	Magnetite-Gabbro
TW1-3	62.0	62.1	Magnetite-Gabbro
TW1-4	85.5	85.7	Magnetite-Gabbro
TW1-5	109.0	109.1	Magnetite-Gabbro
TW1-6	129.1	129.2	Magnetite-Leucogabbro
TW1-7	155.6	155.8	Magnetite-Gabbro
TW1-8	166.3	166.5	Anorthosite
TW1-9	170.3	170.5	Magnetite-Gabbro
TW1-10	176.9	177.1	Magnetite-Gabbro
TW1-11	206.5	206.6	Anorthosite
TW1-12	210.3	210.5	Olivine-bearing Pyroxenite
TW1-13	212.7	212.8	Olivine- and Magnetite-bearing Feldspathic Pyroxenite
TW1-14	213.3	213.4	Olivine-bearing Magnetite-Gabbro
TW1-15	221.8	221.9	Magnetite-Gabbro
TW1-16	250.7	250.8	Magnetite-Gabbro (with grantic veining and alteration)
TW1-17	339.7	339.8	Gabbro
TW1-18	389.9	390.0	Gabbro
TW1-19	468.0	468.1	Leucogabbro
TW1-20	476.7	476.8	Pyroxenite (altered)
TW1-21	498.4	498.6	Leucogabbronorite
TW1-22	544.0	544.2	Olivine-rich Feldspathic Harzburgite
TW1-23	567.4	567.5	Norite
TW1-24	568.0	568.1	Magnetite-bearing Anorthosite
TW1-25	576.8	577.0	Magnetite-bearing Gabbronorite
TW1-26	584.1	584.3	Leucogabbronorite
TW1-27	595.4	595.5	Melagabbronorite
TW1-28	603.1	603.3	Ol-bearing Gabbronorite
TW1-29	614.4	614.5	Leucogabbronorite
TW1-30	618.2	618.4	Melagabbronorite
TW1-31	627.5	627.6	Gabbronorite
TW1-32	636.9	637.0	Leucogabbronorite (Taxitic)
TW1-33	647.1	647.4	Gabbronorite
TW1-34	647.7	647.8	Gabbronorite
TW1-35	648.2	648.4	Gabbronorite
TW1-36	648.4	648.7	Gabbronorite
TW1-37	668.3	668.6	Gabbronorite
TW1-38	668.6	668.7	Leucogabbronorite
TW1-39	685.9	686.1	Melagabbronorite
TW1-40	698.5	698.6	Granite gneiss

6.2.1. Sample preparation for geochemical analysis

The process of sample preparation for whole rock geochemical analysis also involved the selection of a representative section of each of the aforementioned TW1 borehole drill core samples. The samples were all cut using the diamond-tipped rock saw to produce 5-7 cm sections of drill core to be crushed and milled into a fine powder for geochemical analysis. Each sample was crushed using the jaw crusher in the Geosciences sample preparation facility at the University of the Witwatersrand, to produce centimetre-sized chips and fragments. The rock-chip samples were placed in the *Dickie & Stockler TS-250* swing mill, where the machine was run for two minutes, thereby pulverising the chips and producing very fine powders. Throughout this process, the utmost care and consideration was focused towards preventing contamination of the samples as well as ensuring that the minimal amount of sample mass was lost throughout the crushing and milling process. All machinery and apparatus were cleaned meticulously throughout the sample preparation process to ensure no contamination. The milled aliquots of between 90 g and 100 g were packed for chemical analysis and sent to the *Earth Laboratory* at the University of the Witwatersrand.

Sample preparation for X-ray Fluorescence (XRF) geochemical analysis was carried out in two separate ways for the bulk major elements and trace elements respectively. The bulk major element oxides for each of the forty samples were determined using the fused disk method where the milled sample powders were heated to 1000 ˚C in order to determine the loss on ignition (LOI). The samples were then mixed with a chemical flux – Johnson-Matthey spectroflux JM100B (80% Lithium Metaborate and 20% Lithium Tetraborate) –, heated to 1000 ˚C and then pressed into a fused disk for analysis. The trace elements for the forty samples, on the other hand, were determined using a pressed pellet method whereby 6 g of each of the milled sample powders were combined with 5-6 drops of a 4% polyvinyl alcohol (Mowiol) binding agent, left out to dry for 24 hours and then pressed into a pellet mould at 10 tons per square inch. The fused disks and pressed pellets for each of the forty samples were all analysed using a *PANanalytical PW2404* XRF machine. The major and trace element geochemical data obtained from XRF analyses during this study are provided in Appendix 2.

6.3. Geochemical Results

6.3.1. CIPW Normative Mineralogy Classification

The CIPW norms for each of the forty samples were calculated from their respective major oxide compositions. This was done to identify the equilibrium mineral assemblages present, to highlight the variation of the four major minerals (plagioclase, orthopyroxene, clinopyroxene and olivine) between the various units, and provided a basic classification of the samples taken from TW1.

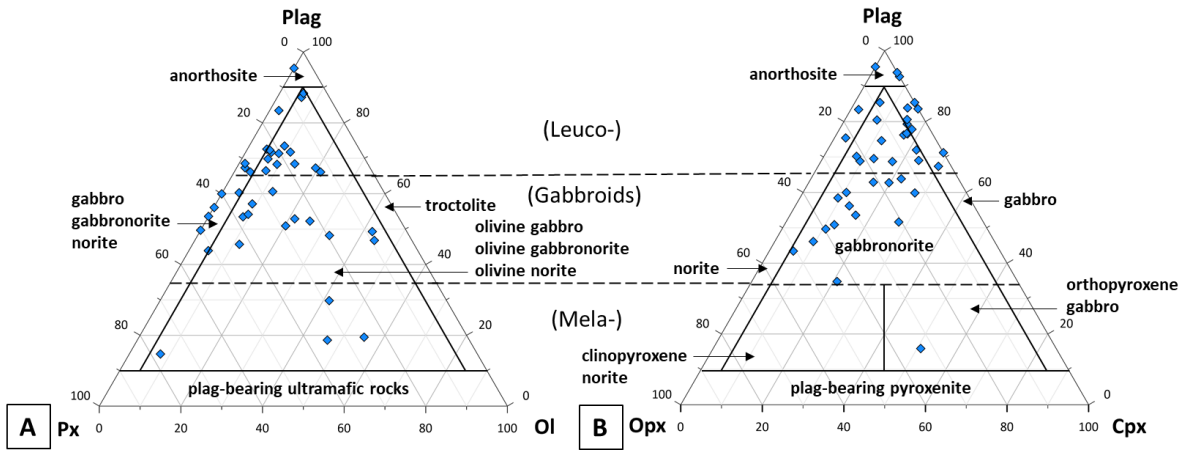

Figure 6.1. *Modal classification* ***A)*** *Plag-Px-Ol and* ***B)*** *Plag-Opx-Cpx ternary diagrams with the CIPW norm calculations for all forty samples plotted on each (Adapted from Streckeisen, 1976 and Le Maitre et al., 2002).*

The ternary Plag-Px-Ol and Plag-Opx-Cpx diagrams *A* and *B* of *Figure 6.1.* show the rock classification for the forty samples according to the ternary diagrams of the Streckeisen (1976) modal classification of gabbroic rocks. *Figure 6.1. A* illustrates that the majority of samples plot within the normal (gabbroic) to leucocratic gabbro-gabbronorite-norite fields and respective olivine-bearing equivalents, with only one sample plotting in the anorthosite field. No samples plot within the troctolite field of the Plag-Px-Ol ternary which is expected considering the absence of troctolite in the TW1 core. A total of four samples plot within the melanocratic and olivine-bearing gabbro-gabbronorite-norite field of *Figure 6.1. A.* No samples plot within the ultramafic fields of either diagrams. This is likely to be due to fact that the normative mineralogy of the samples taken from the TW1 core are representative of upper RLS rock types that tend to be more felsic, and therefore other mafic and ultramafic components within the samples are limited in proportion.

Rocks falling within the gabbro-gabbronorite-norite fields can be further subdivided using the ternary diagram of *Figure 6.1. B* (Le Maitre *et al*., 2002). The samples largely plot within the leucogabbro and normal to leucogabbronorite fields, with three samples plotting within the anorthosite field and a further two samples plotting in the leuconorite field. This discrepancy between the number of samples plotting within the anorthosite fields in each of the two mafic ternary diagrams of *Figure 6.1.* is the result of the change in end members between the pair.

6.3.2. Major Element Oxides

The major element chemistry of the Upper and Main Zone lithologies at Tweespalk (anorthosites, gabbros, gabbronorites, norites, pyroxenites and feldspathic Harzburgites) have been modelled as a function of the proportions of clinopyroxene (Cpx), orthopyroxene (Opx), plagioclase (Plag), and olivine (Ol) the rocks contain. Igneous rocks generally contain aluminium, calcium and sodium which

reflect the modal proportions of feldspars, while pyroxene and olivine are both reflected by the modal proportions of MgO and Fe_2O_3. Eales *et al.*, (1986) stated that the major element oxide parameters of Al_2O_3, CaO, Fe_2O_3 and MgO can be used in the classification of igneous rock types defined by triangular fields within various binary diagrams. It should be noted that samples plotting significantly outside of the triangular compositional fields in *Figure 6.2.*, contain a substantial amount of magnetite and other minor accessory minerals.

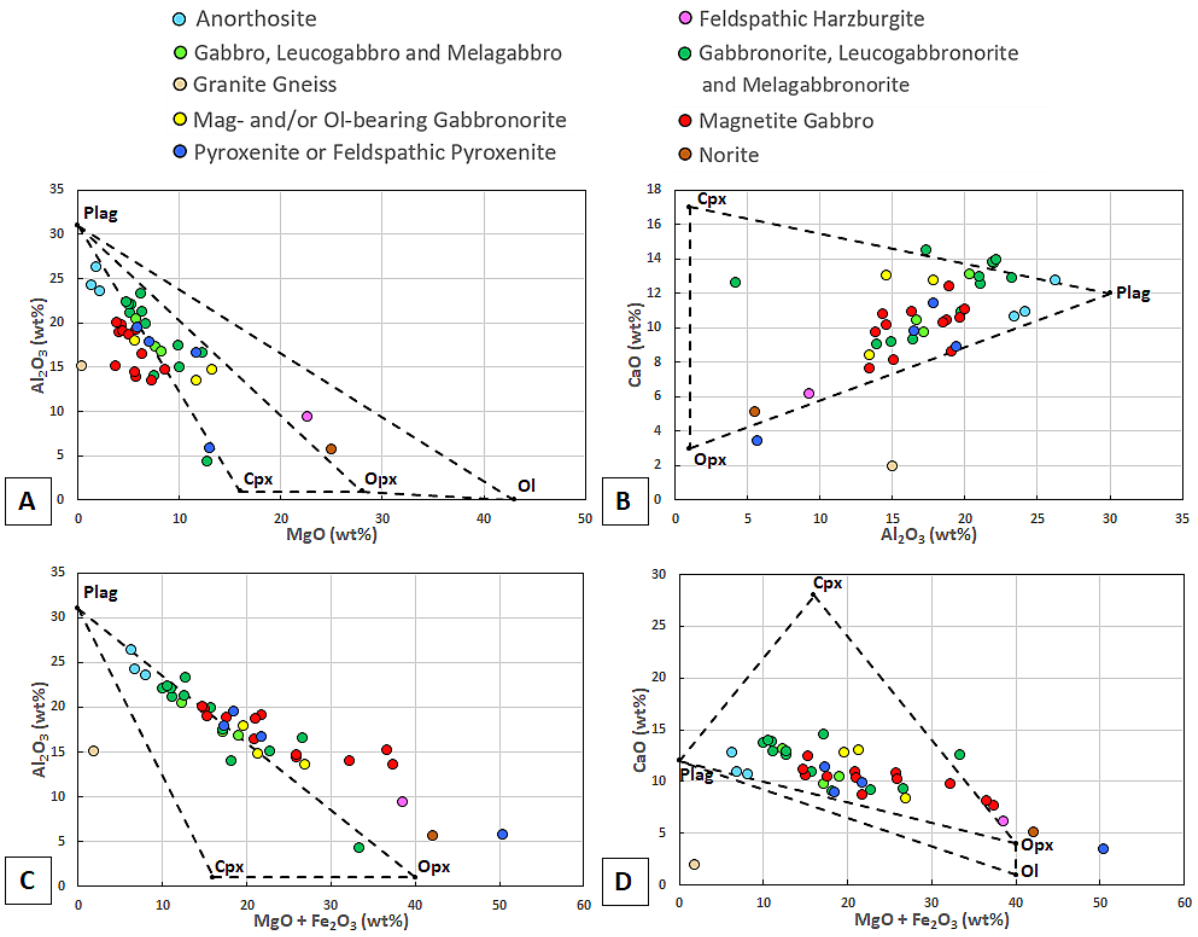

Figure 6.2. *Major element geochemical plots of* ***A)*** *Al_2O_3 vs MgO* ***B)*** *CaO vs Al_2O_3* ***C)*** *Al_2O_3 vs MgO + Fe_2O_3 and* ***D)*** *CaO vs MgO + Fe_2O_3 for the TW1 samples, showing the compositions of the different rock types compared to the endmember minerals of plagioclase, orthopyroxene, clinopyroxene and olivine.*

The major element chemistry of the TW1 lithologies plotted in *Figure 6.2.* illustrate the various trends with regards to their major oxide compositions and predominantly plot within the Plag-Cpx-Opx endmember fields of each figure. *Figure 6.2. A, C* and *D* highlight the relationship of decreasing MgO and Fe_2O_3 compositions with increasing Al_2O_3 or CaO compositions, which illustrates the overall transition of the rock types from the more mafic and melanocratic gabbronorites, norite, pyroxenites and feldspathic harzburgite that contain higher proportions of pyroxene and olivine minerals, towards more plagioclase-rich anorthosites and leucocratic gabbroic units.

The norite sample TW1-24 that plots abnormally towards the plagioclase endmember should rather be classified as an anorthosite, as this coincides with the observations made in *Chapter 6* that the sample exhibits a patchy or mottled texture and is rich in plagioclase. The samples that plot outside of the triangular fields in *Figure 6.2. C* are indicative of the presence of magnetite in the rocks, with a few gabbronorites that were not characterised as being magnetite-bearing – due to the significantly low proportions seen in core and thin sections – displaying high Fe_2O_3 contents associated with magnetite.

6.3.3. Geochemical Variations with Depth

A number of different geochemical parameters within a bulk geochemistry dataset are commonly used to evaluate the elemental changes within a differentiated magmatic stratigraphy such as the Bushveld Complex. These geochemical parameters highlight certain trends or variations that are integral to the understanding of the emplacement and formation processes of an intrusive sequence.

The differentiation and possible influx of a new magma within a magma chamber can be interpreted using selected major element oxide and trace element concentrations and ratios, these key parameters include: (1) the ratio of Sr:Al_2O_3 which can be used to indicate an influx of new magma into the chamber, (2) the ratio of magnesium to iron in the form of the magnesium number (Mg#) which can indicate whether a magma is evolved or more primitive, (3) the ratio of Al_2O_3:FeO + MgO shows the changing proportions of plagioclase and pyroxene and can be a similar indication of possible magma influxes, (4) the SiO_2:Al_2O_3 ratio which can be used to differentiate between different packages of rocks with different compositions that formed from different magma injections, (5) the CaO:Al_2O_3 is used as a potential indicator towards magma contamination by the country rocks (Kinnaird, 2005).

Depth profiles of selected major and trace elements throughout the TW1 core are shown in *Figures 6.3.* and *6.4.* respectively. Through the TW1 borehole, from the base of the succession upwards, the SiO_2:Al_2O_3 ratio remains relatively constant around 3.11 (*Figure 6.3 A*). The Al_2O_3 content generally shows a similar consistency throughout the stratigraphy, averaging around 17.19 wt% with a slightly greater dispersion between samples (*Figure 6.3. B*). The CaO content follows a marginally decreasing trend from the base of the borehole, upwards (*Figure 6.3 C*). The Mg# displays a progressive decrease with decreasing depth, ranging from values of around 49.25 near the base to 24.65 at the top of the borehole (*Figure 6.3 D*).

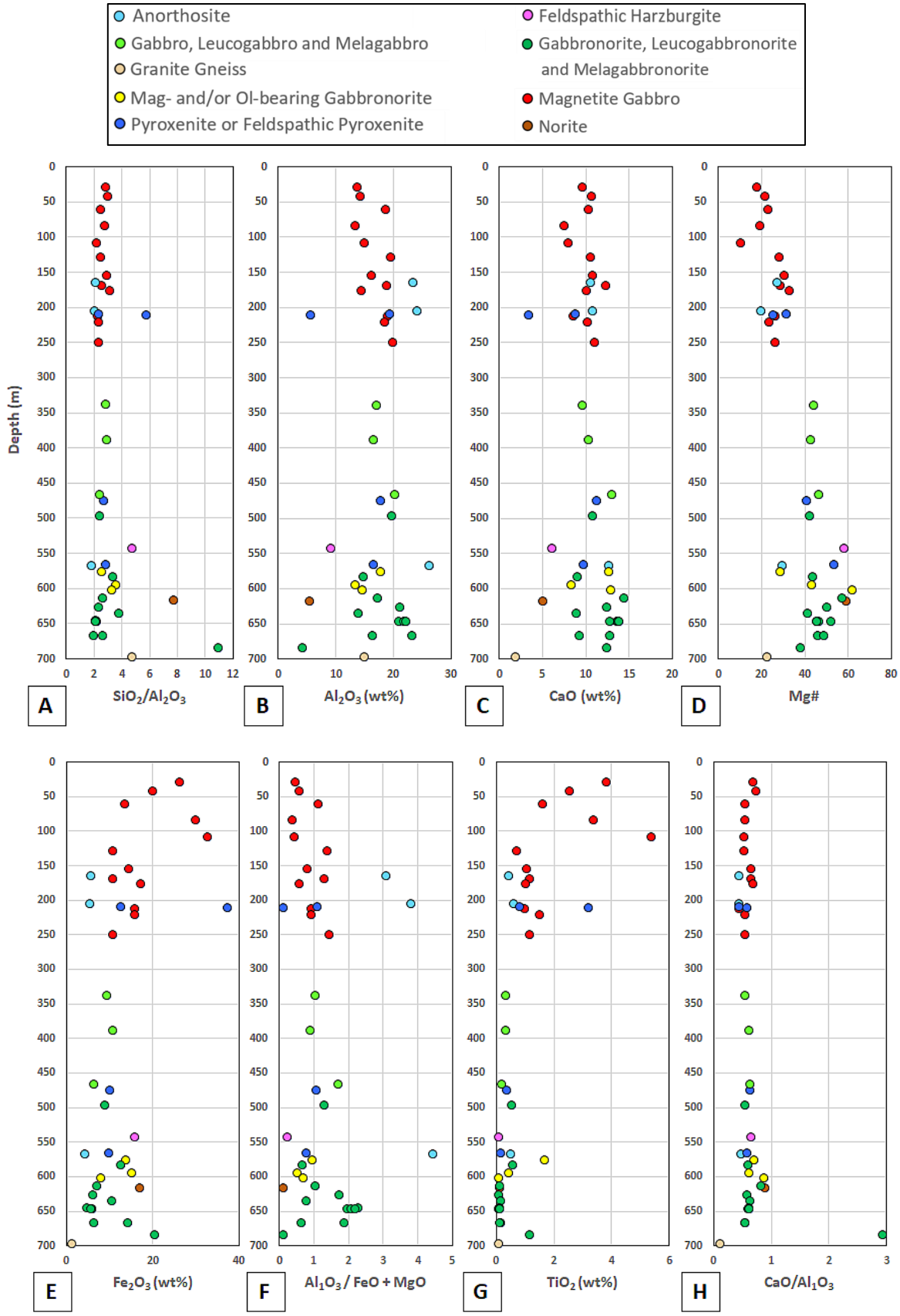

Figure 6.3. *Major element oxide geochemical variations with depth in borehole TW1,* ***A)*** *SiO_2 /Al_2O_3* ***B)*** *Al_2O_3* ***C)*** *CaO* ***D)*** *Mg#* ***E)*** *Fe_2O_3* ***F)*** *Al_2O_3/FeO + MgO* ***G)*** *TiO_2* ***H)*** *CaO/Al_2O_3.*

The Al_2O_3:FeO+MgO (*Figure 6.3 F*) and CaO:Al_2O_3 contents both remain fairly consistent throughout, only the anorthosites and a package of gabbronorites at a depth of ~560 m in the Al_2O_3:FeO+MgO ratio, show elevated values from the average of 1.24. A sharp spike in the CaO:Al_2O_3 TW1-39 at the base of the magmatic stratigraphy suggests magma contamination as a result interaction with the granitic gneiss country rock (*Figure 6.3 H*). The Fe_2O_3 values are broadly constant throughout the borehole, but show notable increases in the magnetite gabbro samples towards the top of the succession (*Figure 6.3 E*). The TiO_2 contents in *Figure 6.3. G* generally mirror this Fe_2O_3 relationship with depth, displaying similarly high contents in the magnetite gabbros in the Upper Zone. A discrete increase is also observed within a package of magnetite-bearing gabbronorites and an anorthosite, between depths of 544.0 m and 595.4 m.

The consistent nature of the SiO_2:Al_2O_3 ratio in *Figure 6.3. A* suggests that there was no significant new influx of magma during emplacement and that the stratigraphy at Tweespalk formed from a single magma source with little addition of new magma. With mantle olivine compositions of Fo_{88}-Fo_{98} defining a primary melt that has a Mg# of 65 (Gill, 2010), the Mg# near the base of the magmatic stratigraphy is around 50 and then decreases progressively towards the top of the stratigraphy. This reflects an initially more primitive magma that evolved upwards as a result of differentiation. A measure for potential magma contamination is indicated by the CaO:Al_2O_3 ratio. Pure plagioclase has a CaO:Al_2O_3 ratio of 0.6, so any significant deviation from this value suggests magma contamination. The CaO:Al_2O_3 ratio averages 0.67 in the TW1 core which indicates a lack of contamination in the various rock types throughout the stratigraphy, however the gabbronorite of sample TW1-39 shows a major increase which is likely to have been a result of contamination or alteration at the contact with the granite gneiss footwall.

The Sr:Al_2O_3 plot in *Figure 6.4. A* shows the ratio to be slightly increasing from the base upwards, with values ranging from around 12.38 at the bottom of the stratigraphy through to an average value of 15.16 at the top. The gradual increase of the Sr:Al_2O_3 ratio upwards through the Tweespalk succession is indicative of it having formed from the same magma, with no sudden changes observed in the depth profile.

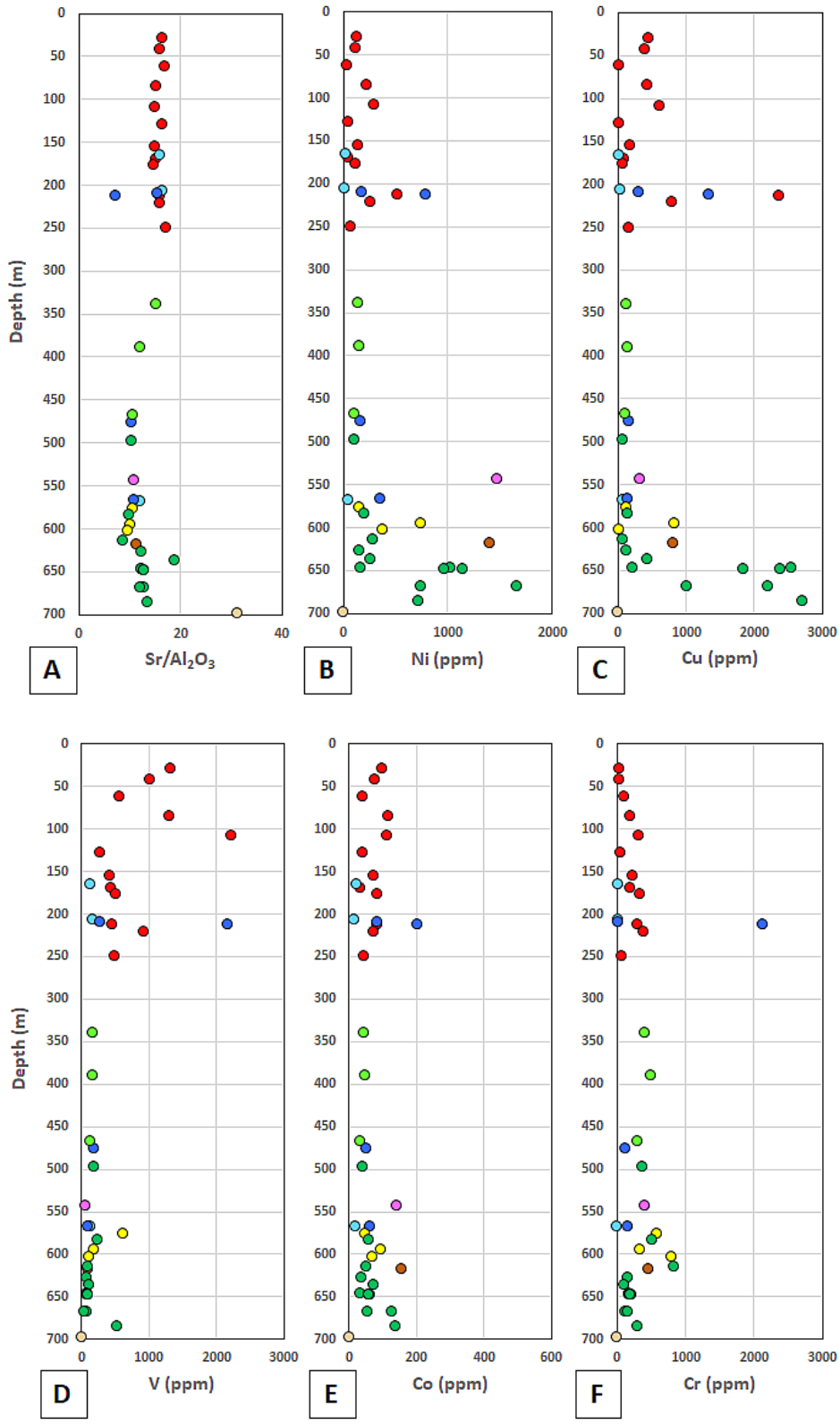

Figure 6.4. *Major and trace element geochemical variations with depth in borehole TW1,* ***A)*** *Sr/Al_2O_3* ***B)*** *Ni* ***C)*** *Cu* ***D)*** *V* ***E)*** *Co* ***F)*** *Cr. Symbols as in seen in Figure 7.3.*

The Ni and Cu contents display extremely similar trends throughout the Tweespalk magmatic package, with generally low values amongst the majority of the samples (*Figure 6.4. B* and *C*). Both trace

elements also show significant enrichments in Ni (up to 1668.82 ppm) and Cu (up to 2709.51 ppm) contents at depths between 210-222 m and 595-686 m within the stratigraphy. Noting that not all the gabbronorite samples show elevated Ni and Cu contents, and that these enrichments are locally confined to basal gabbronorites below 637 m (Ni contents >720 ppm and Cu contents >816 ppm). This increasing Ni is a good reflection of the olivine content with the rock.

There is a remarkably similar trend between the V contents with height and the TiO_2 and – to a lesser extent – Fe_2O_3 major oxide contents shown in *Figures 6.3. E* and *G*. The Co and Cr plots of *Figure 6.4. E* and *F* show negligible variation with depth and remain fairly constant around 72 ppm and 308 ppm individually. It is interesting to note that the olivine- and magnetite-bearing feldspathic pyroxenite of TW1-13 at a depth of 212.7 shows considerable enrichments in the majority of the trace elements relative to other samples, most notably V, Cr, Co, Ni, Cu, Zn, and Pb.

The observed geochemical characteristics of the TW1 borehole are largely reflective of a typical upper RLS geochemical signature in the northern limb. The succession displays an overall progression from a more primitive magma at the base, towards a more evolved magma at the top – a common feature throughout the RLS stratigraphy. No significant influx of new magma was recorded in the geochemical profile, indicating that the magmatic stratigraphy at Tweespalk formed from a single magma source whilst also having been largely unaffected by country rock contamination. The geochemical data interpreted in this chapter does not fully explain the subdivision of the observed stratigraphy at Tweespalk into a UZ and a MZ as proposed in the previous chapters and will be discussed in greater detail in the next chapter. The information gathered from the previous three chapters allows for a structured and detailed analysis of the Tweespalk core relative to the geology observed throughout the rest of the northern limb.

Chapter Seven

Discussion and Conclusions

7.1. Discussion

The stratigraphic succession of the northern limb Bushveld rocks at Tweespalk, coupled with the respective lithological, mineralogical, and geochemical variations observed throughout the studied TW1 core, have allowed for a greater understanding of the local geology. This has provided an improved platform to further evaluate the relationship of this magmatic stratigraphy and mineralisation – or lack thereof – within the greater context of the northern limb. This discussion aims to address all of the stated objectives and highlight the main findings from the respective studies carried out in *Chapters 4*, *5* and *6* in order to effectively assess the correlation of this package of Bushveld rocks with the rest of the known northern limb stratigraphy, as well as the Aurora and Waterberg projects further north.

The Tweespalk property has an extremely thin cover succession of unconsolidated alluvium and weathered Karoo Supergroup sedimentary units which is relatively similar to the cover sequences of the rest of the northern limb stratigraphy where volcanic units are absent at the top of the stratigraphy. The magmatic stratigraphy is not truncated by overlying granite and granophyre volcanic units (observed predominantly above the western portions of the northern limb stratigraphies) and Rooiberg volcanics (at the top of the eastern and western limb stratigraphies). As a result, the Tweespalk area shows comparisons with the thin, ~10 m to ~50 m thick sedimentary cover directly overlying magmatic rocks of the RLS at farm localities such as Grasvally, Turfspruit, Overysel, Aurora and Waterberg. The Waterberg exploration area also displays this thin sedimentary cover, however it is separated from the RLS rocks by a 120-700 m thick succession of Waterberg red-bed sandstone, arkose and conglomerate sedimentary units and a dolerite sill (McCreesh, 2016; Kinnaird *et al*., 2017).

The underlying magmatic succession of RLS rocks at Tweespalk that continues to a depth of 696 m, exhibit broadly similar stratigraphic features to that of the upper portions of the known northern limb and Bushveld Complex mafic and ultramafic stratigraphies and are locally representative of the Upper and Main Zone lithologies observed in the northern limb. As discussed previously, the exploration drilling carried out at Tweespalk suggested that the local geology comprised of predominantly Upper Zone lithologies, with limited Main Zone present (Maier *et al*., 2007). The return of relatively poor assay test results for PGEs and BMSs throughout the PTM boreholes, signified the absence of any economically significant mineralisation. This perceived lack of any Main Zone and the nonappearance

of Platreef lithologies in particular – the high grade Platreef mineralisation of the northern limb being the primary focus of exploration and mining companies at the time (Kinnaird and McDonald, 2018) – is the reason behind the discontinued exploration and study of the area.

On the basis of the detailed study of the TW1 drill core in *Chapter 4*, it is evident that the magmatic stratigraphy at Tweespalk comprises both Upper Zone and Main Zone lithologies, despite previous interpretations of the geology indicating that only the Upper Zone of the RLS was present. The magmatic stratigraphy at Tweespalk therefore comprises a thick succession of Upper Zone rocks that overly a relatively thin portion of Main Zone resting on the Archaean footwall.

The majority of gabbro, gabbronorite and anorthosite units that make up the plagioclase-rich Upper Zone contain cumulus magnetite in relative abundance. The zone also displays a number of individual magnetite layers and stringers which are common throughout most of the northern limb Upper Zone. The first appearance of magnetite is observed at a depth of 596.3 m, with the proportions of magnetite within the units generally increasing with decreasing depth. The first significant volume of magnetite is observed at 541.2 m, which is ~55.1 m above the first appearance in the stratigraphy. This section of units that are magnetite-bearing – but in relatively low proportions – is evident in samples TW1-22 through to TW1-27 (*Figure 5.6. and Figure 5.4. A* and *B*). A comparatively magnetite-barren section (~203.4 m) of gabbros and granitic veining is also noted between the depths of 546.1 m and 252.7 m. The highest volumes of magnetite are present within the upper portion of Tweespalk stratigraphy.

The section of rocks that lies between the first appearance and first significant volume of magnetite (596.3 m – 541.2 m), is made up of gabbronorites, norites, feldspathic pyroxenites, feldspathic harzburgites and an anorthosite unit. This interval of rocks can be divided in two portions, a lower portion that comprises of predominantly gabbronorite and norite and an upper portion of gabbronorite, feldspathic harzburgite and feldspathic pyroxenite. This subdivision is placed at the end of a norite unit situated towards the middle of the section, at a depth of 566.1 m. The discrete change in lithologies between the two portions of the ~55.1 m interval, marks the broad transition from Main Zone to Upper Zone within the Tweespalk stratigraphy.

Olivine is particularly common throughout the majority of units extending from the base of stratigraphy through to a depth of 541.2 m. Aside from a localised enrichment in olivine content observed at 210.3 m, olivine is limited within the lithologies above 541.2 m. This disparity in olivine content also highlights the transition between Main and Upper Zone lithologies, with olivine typically more common in the gabbro- and gabbronorite- dominated Main Zone of the Bushveld stratigraphy. Another key feature observed that highlights this transition into the Main Zone stratigraphy, is the increasing homogeneity of particularly gabbronorite units towards the base of succession (*Figures 5.6.*

and *6.5.*), in contrast to gabbronorite units in the upper portions of the stratigraphy, which have shown to be considerably less homogeneous.

The placement of the boundary between the UZ and MZ at Tweespalk requires the consideration of a number of key factors. The primary factor is the delineation of the depth at which the first significant presence of cumulus magnetite is observed within the stratigraphy. The second factor considered is the placement of the UZ-MZ boundary, by Ashwal *et al*. (2005) and McCreesh (2016), where a sharp change in magmatic susceptibility is observed within the stratigraphy (~42 m and ~100 m below the first presence of magnetite in the Bellevue and Waterberg core respectively). Lastly, typical Main Zone lithologies need to be present within the stratigraphy in order for the boundary between the two zones to be established. Considering all of these factors, the boundary between the UZ and MZ at Tweespalk is placed at a depth of 566.1 m, at the contact between a norite and overlying gabbronorite, ~24.9 m below the first magnetite-bearing unit.

In terms of the major oxide and trace element geochemical characteristics observed throughout the Tweespalk core in *Chapter 6*, the SiO_2:Al_2O_3 ratio, the Al_2O_3:FeO+MgO ratio and CaO:Al_2O_3 ratio, all remain relatively constant throughout the TW1 profile. The Al_2O_3 content exhibits a very similar pattern and consistency throughout the stratigraphy. The consistency of the SiO_2:Al_2O_3 ratio is indicative of package of rocks formed from a single dominant magma intrusion, which suggests that there was no significant magma influx during the emplacement process. It is known from literature on the Bushveld as a whole, that the Upper Zone formed from a new and different magma source to that of the Main Zone, with this new influx of magma occurring around the Pyroxenite Marker – which lies below the UZ-MZ boundary. This implies that the lithologies of the Tweespalk stratigraphy all formed from the Upper Zone magma, with the small portion Main Zone lithologies observed being representative of Main Zone stratigraphy that forms from the same Upper Zone magma between the pyroxenite marker and the UZ-MZ boundary. However, this injection of new magma may have occurred approximately 150 m below the stratigraphic position of the Pyroxenite Marker as suggested by Nex *et al*. (2002), with fractional crystallisation processes continuing above the marker, into the Upper Zone.

The slightly increasing Sr:Al_2O_3 ratio with decreasing depth, shows no abrupt changes throughout the profile, which signifies once more that the stratigraphy formed from a single influx of magma. The progressively increasing Mg# from the base of the sequence to the top, suggests the stratigraphy developed from an initially more primitive magma towards a more evolved magma. This is the result of differentiation during emplacement and crystallisation, from the more mafic upper MZ to the more felsic UZ rocks. The Fe_2O_3 and TiO_2 contents which show a uniquely similar pattern, also demonstrate

the transition from magnetite-bearing UZ rocks through to magnetite-poor MZ rocks, with this being supported by the subtly decreasing CaO content with decreasing depth.

A relatively important geochemical parameter in the northern limb is the CaO:Al_2O_3 ratio, as it gives a good indication type of basement rock intruded and subsequently degree of interaction. At Tweespalk, the ratio tends to be rather consistent throughout, which suggests a lack of contamination of the intruding magma by the country rocks. A sharp spike seen in the CaO:Al_2O_3 ratio of the gabbronorite sample TW1-39, is reflective of the contact interaction of the magma with the granite gneiss footwall. Contamination of the Bushveld magma is particularly common in areas of the northern limb that have a Transvaal metasedimentary footwall. This lack of contamination at Tweespalk is possibly another reason for the absence of any significant mineralisation. The reasoning behind this being that the contamination of intruding Bushveld magma through country rock interaction and assimilation (especially of sulphur), is an integral factor in the formation of sulphide mineralisation.

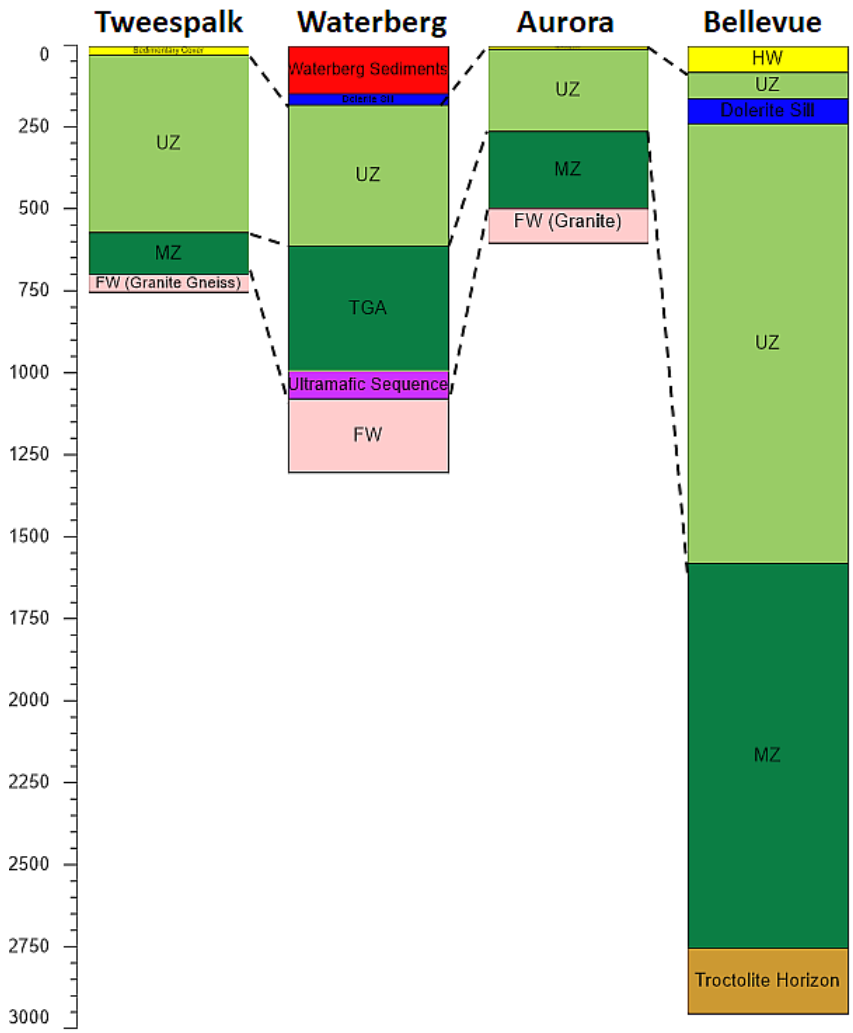

Figure 7.1. *Simplified core logs representing and comparing the general stratigraphy of the northern limb at Tweespalk, Waterberg (After Huthmann et al., 2018), Aurora (After McDonald* et al.*, 2017) and Bellevue (After Ashwal* et al.*, 2005).*

The Tweespalk core shows similar stratigraphic features to that of the Bushveld Complex stratigraphy, and to the northern limb in particular (*Figure 8.1.*). Despite these similarities, the overall magmatic stratigraphy is significantly thinner when compared with the general thicknesses of stratigraphies throughout the rest of the known northern limb and Bushveld. The Upper Zone at Tweespalk is estimated to reach a thickness of ~540 m, whereas the Upper Zones of the western limb, eastern limb and in the Bellevue core further to the southwest of Tweespalk, reach maximum thicknesses of ~1700 m, ~2000 m and ~1190 m respectively. Relative to the Waterberg and Aurora projects further north of the main northern limb, the overall thickness of each magmatic zone at Tweespalk is fairly similar, with the Waterberg being the thickest of the three, but also comprising of the thickest portion of sedimentary cover.

Another key feature missing from the Tweespalk core, is the presence of a Troctolite Marker or any unit of troctolite entirely. The absence of troctolite, a characteristic feature commonly observed towards the centre of a typical northern limb MZ sequence, indicates that the section of MZ stratigraphy present at Tweespalk is representative of only a small portion of upper MZ. The lack of any Transvaal Supergroup xenoliths throughout the section, coupled with the presence of grantic veining, suggests that the Bushveld intrusion and formation at Tweespalk was controlled by the local basement high of granite gneiss (*Figure 3.5.*). This basement continues to rise towards surface further north, before sloping down below the magmatic stratigraphy at Waterberg, where it then rises again in a northerly extension.

This local basement high prevented the development of the full Bushveld stratigraphy at Tweespalk. Mineralisation within the Bushveld and northern limb stratigraphies is believed to occur as a result of two principal factors, namely. The incorporation of sulphur, silica or iron caused by footwall rock interaction and contamination is the first factor, a common process throughout the Bushveld Complex (Kinnaird, 2005; Holwell, 2006; Holwell and McDonald, 2006). The other factor that promotes mineralisation is the intermixing of a new magma influx with an already present resident magma in the chamber (Irvine *et al*., 1983; McDonald and Holwell, 2011). The second factor played a pivotal role in the mineralisation of pyroxenite/harzburgite ultramafic and troctolite-gabbronorite-anorthosite sequences at Waterberg (Kinnaird *et al*., 2017). Based on the evidence provided in this study, it is unlikely that either of these processes occurred in the Tweespalk area. McDonald and Holwell (2006) mentioned that the fluid-rock interaction – integral to the formation ore bodies such as the Platreef – is least prevalent where the basement rock is impermeable Archaean granite gneiss as opposed to a dolomite footwall seen at Sandsloot, for example. This lack of contamination of Bushveld magma by

a metasedimentary footwall as well as there being no intermixing of a resident and new magma influx, is the suggested reason for the absence of any substantial mineralisation.

7.2. Conclusions

This study presents the first significant description of the Rustenburg Layered Suite stratigraphy present at the Tweespalk farm in northern limb of the Bushveld Complex. Specific mineralogical and whole-rock geochemical studies were carried out in order to fully characterise the magmatic stratigraphy at Tweespalk, and compare this succession of rocks to the rest of the known Bushveld Complex and northern limb in particular. The results of the study confirm that the local magmatic succession broadly correlates with that of the typical Bushveld and northern limb stratigraphies. Despite these shared lithological and geochemical characteristics, the stratigraphy at Tweespalk only comprises of Main Zone and Upper Zone lithologies, with the rest of the RLS zones below the MZ being absent.

The stratigraphy at Tweespalk is significantly thinner when compared to the average RLS package thickness observed throughout the northern limb. The identification of a small portion of MZ lithologies towards the base of the stratigraphy, coupled with the lack of a MZ Troctolite or Pyroxenite Marker, suggests that the Tweespalk stratigraphy is representative of predominantly UZ lithologies that overly a thin section of upper MZ sitting on the granite gneiss footwall. The small portion of MZ observed however, is likely to have formed from the same new UZ magma influx that typically occurs near the Pyroxenite Marker throughout the rest of the Bushveld.

In terms of mineralisation, the relatively minor presence of sulphide mineralisation at Tweespalk is largely confined within this smaller upper portion of MZ gabbronorites, situated near the base of the stratigraphy. The lack of any significant mineralisation compared to the rest of the northern limb is largely due to the non-occurrence of either of the two main mineralisation-forming processes in the Bushveld at Tweespalk. These being the lack of any significant assimilation of sulphur as a result of footwall contamination, and no geochemical evidence to suggest the intermixing of a new magma influx with residual magma in the chamber.

In conclusion, the results of the study suggest that the geology of the magmatic stratigraphy at Tweespalk stratigraphy broadly correlates with the northern limb stratigraphy and the rest of the known Bushveld Complex. The absence of any significant mineralisation within the area has been attributed to the rise of the local granite gneiss basement, which prevented the development of the full RLS and more specifically the Platreef-bearing Main Zone in the northern limb. This, coupled with

the presence of a relatively impermeable and unreactive basement granite gneiss, are the primary reasons behind the limited PGE and base-metal sulphide mineralisation observed at Tweespalk.

References

Andrews, M. 2015. The use of chemostratigraphy and geochemical vectoring as an exploration tool for platinum group metals in the Platreef, Bushveld Complex, South Africa: A case study on the Tweefontein and Sandsloot farms. *M.Sc. Thesis, University of the Western Cape, South Africa (unpublished)*, 1 - 158.

Armitage, P.E.B., McDonald, I., Edwards, S.J. and Manby, G.M. 2002. Platinum-group elements mineralization in the Platreef and calc-silicate footwall at Sandsloot, Potgietersrus District, South Africa. *The Institution of Mining and Metallurgy*, 32 - 45.

Armitage, P.E.B., McDonald, I. and Tredoux, M. 2007. A geological investigation of the Waterberg hydrothermal platinum deposit, Mookgophong, Limpopo Province, South Africa. *Applied Earth Science*, 116: 113 - 129.

Armitage, P.E.B. 2011. Development of the Platreef in the Northern Limb of the Bushveld Complex at Sandsloot, Mokopane District, South Africa. *PhD Thesis, The University of Greenwich, United Kingdom,* 1 - 185.

Ashwal, L.D., Webb, S.J. and Knoper, M.W. 2005. Magmatic stratigraphic in the Bushveld Northern Lobe: continuous geophysical and mineralogical data from the 2950 m Bellevue drillcore. *South African Journal of Geology,* 108: 199 - 232.

Barnes, S.-J., Maier, W.D. and Ashwal, L. D. 2004. Platinum-group elements distribution in the Main Zone and Upper Zone of the Bushveld Complex, South Africa. *Chemical Geology*, **208**, 293-317.

Barton, J.M., Cawthorn, R.C. and White, J.A. 1986. The role of contamination in the evolution of the Platreef of the Bushveld Complex. *Economic Geology*, 81: 1096 - 1104.

Buchannan, P.C. 1977. Cryptic variation in minerals from the Bushveld Complex of the Bethal area. *Transactions of the Geological Society of South Africa*, 80: 49 - 52.

Buchanan, P.C. 2006. *The Rooiberg Group*. In: Johnson, M.R., Anhaeusser, C.R. and Thomas, R.J. (eds.), The Geology of South Africa. Geological Society of South Africa Johannesburg and the Council for Geoscience, Pretoria. 282 - 289.

Buick, I.S., Mass, R. and Gibson, R. 2001. Precise U-Pb titanite age constraints on the emplacement of the Bushveld Complex, South Africa. *Journal of the Geological Society of London*, 158: 3 - 6.

Cameron, E.N. 1978. The Lower Zone of the Eastern Bushveld Complex in the Olifants River trough. *Journal of Petrology*, 19: 437 - 462.

Cameron, E.N. 1980. Evolution of the Lower Critical Zone, central sector, eastern Bushveld Complex and its chromite deposits. *Economic Geology*, 75(6): 845 - 871.

Cameron, E.N. 1982. The upper critical zone of the eastern Bushveld Complex: Precursor of the Merensky Reef. *Economic Geology*, 77: 1307 - 1327.

Cawthorn, R.G., Meyer, S.P. and Kruger, F.J. 1991. Major addition of magma at the Pyroxenite Marker in the western Bushveld Complex, South Africa. *Journal of Petrology*, 32: 739 - 763.

Cawthorn, R.G. and Lee, C. 1998. Field excursion guide to the Bushveld Complex. 8th International Platinum Symposium, Geological Survey of South Africa: 113.

Cawthorn, R.G. and Walraven, F. 1998. Emplacement and crystallization time for the Bushveld Complex. *Journal of Petrology*, 39: 1669 - 1687.

Cawthorn, R.G. 1999. Platinum-group element mineralization in the Bushveld Complex – A critical reassessment of geochemical models. *South African Journal of Geology*, 102: 268 - 281.

Cawthorn, R.G. and Webb, S.J. 2001. Connectivity between the western and eastern limbs of the Bushveld Complex. *Tectonophysics*, 330: 195 - 209.

Cawthorn, R.G., Merkle, R.W.K. and Viljoen, M.J. 2002. *Platinum-Group Element Deposits in the Bushveld Complex, South Africa*. In: Cabri, L.J. (ed.), The geology, geochemistry, mineralogy and mineral beneficiation of platinum-group elements. Canadian Institute of Mining, Metallurgy and Petroleum Special Issue. 54: 389 - 430.

Cawthorn, R.G., Eales, H.V., Walraven, F., Uken, R. and Watkeys, M.K. 2006. *The Bushveld Complex*. In: Johnson, M.R., Anhaeusser, C.R. and Thomas, R.J. (eds.), The Geology of South Africa. Geological Society of South Africa Johannesburg and the Council for Geoscience, Pretoria. 261 - 281.

Cheney, E.S. and Twist, D. 1991. The conformable emplacement of the Bushveld mafic rocks along a regional unconformity in the Transvaal succession of South Africa. *Precambrian Research*, 52: 115 - 132.

Cheney, E.S. 1996. Sequence stratigraphy and plate tectonic significance of the Transvaal succession of southern Africa and its equivalent in Western Australia. *Precambrian Research*, 79: 3 - 24.

Clarke, B.M., Uken, R., Watkeys, M.K. and Reinhardt, J. 2005. Folding of the Rustenburg layered suite adjacent to the Steelpoort pericline: Implications for syn-Bushveld tectonism in the eastern Bushveld Complex. *South African Journal of Geology*, 108: 397 - 412.

Clarke, B., Uken, R. and Reinhardt, J. 2009. Structural and compositional constraints on the emplacement of the Bushveld Complex, South Africa. *Lithos*, 111(2): 21 - 36.

Coertze, F.J., Jansen, H. and Walraven, F. 1977. The transition from the Transvaal Sequence to the Waterberg Group. *Transactions of the Geological Society of South Africa*, 80: 145 - 156.

Coertze, F.J., Burger, A.J., Walraven, F., Marlow, A.G. and MacCaskie, D.R. 1978. Field relations and age determinations in the Bushveld Complex. *Transactions of the Geological Society of South Africa*, 81: 1 - 11.

Coggon, J.A., Nowell, G.M., Pearson, D.G., Oberthür, T., Lorand, J.-P., Melcher, F. and Parman, S.W. 2012. The ^{190}Pt-^{186}Os decay system applied to dating platinum-group element mineralization of the Bushveld Complex, South Africa. *Chemical Geology*, 303: 48 - 60.

Cousins, C.A. 1959. The structure of the mafic portion of the Bushveld Igneous Complex. *Transactions of the Geological Society of South Africa*, 62: 174 - 189.

Cousins, C.A. and Feringa, G. 1964. *The chromite deposits of the western belt of the Bushveld Complex*. In: Haughton, S.H. (ed.), The geology of some ore deposits in southern Africa. Geological Society of South Africa, Johannesburg. 2: 183 - 202.

Cronje, L.J. 2017. An evaluation of chromitiferous layers and their host rocks in the Platreef, on the Turfspruit and Zwartfontein properties: A comparative study with the main Bushveld Complex. *M.Sc. Thesis, University of the Witwatersrand, South Africa (unpublished),* 1 - 119.

Dalziel, I.W.D., Mosher, S. and Gahagan, L.M. 2000. Laurentia–Kalahari collision and the assembly of Rodinia. *Journal of Geology*, 108: 499 - 513.

de Kock, M.O., Evans, D.A.D. and Beukes, N.J. 2009. Validating the existence of Vaalbara in the Neoarchean. *Precambrian Research*, 174: 145 - 154.

De Wit, M.J., De Ronde, C.E.J., Tredoux, M., Roering, C., Hart, R.J., Armstrong, R.A., Green, R.W.E., Peberdy, E. and Hart, R.A. 1992. Formation of an Archaean continent. *Nature*, 357: 553 - 562.

Eales, H.V. 1987. *Upper Critical Zone chromitite layers at R.P.M. Union Section Mine, western Bushveld Complex*. In: Stowe, C.W. (ed.), Evolution of chromium ore fields. Van Nostrand Reinhold, New York. 109-143.

Eales, H.V., Marsh, J.S., Mitchell, A.A., de Klerk, W.J., Kruger, F.J. and Field, M. 1986. Some geochemical constraints upon models for the crystallization of the upper critical zone-main zone interval, northwestern Bushveld Complex. *Mineralogical Magazine*, 50: 567-582.

Eales, H.V. and Cawthorn, R.G. 1996. *The Bushveld Complex*. In: Cawthorn, R. G. (ed.), Layered Intrusions. Elsevier, Amsterdam, 181-230.

Engelbrecht, J.P. 1985. The chromites of the Bushveld Complex in the Nietverdiend area. *Economic Geology*, 80: 896 - 910.

Eriksson, P.G., Schweitzer, J.K., Bosch, P.J.A., Schreiber, U.M., van Devender, J.L. and Hatton, C.J. 1993. The Transvaal Sequence: an overview. *Journal of African Earth Sciences*, 16: 25 - 51.

Eriksson, P.G. and Reczko, B.F.F. 1995. The sedimentary and tectonic setting of the Transvaal Supergroup floor rocks to the Bushveld Complex. *Journal of African Earth Sciences*, 21(4): 487 - 504.

Eriksson, P.G., Catuneanu, O., Els, B.G., Bumby, A.J., van Rooy, J.L. and Popa, M. 2005. Kaapvaal Craton: Changing first- and second-order controls on sea level from c. 3.0 Ga to 2.0 Ga. *Sedimentary Geology*, 176(2): 121 - 148.

Finn, C.A., Bedrosia, P.A., Cole, J.C., Khoza, T.D. and Webb, S.J. 2015. Mapping the 3D extent of the Northern lobe of the Bushveld layered mafic intrusion from geophysical data. *Precambrian Research*, 268: 279 - 294.

Furness, J. 2004. PTM advances SA exploration projects. [Online]. Available: http://www.miningweekly.com/article/ptm-advances-sa-exploration-projects-2004-06-07. [Accessed 01 June 2018].

Gill, R. 2010. Igneous Rocks and Processes: A practical guide. *Blackwell Publishing*, 1 - 415.

Good, N. and de Wit, M.J. 1997. The Thabazimbi-Murchison Lineament of the Kaapvaal Craton, South Africa: 2700 Ma of episodic deformation. *Journal of the Geological Society*, 154: 93 - 97.

Gore, J., James, D.E., Zengeni, T.G. and Gwavava, O. 2009. Crustal structure of the Zimbabwe Craton and the Limpopo Belt of Southern Africa: New constraints from seismic data and implications for its evolution. *South African Journal of Geology*, 112: 213 - 228.

Grobler, D.F., Brits, J.A.N., Maier, W.D. and Crossingham, A. 2018. Litho- and chemostratigraphy of the Flatreef PGE deposit, northern Bushveld Complex. *Mineralium Deposita*, 54: 3 - 28.

Hall, A.L. 1932. The Bushveld Igneous Complex of the Central Transvaal. *Geological Society of South Africa Memoir*, 28: 544.

Harmer, R.E. and Sharpe, M.R. 1985. Field relations and strontium isotope systematics of the marginal rocks of the eastern Bushveld Complex. *Economic Geology*, 80: 813 - 837.

Harmer, R.E. and von Gruenewaldt, G. 1991. A review of magmatism associated with the Transvaal Basin – Implications for its tectonic setting. *South African Journal of Geology*, 94: 104 - 122.

Harmer, R.E. and Armstrong, R.A. 2000. New precise dates on the acid phase of the Bushveld and their implications. Abstracts, National Research Foundation. *Workshop on the Bushveld Complex*, Burgersfort, 12th - 18th of November.

Harmer, R.E., McDonald, I., Holwell, D.A., Hughes, H.S.R. and Boyce, A.J. 2017. Aurora PGE-Cu-Ni-Au Project: Main Zone- hosted PGE mineralisation in the Northern Limb of the Bushveld Complex. *GSSA Conference, South Africa*.

Hatch, F.H. and Corstorphine, G.S. 1905. *The Geology of South Africa*. Macmillan and Co., London. 394.

Hatton C.J. and von Gruenewaldt, G. 1987. *The geological setting and petrogenesis of the Bushveld chromitite layers*. In: Stow, C.W. (ed), Chromite deposits through time. International Geological Congress, Washington. 109 - 142.

Hatton, C.J. and Schweitzer, J.K. 1995. Evidence for synchronous extrusive and intrusive Bushveld magmatism. *Journal of African Earth Sciences*, 21: 579 - 594.

Hoffman, P.F. 1991. Did the breakout of Laurentia turn Gondwanaland inside-out?. *Science*, 252: 1409 - 1412.

Holwell, D.A. 2006. The roles of magmatism, contamination and hydrothermal processes in the development of the Platreef mineralisation, Bushveld Complex, South Africa. *Ph.D. Thesis (unpublished)*, 1 - 285.

Holwell, D.A. and Jordaan, A. 2006. Three-dimensional mapping of the Platreef at the Zwartfontein South mine: Implications for the timing of magmatic events in the northern limb of the Bushveld Complex. *Transactions of the Institute of Mining and Metallurgy*, 115: 41 - 48.

Holwell D.A. and McDonald, I. 2006. Petrology, geochemistry, and the mechanisms determining the distribution of platinum group element and base metal sulfide mineralisation in the Platreef at Overysel, northern Bushveld Complex, South Africa. *Mineralium Deposita*, 41: 575 - 598.

Holwell, D.A., McDonald, I. and Armitage, P.E.B. 2006. Platinum group mineral assemblages in the Platreef at the Sandsloot mine, northern Bushveld Complex, South Africa. *Mineralogical Magazine*, 70: 83 - 101.

Holwell, D.A., Jones, A., Smith, J.W. and Boyce, A.J. 2013. New mineralogical and isotopic constraints on Main Zone hosted PGE mineralisation at Moorddrift, northern Bushveld Complex. *Mineralium Deposita*, 48: 675-686.

Holzer, L., Frei, R., Barton, J.M. and Kramers, J.D. 1998. Unravelling the record of successive high-grade events in the Central Zone of the Limpopo Belt using Pb single phase dating of metamorphic minerals. *Precambrian Research*, 87: 87 - 115.

Hulbert, L.J. and von Gruenewaldt, G. 1982. Nickel, copper, and platinum mineralisation in the Lower Zone of the Bushveld Complex, south of Potgietersrus. *Economic Geology*, 77: 1296 - 1306.

Hulbert, L.J. 1983. A petrographical investigation of the Rustenburg Layered Suite and associated mineralisation south of Potgietersrus. *Ph.D. Thesis, University of Pretoria, South Africa (unpublished)*, 1 - 501.

Hulbert, L.J. and Von Gruenewaldt, G. 1985. Textural and compositional features of chromite in the lower and critical zones of the Bushveld complex south of Potgietersrus. *Economic Geology*, 80: 872 - 895.

Hutchinson, D., Kinnaird, J.A. and Schurmann, L.W. 2004. Complex multi-stage mineralisation history in the southern sector of the Platreef, Bushveld Complex, South Africa. *GeoscienceAfrica Abstract Volume*, University of the Witwatersrand, 12th-16th July.

Huthmann, F.M., Yudovskaya, M.A., Frei, D. and Kinnaird, J.A. 2016. Geochronological evidence for an extension of the Northern Lobe of the Bushveld Complex, Limpopo Province, South Africa. *Precambrian Research*, 280: 61 - 75.

Huthmann, F.M., Yudovskaya, M.A., Kinnaird, J.A., McCreesh, M. and McDonald, I. 2018. Geochemistry and PGE of the lower mineralized Zone of the Waterberg. *Ore Geology Reviews*, 92: 161 - 185.

Irvine, T.N., Keith, D.W. and Todd, S.G. 1983. The JM platinum-palladium reef of the Stillwater Complex, Montana; II, Origin by double-diffusive convective magma mixing and implications for the Bushveld Complex. *Economic Geology*, 78: 1287 - 1334.

Kekana, S.M. 2014. An investigation of the mineralisation controls in the upper section of the Platreef in the southern sector, on Turfspruit, northern limb, Bushveld Complex, South Africa. *M.Sc. Thesis, University of the Witwatersrand, South Africa*, 1 - 128.

Kekana, S.M. and Broughton, D. 2011. New observations and exploration developments at Turfspruit. 4th Platreef Workshop January 14-16, Mokopane, South Africa.

Kinnaird, J.A., Kruger, F.J., Nex, P.A.M. and Cawthorn, R.G. 2002. Chromitite formation – A key to understanding processes of platinum enrichment. *Applied Earth Science*, 111: 23 - 35.

Kinnaird, J.A. 2005. Geochemical evidence for the multiphase emplacement in the southern Platreef. *Applied Earth Science (Transactions of the Institute of Mining and Metallurgy)*, 144: 225 - 242.

Kinnaird, J.A. and McDonald, I. 2005. An introduction to the mineralisation in the northern limb of the Bushveld Complex. *Transactions of the Institution of Mining and Metallurgy*, 114: 194 - 198.

Kinnaird, J.A., Hutchinson, D., Schürmann, L.W., Nex, P.A.M. and de Lange, R. 2005. Petrology and mineralisation of the southern Platreef: northern limb of the Bushveld Complex, South Africa. *Mineralium Deposita*, 40: 576 - 597.

Kinnaird, J.A., Yudovskaya, M.A., Naldrett, A.J., Botha, M.J. and Chunnett, G.K. 2012. PGE mineralisation in the main Zone of the Northern Limb of the Bushveld Complex. 12th *International Ni-Cu (PGE) Symposium*, Guiyang, China, 1 - 4.

Kinnaird, J.A. and Nex, P.A.M. 2015. An overview of the Platreef. In: Platinum-group element (PGE) mineralisation and resources of the Bushveld Complex, South Africa. *Council for Geoscience, Pretoria*. 193 - 342.

Kinnaird, J.A., Yudovskaya, M.A., McCreesh, M.J.G., Huthmann, F.M. and Botha, T.J. 2017. The Waterberg Platinum Group Element Deposit: Atypical mineralization in mafic-ultramafic rocks of the Bushveld Complex, South Africa. *Economic Geology*, 112: 1367 - 1394.

Kruger, F.J. and Marsh, J.S. 1982. Significance of $^{87}Sr/^{86}Sr$ ratios in the Merensky cyclic unit of the Bushveld Complex. *Nature*, 298: 53 - 55.

Kruger, F.J., Cawthorn, R.G., Meyer, P.S. and Walsh, K.L. 1986. Sr-isotopic, chemical and mineralogical variations across the pyroxenites marker and in the Upper Zone of the western Bushveld Complex. In: Geocongress '86. Geological Society of South Africa, Johannesburg. 609 - 612.

Kruger, F.J. 1990. The stratigraphy of the Bushveld Complex: A reappraisal and relocation of the Main Zone boundaries. *South African Journal of Geology*, 93(2): 376 - 381.

Kruger, F.J. 1992. The origin of the Merensky cyclic unit: Isotopic and mineralogical evidence for an alternative orthomagmatic model. *Australian Journal of Earth Science*, 39: 255 - 261.

Kruger, F.J. 1999. *The Bushveld Complex unconformity related ore deposits: An isotopic perspective*. In: Stanley *et al*. (eds.), Mineral Deposits: Processes to Processing. Balkema, Rotterdam. 373-378.

Kruger, F.J. 2005. Filling the Bushveld Complex magma chamber: Lateral expansion, roof and floor interaction, magmatic unconformities, and the formation of giant chromitite, PGE and Ti-V-magnetitite deposits. *Mineralium Deposita*, 40: 451 - 472.

Le Bas, M.J. and Streckeisen, A.L. 1991. The IUGS systematics of igneous rocks. *Journal of the Geological Society*, 1485(5): 825 - 833.

Lee, C.A. 1996. *A review of mineralisation in the Bushveld Complex and some other layered mafic intrusions*. In: Cawthorn, R.G. (ed.), Layered Intrusions. Elsevier, Amsterdam. 103 - 146.

Le Maitre, R.W. (Editor), Streckeisen, A., Zanettin, B., Le Bas, M.J., Bonin, B., Bateman, P., Bellieni, G., Dudek, A., Efremova, S., Keller, J., Lameyre, J., Sabine, P.A., Schmid, R., Sorensen, H. and Woolley, A.R. 2020. *Igneous Rocks: A Classification and Glossary of Terms* (2nd Edition). Cambridge, Cambridge University Press.

Lenhardt, N. and Eriksson, P.G. 2012. Volcanism of the Palaeoproterozoic Bushveld Large Igneous Province: The Rooiberg Group, Kaapvaal Craton, South Africa. *Precambrian Research*, 215: 82-94.

Lenhardt, N., Masango, S., Jolayemi, O., Lenhardt, S., Peeters, G. and Eriksson, P. 2017. The Paleoproterozoic (~2.06 Ga) Rooiberg Group, South Africa: Dominated by extremely high-grade lava-like and rheomorphic ignimbrites? New observations and lithofacies analysis. *Journal of African Earth Sciences*, 131: 213 - 232.

Lenthall, D.H. 1973. A proposed nomenclature system for the granophyres associated with the Bushveld Complex. *Transactions of the Geological Society of South Africa*, 76: 75 - 76.

Letts, S., Torsvik, T.H., Webb, S.J. and Ashwal, L.D. 2011. *New Palaeoproterozoic palaeomagnetic data from the Kaapvaal Craton, South Africa*. In: Van Hinsbergen, D.J.J., Buiter, S.J.H., Torsvik, T.H., Gaina, C. and Webb, S.J. (eds.), The formation and evolution of Africa: A synopsis of 9.8 Ga of earth history. Geological Society, London, Special Publications. 357: 9 - 26.

Li, Z.X., Bogdanova, S.V., Collins, A.S., Davidson, A., De Waele, B., Ernst, R.E., Fitzsimmons, I.C.W., Fuck, R.A., Gladkochub, D.P., Jacobs, J., Karlstrom, K.E., Lu, S., Natapov, L.M., Pease, V., Pisarevsky, S.A., Thrane, K. and Vernikovsky, V. 2008. Assembly, configuration and break-up history of Rodinia: A synthesis. *Precambrian Research*, 160: 179 - 210.

Lomberg, K.G. 2012. Exploration Results and Mineral Resources Estimation for the Waterberg Platinum Project South Africa (Latitude 23°21'53" S, Longitude 28°48'23" E). Platinum Group Metals (RSA) (Pty) Ltd (Internal report).

Maier, W.D., Barnes, S.-J., Teigler, B., de Klerk, W.J. and Mitchell, A.A. 1996. Cu/Pd and Cu/Pt of silicate tocks in the Bushveld Complex: Implications for platinum-group element exploration. *Economic Geology*, 91: 1151 - 1158.

Maier, W.D., de Klerk, L., Blaine, J., Manyeruke, T.D., Barnes, S.-J., Stevens, M.V.A. and Mavrogenes, J.A. 2008. Petrogenesis of contact-style PGE mineralisation in the northern limb of the Bushveld Complex: Comparison of data from the farms Rooipoort, Townlands, Drenthe, and Nonnenwerth. *Mineralium Deposita*, 43: 255 - 280.

Maier, W.D. and Groves, D.I. 2011. Temporal and spatial controls on the formation of magmatic PGE and Ni-Cu deposits. *Mineralium Deposita*, 46: 841 - 857.

Maier, W.D., Barnes, S.-J. and Groves, D.I. 2013. The Bushveld Complex, South Africa: Formation of platinum-palladium, chrome- and vanadium-rich layers via hydrodynamic sorting of a mobilised cumulate slurry in a large, relatively slowly cooling, subsiding magma chamber. *Mineralium Deposita*, 48: 1 - 56.

Manyeruke, T.D., Maier, W.D. and Barnes, S.-J. 2005. Major and trace element geochemistry of the Platreef on the farm Townlands, northern Bushveld Complex. *South African Journal of Geology*, 108: 381 - 396.

McCourt, S. and Armstrong, R.A. 1998. SHRIMP U-Pb zircon geochronology of granites from the Central Zone, Limpopo Belt, Southern Africa: Implications for the age of the Limpopo Orogeny. *South African Journal of Geology*, 101: 329 - 338.

McCreesh, M.J.G. 2016. An investigation of the mineralisation in the Waterberg Platinum-Group Element deposit, South Africa. *M.Sc. Thesis, University of the Witwatersrand, South Africa (unpublished)*, 1 - 256.

McDonald, I., Ohnenstetter, S., Rowe, J.P., Tredoux, M., Pattrick, R.A.D. and Vaughand, D.J. 1999. Platinum precipitation in the Waterberg deposit, Naboomspruit, South Africa. *South African Journal of Geology*, 102: 184 - 191.

McDonald, I., Holwell, D.A. and Armitage, P.E.B. 2005. Geochemistry and mineralogy of the Platreef and "Critical Zone" of the northern lobe of the Bushveld Complex, South Africa: Implications for Bushveld stratigraphy and the development of PGE mineralisation. *Mineralium Deposita*, 40(5): 526 - 549.

McDonald, I. and Holwell, D.A. 2011. Geology of the Northern Bushveld Complex and the setting and genesis of the Platreef Ni-Cu-PGE deposit. *Reviews in Economic Geology*, 17: 297 - 327.

McDonald, I., Harmer, R.E., Holwell, D.A., Hughes, H.S.R. and Boyce, A.J. 2017. Cu-Ni-PGE mineralisation at the Aurora Project and potential for a new PGE province in the Northern Bushveld Main Zone. *Ore Geology Reviews*, 80: 1135 - 1159.

Merensky, H. 1925. The platinum areas of Lydenburg. *South African Mining and Engineering Journal*, 474 - 476.

Meyer, R. and de Beer, J.H. 1987. Structure of the Bushveld Complex from resistivity measurements. *Nature*, 325: 610 - 612.

Mitchell, A.A. 1990. The stratigraphy, petrography and mineralogy of the Main Zone of the northwestern Bushveld Complex. *South Africa Journal of Geology*, 93: 818 - 831.

Molengraaf, G.A.F. 1898. Report of the State Geologist of the South African Republic for the year 1897. *Transactions of the Geological Society of South Africa*, 4: 119 - 147.

Molyneux, T.G. 1974. A geological investigation of the Bushveld Complex in Sekhukhuneland and part of the Steelport Valley. *Transactions of the Geological Society of South Africa*, 77: 329 - 338.

Moore, J.M., Tsikos, H. and Polteau, S. 2001. Deconstructing the Transvaal Supergroup, South Africa: Implications for Paleoproterozoic paleoclimate models. *Journal of African Earth Sciences*, 33(4): 437 - 444.

Naldrett, A.J. 2004. Magmatic Sulfide Deposits: Geology, Geochemistry and Exploration. Springer, New York. 1 - 730.

Nex, P.A.M., Kinnaird, J.A., van der Vyver, B.A., Ingle, L.J. and Cawthorn, R.G. 1998. A new stratigraphy for the Main Zone of the Bushveld Complex, in the Rustenburg area. *South Africa Journal of Geology*, 101(3): 215 - 223.

Nex, P.A.M., Cawthorn, R.G. and Kinnaird, J.A. 2002. Geochemical effects of magma addition: compositional reversals and decoupling of trends in the Main Zone of the western Bushveld Complex. *Mineralogical Magazine*, 66: 833 - 856.

Nex, P.A.M. and Kinnaird, J.A. 2004. The Platreef: it is not as easy as A, B, C. *Geoscience Africa 2004 conference, University of the Witwatersrand, Johannesburg, South Africa*. 494 - 495.

Nex, P.A.M. 2005. The structural setting of mineralisation on Tweefontein Hill, northern limb of the Bushveld Complex, South Africa. *Transactions of the Institute of Mining and Metallurgy*, 114: 243 - 251.

Nex, P.A.M., Kinnaird, J.A., Jones, B. and Colloty, A. 2006. Platreef rock type definitions and descriptions. *Anglo Platinum Technical Report*.

Nomade, S., Renne, P.R. and Merkle, R.K.W. 2004. $^{40}Ar/^{39}Ar$ age constraints on ore deposition and cooling of the Bushveld Complex, South Africa. *Journal of the Geological Society London*, 161(3): 411 - 420.

Olsson, J.R., Söderlund, U., Hamilton, M.A., Klausen, M.B. and Helffrich, G.R. 2011. A late Archaean radiating dyke swarm as possible clue to the origin of the Bushveld Complex. *Nature Geoscience*, 4: 865-869.

PTM Annual Report. 2004. Form 20-F 2004 Annual Report. [Online]. Available: http://www.sec.gov/Archives/edgar/data/1095052/000113717105000293/main20f.html. [Accessed 24 June 2018].

PTM Annual Report. 2012. Time to mine 2012 Annual Report. [Online]. Available: https://s1.q4cdn.com/169714374/files/doc_financials/2012/PTM_2012_AR_v001_t26pgi.pdf. [Accessed 25 June 2018].

Reisberg, L., Tredoux, M., Harris, C., Coftier, A. and Chaumba, J. 2011. Re and Os distribution and Os isotope composition of the Platreef at the Sandsloot-Mogolakwena mine, Bushveld Complex, South Africa. *Chemical Geology*, 281: 352 - 363.

Robb, L.J. 2005. *Introduction to Ore-Forming Processes*. Blackwell Publishing, Oxford.

Robb, L.J., Brandl, G., Anhaeusser, C.R. and Poujol, M. 2006. *Archaean Granitoid Intrusions*. In: Johnson, M.R., Anhaeusser, C.R. and Thomas, R.J. (eds.), The Geology of South Africa. Geological Society of South Africa Johannesburg and the Council for Geoscience, Pretoria. 282 - 289.

Rogers, J.J.W. 1996. A history of continents in the past three billion years. *Journal of Geology*, 104: 91 - 107.

Schoenberg, R., Kruger, F.J., Nägler, T.F., Meisel, T. and Kramers, J.D. 1999. PGE enrichment in chromitite layers and the Merensky Reef of the western Bushveld Complex: A Re-Os and Rb-Sr isotope study. *Earth and Planetary Science Letters*, 172: 49 - 64.

Schurmann, L.W., Grabe, P-J. and Steenkamp, C.J. 1998. *Chromium*. In: Wilson, M.G.C. and Anhaeusser, C.R. (eds.), The Mineral Resources of South Africa. Council for Geoscience, Pretoria. 16: 90 - 105.

Schweitzer, J.K., Hatton, C.J. and De Waal, S.A. 1995. Regional lithochemical stratigraphy of the Rooiberg Group, upper Transvaal Supergroup: a proposed new subdivision. *South African Journal of Geology*, 98: 245 - 255.

Scoates, J.S. and Friedmann, R.M. 2008. Precise Age of the platiniferous Merensky Reef, Bushveld Complex, South Africa, by the U-Pb Zircon Chemical Abrasion ID-TIMS Technique. *Economic Geology*, 103: 465 - 471.

Scoon, R.N. and Teigler, B. 1994. Platinum-group element mineralisation in the Critical Zone of the western Bushveld Complex: Sulfide-poor chromitites below the UG2. *Economic Geology*, 89: 1094 - 1121.

Scoon, R.N. and Mitchell, A.A. 2012. The Upper Zone of the Bushveld Complex at Roossenekal, South Africa: Geochemical stratigraphy and evidence of multiple episodes of magma replenishment. *South African Journal of Geology*, 115: 515 - 534.

Sharpe, M.R. and Chadwick, B. 1982. Structures in Transvaal Sequence rocks within and adjacent to the Eastern Bushveld Complex. *Transactions of the Geological Society of South Africa*, 85: 29 - 41.

Silver, P.G., Fouch, M.J., Gao, S.S., Schmitz, M., and Kaapvaal Seismic Group. 2004. Seismic anisotropy, mantle fabric, and the magmatic evolution of Precambrian southern Africa. *South African Journal of Geology*, 107(5): 45 - 58.

Smith, J.W., Holwell, D.A. and McDonald, I. 2014. Precious and base-metal geochemistry and mineralogy of the Grasvally-Norite-Pyroxenite-Anorthosite (GNPA) member, northern Bushveld Complex, South Africa: Implications for a multistage emplacement. *Mineralium Deposita*, 49: 667 - 692.

South African Committee for Stratigraphy. 1980. In: Kent, L.E. (ed.), *Stratigraphy of South Africa Part 1: Lithostratigraphy of the Republic of South Africa, South West Africa/Namibia and the Republics of Bophuthatswana, Transkei, and Vend*a. Handbook of the Geological Survey of South Africa, Pretoria. 8: 223 - 231.

Streckeisen, A. 1976. To each pluton rock its proper name. *Earth-Science Reviews*, 12(1): 1 - 33.

Tankard, A J., Jackson, M.P.A., Eriksson, K.A., Hobday, D.K., Hunter, D.A. and Minter, W.E.L. 1982. *Crustal evolution of Southern Africa: 3,8 billion years of earth history*. Springer-Verlag, New York. 523.

Tanner, D., Mavrogenes, J.A., Arculus, R.J. and Jenner, F.E. 2014. Trace element stratigraphy of the Bellevue core, northern Bushveld: Multiple magma injections obscured by diffusive processes. *Journal of Petrology*, 55: 859 - 882.

Tanner, D., McDonald, I., Harmer, R.E. and Hughes, H.S.R. 2017). Sulfide melt evolution in the Volspruit project: The most primitive, yet most contaminated platinum group element (PGE) deposit in the Bushveld Complex?. *Applied Earth Science*, 126(2): 96 - 97.

Teigler, B. and Eales, H.V. 1996. The Lower and Critical Zones of the western limb of the Bushveld Complex as intersected by the Nooidedagte boreholes. *Bulletin, Geological Society of South Africa*, 11: 126.

Twist, D. and French, B.M. 1983. Voluminous acid volcanism in the Bushveld Complex: a review of the Rooiberg Felsite. *Bulletin Volcanologique*. 46(3), 225 - 242.

Uken, R. and Watkeys, M.K. 1997. Diapirism initiated by the Bushveld Complex, South Africa. *Geology*, 25: 723 - 726.

Uken, R. 1999. The geology and structure of the Bushveld Complex metamorphic aureole in the Olifants River area. *Ph.D. Thesis (unpublished)*, *University of Natal, South Africa*, 1 - 277.

van der Merwe, M.J. 1976. The layered sequence of the Potgietersrus limb of the Bushveld Complex. *Economic Geology*, 71(7): 1337 - 1351.

van der Merwe, M.J. 1978. The geology of the basic and ultramafic rocks of the Potgietersrus limb of the Bushveld Complex. *Ph.D. Thesis (unpublished), University of the Witwatersrand, South Africa*, 1 - 176.

van der Merwe, M.J. 2008. The geology and structure of the Rustenburg Layered Suite in the Potgietersrus/Mokopane area of the Bushveld Complex, South Africa. *Minaralium Deposita*, 43: 405 - 419.

van Kranendonk, M.J., Hickman, A.H., Smithies, R.H., Nelson, D.R. and Pike, G. 2002. Geology and tectonic evolution of the Archean North Pilbara Terrain, Pilbara Craton, Western Australia. *Economic Geology*, 97: 695 - 732.

Venmyn-Rand, 2010. Independent Technical Experts Report on the Mineral Assets of Sylvania Resources Limited – In the Form of a Competent Persons Report, Venmyn-Rand (Pty) Limited 151.

Visser, W.J. and McWha, M. 2005. NI 43-101 Technical Report on the Tweespalk and War Springs (Oorlogsfontein) Northern Limb Platinum Properties, Platinum Group Metals (Pty) Limited, 63.

von Gruenewaldt, G. 1973. The Main and Upper zones of the Bushveld Complex in the Roossenekal area, eastern Transvaal. Transactions of the *Geological Society of South Africa*, 76: 53 - 61.

von Gruenewaldt, G., Sharpe, M.R. and Hatton, C.J. 1985. The Bushveld Complex: Introduction and Review. *Economic Geology*, 80: 803 - 812.

Wager, L. R. and Brown, G. M. 1968. *Layered igneous rocks*. *Oliver and Boyd, Edinburg*, 588.

Wagner, P.A. 1925. Platinum deposits in the western part of the Lydenburg District. *South African Journal of Industries*, 8: 90 - 113.

Wagner, P.A. 1929. *The platinum deposits and mines of South Africa*. Oliver and Boyd, Edinburgh, 326.

Walraven, F. 1985. Economic aspects of the granophyric rocks of the Bushveld Complex. *Economic Geology*, 80: 1166 - 1180.

Walraven, F. Retief, E.A., Burger, A.J. and Swanepoel, D.J. 1987a. Implications of new U-Pb zircon age dating on the Nebo Granite of the Bushveld Complex. *Transactions of the Geological Society of South Africa*, 90: 344 - 351.

Walraven, F. 1987b. Textural, geochemical and genetic aspects of the granophyric rocks of the Bushveld Complex. *Geological Survey of Southern Africa Memoir,* 72: 153.

Walraven, F., Armstrong, R.A. and Kruger, F.J. 1990. A chronostratigraphic framework for the north-central Kaapvaal craton, the Bushveld Complex and the Vredefort structure. *Tectonophysics*, 171: 23 - 48.

Walraven, F. and Hattingh, E. 1993. Geochronology of the Nebo Granite, Bushveld Complex. *South African Journal of Geology*, 96: 31 - 41.

White, J.A. 1983. The geology and mineralisation of the Platreef of the Potgietersrus limb of the Bushveld Complex. *Symposium on the Bushveld Complex, University of Pretoria*, 102 - 103.

White, J.A. 1994. *The Potgietersrus prospect – Geology and exploration history*. In: Anhaeusser, C.R. (ed.), *Proceedings of the XVth CMMI Congress*. South African Institute of Mining and Metallurgy, Johannesburg, 3: 173 - 181.

Wilson, A.H. 2012. A chill sequence to the Bushveld Complex: Insight into the first stage of emplacement and implications for the parental magmas. *Journal of Petrology*, 53(6): 1123 - 1168.

Wilson, A.H. 2015. The earliest stages of emplacement of the eastern Bushveld Complex: Development of the Lower Zone, Marginal Zone and Ultra Basal Sequence. *Journal of Petrology*, 56(2): 347 - 388.

Wilson, A.H. and Zeh, A. 2015. Emplacement and magma compositions of the lowest succession of the Bushveld Complex. *6th Platreef Workshop, Mokopane, 8th - 10th of May*.

Harmer, R.E. and Armstrong, R.A. 2000. New precise dates on the acid phase of the Bushveld and their implications. Abstracts, National Research Foundation. *Workshop on the Bushveld Complex*, Burgersfort12th-18th November.

Yudovskaya, M.A. and Kinnaird, J.A. 2010. Chromitite in the Platreef (Bushveld Complex, South Africa): Occurrence and evolution of its chemical composition. *Minaralium Deposita*, 45(4): 369 - 391.

Yudovskaya, M.A., Kinnaird, J.A., Sobolev, A.V., Kuzmin, D.V., McDonald, I. and Wilson, A.H. 2013. Petrogenesis of the Lower Zone olivine-rich cumulates beneath the Platreef and their correlation with recognized occurrences in the Bushveld Complex. *Economic Geology*, 108: 1923 - 1952.

Yudovskaya, M.A., Kinnaird, J.A., Udachina, L.V., Distler, V.V. and Kuzmin, D.V. 2014. Role of magmatic and fluid concentrating in formation of platinum mineralization in the Lower Zone and Platreef as follows from composition of phlogopite, cumulus silicates, and sulphide melt, the northern limb of Bushveld Complex. *Geology of Ore Deposits*, 56(6): 451 - 478.

Zeh, A., Gerdes, A. and Barton, M.J. 2009. Archean accretion and crustal evolution of the Kalahari Craton – the Zircon age and Hf isotope record of granitic rocks from the Barberton/Swaziland to the Francistown Arc. *Journal of Petrology*, 50: 933 - 966.

Zeh, A., Ovtacharova, M., Wilson, A.H. and Schaltegger, U. 2015. The Bushveld Complex was emplaced and cooled in less than one million years – results of zirconology, and geotectonic implications. *Earth and Planetary Science Letters,* 418: 103 - 114.

Zeh, A., Wilson, A.H. and Ovtcharova, M. 2016. Source and age of upper Transvaal Supergroup, South Africa: Age-Hf isotope record of zircons in Magaliesberg quartzite and Dullstroom lava, and implications for Paleoproterozoic (2.5-2.0 Ga) continent reconstruction. *Precambrian Research*, 278: 1 - 21.

Zhao, G., Cawood, P.A., Wilde, S.A. and Sun, M. 2002. Review of global 2.1 - 1.8 Ga orogens: Implications for a pre-Rodinia supercontinent. *Earth-Science Reviews*, 59: 125 - 162.

Appendix 1

Core Logging




100
110
120
130
140
150
160
170
180
190
200
Course-grained gabbro with a poikilophitic texture.
A 2 cm magnetite layer with irregular top and bottom contacts.
Continued course-grained gabbro with a poikilophitic texture (No lower contact).
Course-grained gabbro towards course-grained leucogabbro. The gabbro has an oriented ophitic texture and contains ~30 % magnetite. Gabbro becomes increasingly more plagioclase-rich (and less oriented) with depth and with no specific contact or point at which the gabbro becomes more leucocratic (Transitional boundary).
3 cm magnetite stringer which lies 10 cm above the lower contact.
Course-grained leucogabbro (Transitional and irregular lower contact defined by the lower magnetite stringer).
A 2 cm magnetite layer with an irregular top contact, and sharp lower contact.
Anorthosite with 80-90% plagioclase, clinopyroxene and magentite oikocrysts/ porphyrocrysts. The anorthosite appears mottled as a result of the magnetite oikocrysts.
Magnetite-bearing gabbro with ~60% plagioclase.
A 3-4 cm magnetite stringer near the lower contact of the magnetite-gabbro.
Continued magnetite-bearing gabbro with ~60% plagioclase.
Anorthosite with ~90% plagioclase.
Magnetite-bearing gabbro with a transitional and irregular upper contact, and a sharp lower contact (Anorthosite at lower contact looks like leucogabbronorite).
Very course-grained magnetite-bearing anorthosite (10-20% clinopyroxene). The

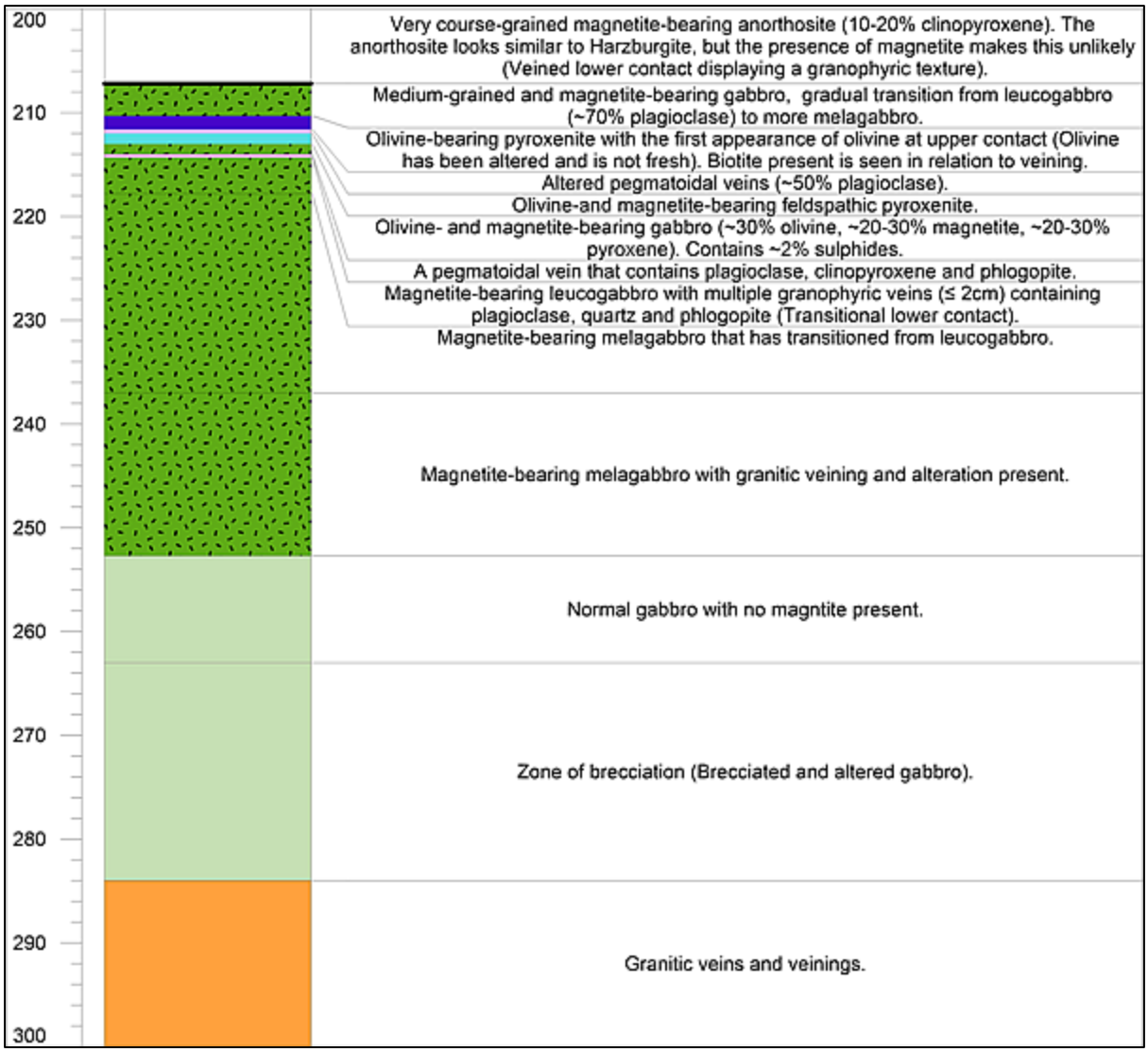
200
210
220
230
240
250
260
270
280
290
300
Very course-grained magnetite-bearing anorthosite (10-20% clinopyroxene). The anorthosite looks similar to Harzburgite, but the presence of magnetite makes this unlikely (Veined lower contact displaying a granophyric texture).
Medium-grained and magnetite-bearing gabbro, gradual transition from leucogabbro (~70% plagioclase) to more melagabbro.
Olivine-bearing pyroxenite with the first appearance of olivine at upper contact (Olivine has been altered and is not fresh). Biotite present is seen in relation to veining.
Altered pegmatoidal veins (~50% plagioclase).
Olivine-and magnetite-bearing feldspathic pyroxenite.
Olivine- and magnetite-bearing gabbro (~30% olivine, ~20-30% magnetite, ~20-30% pyroxene). Contains ~2% sulphides.
A pegmatoidal vein that contains plagioclase, clinopyroxene and phlogopite.
Magnetite-bearing leucogabbro with multiple granophyric veins (≤ 2cm) containing plagioclase, quartz and phlogopite (Transitional lower contact).
Magnetite-bearing melagabbro that has transitioned from leucogabbro.
Magnetite-bearing melagabbro with granitic veining and alteration present.
Normal gabbro with no magntite present.
Zone of brecciation (Brecciated and altered gabbro).
Granitic veins and veinings.

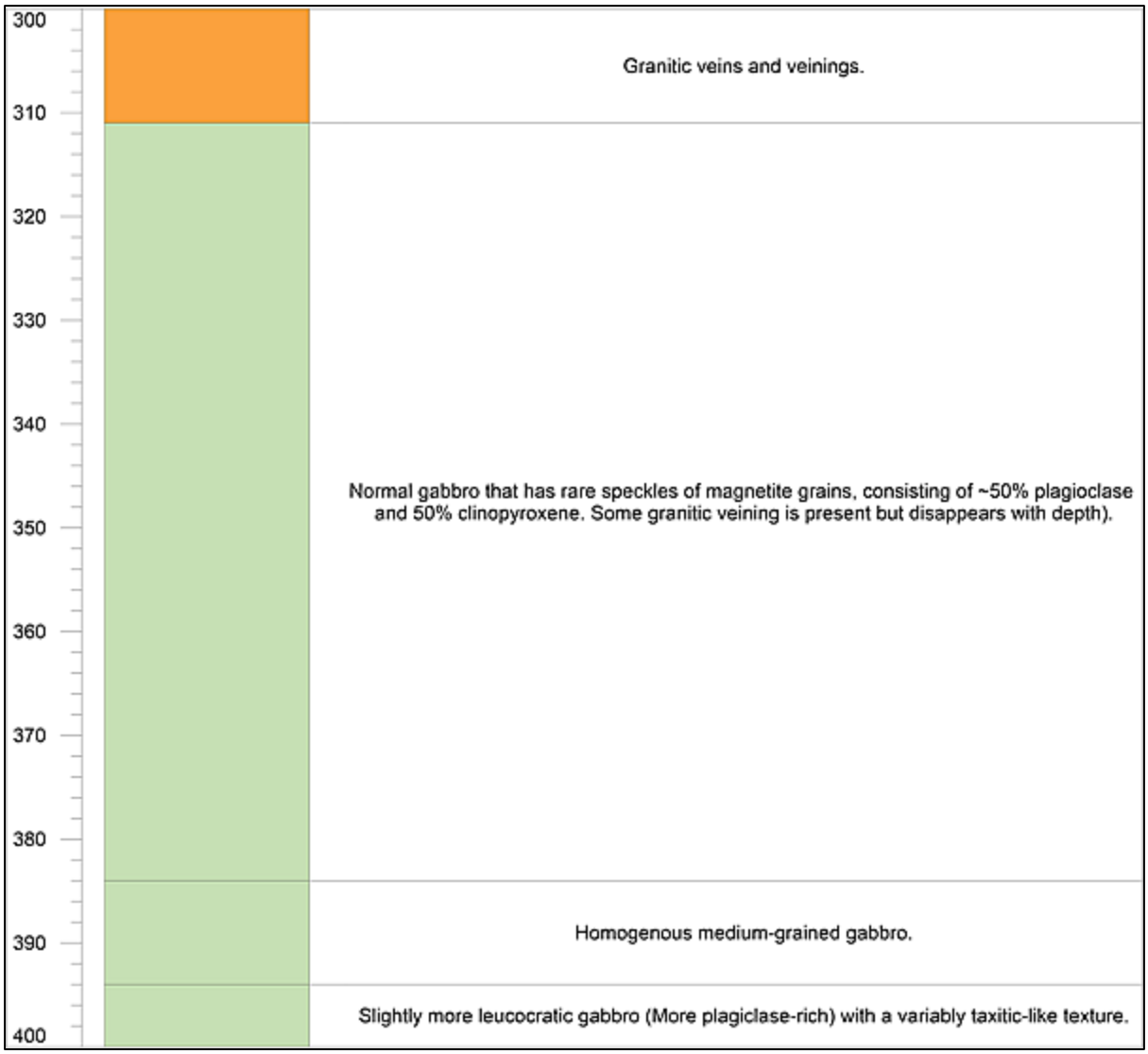
300
310
320
330
340
350
360
370
380
390
400
Granitic veins and veinings.
Normal gabbro that has rare speckles of magnetite grains, consisting of ~50% plagioclase and 50% clinopyroxene. Some granitic veining is present but disappears with depth).
Homogenous medium-grained gabbro.
Slightly more leucocratic gabbro (More plagiclase-rich) with a variably taxitic-like texture.

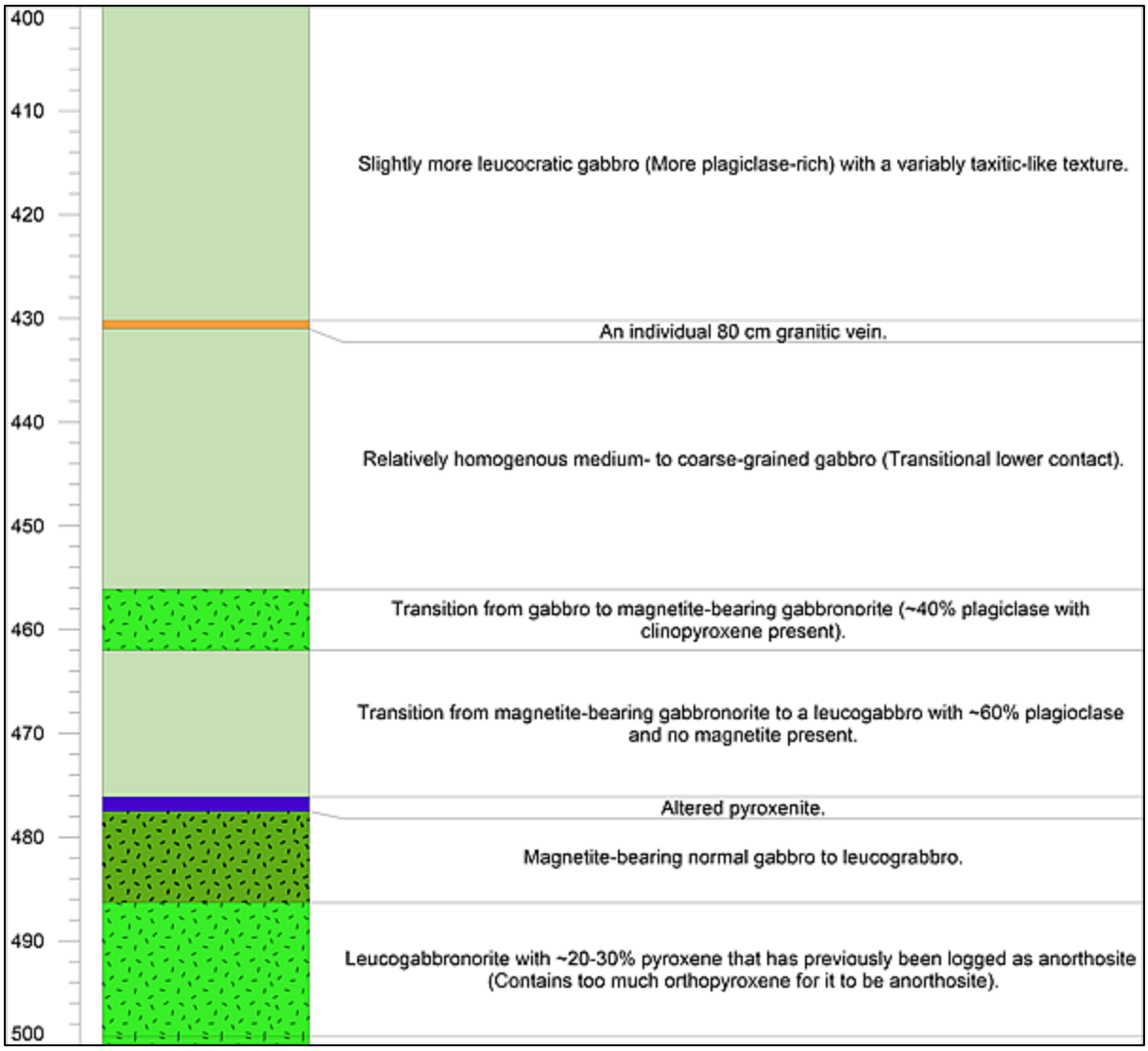
400
410
420
430
440
450
460
470
480
490
500
Slightly more leucocratic gabbro (More plagiclase-rich) with a variably taxitic-like texture.
An individual 80 cm granitic vein.
Relatively homogenous medium- to coarse-grained gabbro (Transitional lower contact).
Transition from gabbro to magnetite-bearing gabbronorite (~40% plagiclase with clinopyroxene present).
Transition from magnetite-bearing gabbronorite to a leucogabbro with ~60% plagioclase and no magnetite present.
Altered pyroxenite.
Magnetite-bearing normal gabbro to leucograbbro.
Leucogabbronorite with ~20-30% pyroxene that has previously been logged as anorthosite (Contains too much orthopyroxene for it to be anorthosite).

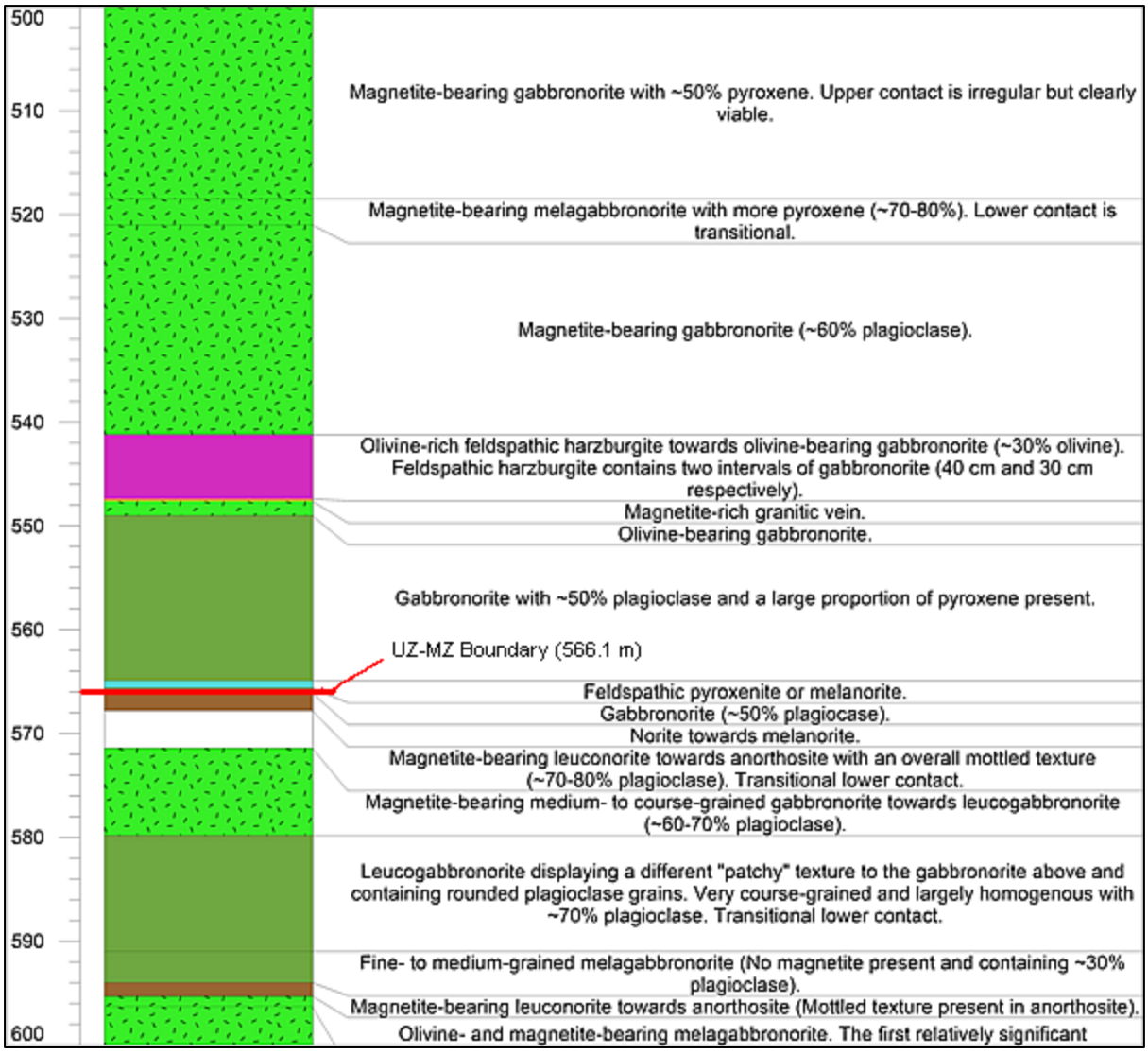
500
510
520
530
540
550
560
570
580
590
600
Magnetite-bearing gabbronorite with ~50% pyroxene. Upper contact is irregular but clearly viable.
Magnetite-bearing melagabbronorite with more pyroxene (~70-80%). Lower contact is transitional.
Magnetite-bearing gabbronorite (~60% plagioclase).
Olivine-rich feldspathic harzburgite towards olivine-bearing gabbronorite (~30% olivine). Feldspathic harzburgite contains two intervals of gabbronorite (40 cm and 30 cm respectively).
Magnetite-rich granitic vein.
Olivine-bearing gabbronorite.
Gabbronorite with ~50% plagioclase and a large proportion of pyroxene present.
UZ-MZ Boundary (566.1 m)
Feldspathic pyroxenite or melanorite.
Gabbronorite (~50% plagiocase).
Norite towards melanorite.
Magnetite-bearing leuconorite towards anorthosite with an overall mottled texture (~70-80% plagioclase). Transitional lower contact.
Magnetite-bearing medium- to course-grained gabbronorite towards leucogabbronorite (~60-70% plagioclase).
Leucogabbronorite displaying a different "patchy" texture to the gabbronorite above and containing rounded plagioclase grains. Very course-grained and largely homogenous with ~70% plagioclase. Transitional lower contact.
Fine- to medium-grained melagabbronorite (No magnetite present and containing ~30% plagioclase).
Magnetite-bearing leuconorite towards anorthosite (Mottled texture present in anorthosite).
Olivine- and magnetite-bearing melagabbronorite. The first relatively significant

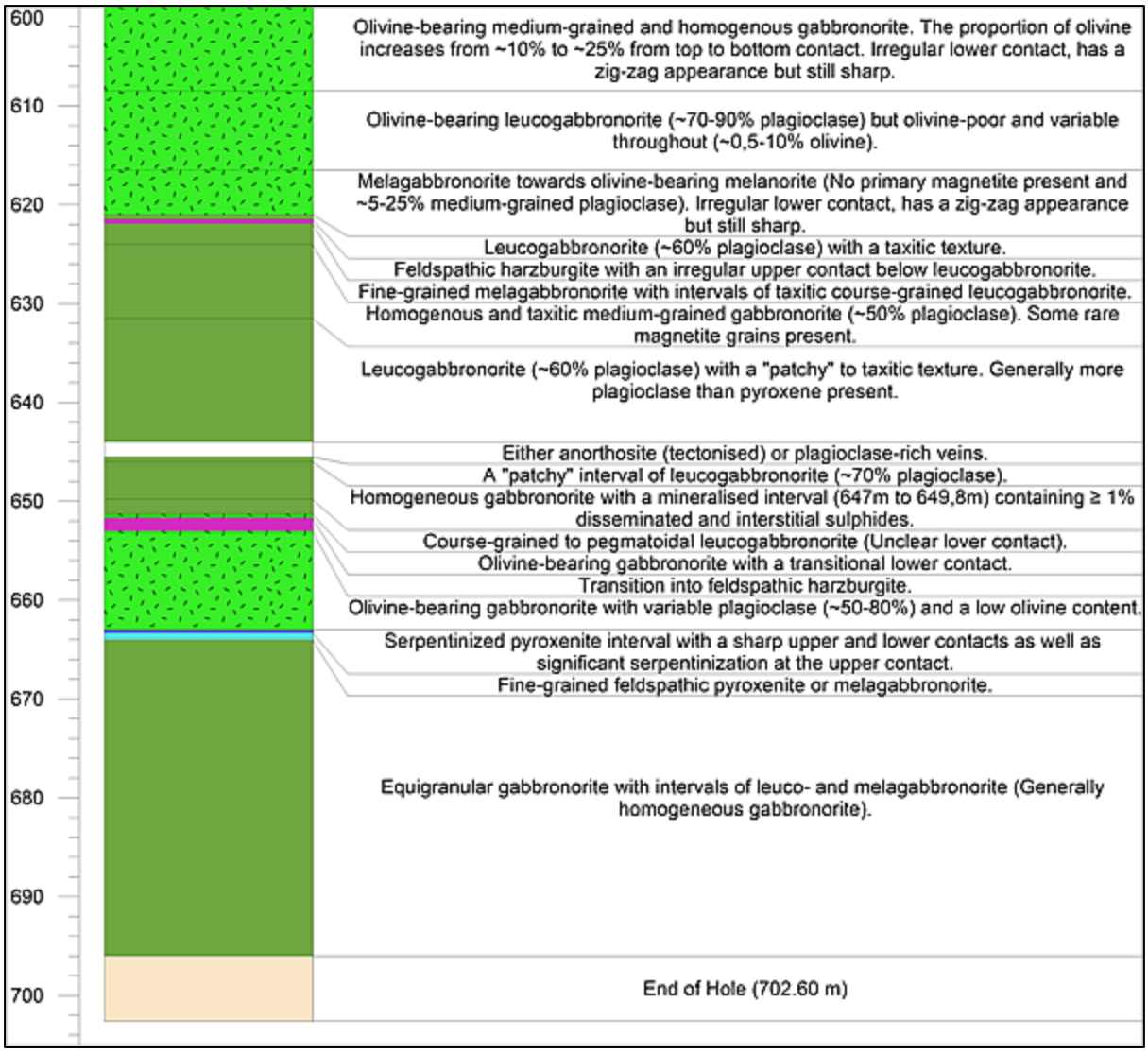
600
610
620
630
640
650
660
670
680
690
700
Olivine-bearing medium-grained and homogenous gabbronorite. The proportion of olivine increases from ~10% to ~25% from top to bottom contact. Irregular lower contact, has a zig-zag appearance but still sharp.
Olivine-bearing leucogabbronorite (~70-90% plagioclase) but olivine-poor and variable throughout (~0,5-10% olivine).
Melagabbronorite towards olivine-bearing melanorite (No primary magnetite present and ~5-25% medium-grained plagioclase). Irregular lower contact, has a zig-zag appearance but still sharp.
Leucogabbronorite (~60% plagioclase) with a taxitic texture.
Feldspathic harzburgite with an irregular upper contact below leucogabbronorite.
Fine-grained melagabbronorite with intervals of taxitic course-grained leucogabbronorite.
Homogenous and taxitic medium-grained gabbronorite (~50% plagioclase). Some rare magnetite grains present.
Leucogabbronorite (~60% plagioclase) with a "patchy" to taxitic texture. Generally more plagioclase than pyroxene present.
Either anorthosite (tectonised) or plagioclase-rich veins.
A "patchy" interval of leucogabbronorite (~70% plagioclase).
Homogeneous gabbronorite with a mineralised interval (647m to 649,8m) containing ≥ 1% disseminated and interstitial sulphides.
Course-grained to pegmatoidal leucogabbronorite (Unclear lover contact).
Olivine-bearing gabbronorite with a transitional lower contact.
Transition into feldspathic harzburgite.
Olivine-bearing gabbronorite with variable plagioclase (~50-80%) and a low olivine content.
Serpentinized pyroxenite interval with a sharp upper and lower contacts as well as significant serpentinization at the upper contact.
Fine-grained feldspathic pyroxenite or melagabbronorite.
Equigranular gabbronorite with intervals of leuco- and melagabbronorite (Generally homogeneous gabbronorite).
End of Hole (702.60 m)

Appendix 2

Whole Rock Geochemical data

Sample	TW1-1	TW1-2	TW1-3	TW1-4	TW1-5	TW1-6	TW1-7	TW1-8	TW1-9	TW1-10	TW1-11	TW1-12	TW1-13	TW1-14
SiO_2 (wt%)	39.64	43.90	46.90	38.27	34.05	49.17	48.11	50.66	48.58	46.12	49.71	46.93	33.58	44.37
TiO_2 (wt%)	3.85	2.58	1.64	3.40	5.42	0.73	1.09	0.46	1.19	1.05	0.65	0.83	3.21	1.00
Al_2O_3 (wt%)	13.89	14.39	18.82	13.46	15.10	19.72	16.37	23.47	18.95	14.62	24.22	19.46	5.77	19.11
Fe_2O_3 (wt%)	26.37	20.25	13.61	30.11	32.84	10.79	14.52	5.92	10.88	17.35	5.49	12.67	37.48	16.06
MnO (wt%)	0.21	0.20	0.14	0.25	0.19	0.15	0.19	0.08	0.13	0.20	0.06	0.12	0.24	0.15
MgO (wt%)	5.87	5.68	4.09	7.32	3.84	4.35	6.46	2.25	4.46	8.71	1.38	5.90	13.02	5.76
CaO (wt%)	9.72	10.74	10.43	7.60	8.06	10.58	10.88	10.63	12.36	10.14	10.89	8.88	3.43	8.62
Na_2O (wt%)	1.88	2.08	2.81	1.73	1.80	2.92	2.28	3.56	2.70	1.98	3.56	2.48	0.13	2.31
K_2O (wt%)	0.21	0.33	0.57	0.22	0.22	0.49	0.25	0.67	0.32	0.21	1.14	0.27	0.26	0.25
P_2O_5 (wt%)	0.02	0.02	0.04	0.03	0.02	0.16	0.05	0.02	0.05	0.03	0.05	0.03	0.02	0.02
Cr_2O_3 (wt%)	0.00	0.00	0.01	0.04	0.08	0.00	0.04	0.00	0.03	0.05	0.00	0.00	0.42	0.05
NiO (wt%)	0.02	0.02	0.01	0.03	0.04	0.01	0.02	0.00	0.01	0.02	0.00	0.03	0.10	0.07
LOI (wt%)	-0.46	0.31	0.56	-1.04	-0.29	0.50	0.01	1.28	0.22	-0.39	1.55	2.00	4.01	2.10
Total (wt%)	101.20	100.50	99.61	101.42	101.35	99.56	100.27	99.01	99.88	100.08	98.70	99.59	101.68	99.87
Sc (ppm)	43.23	47.65	31.38	29.26	32.96	29.77	38.7	20.89	36.51	32.38	17.66	17.09	24.44	19.09
V (ppm)	1329.38	1014.28	573.71	1308.91	2234.3	276.39	425.26	133.72	447.91	509.79	182.62	291.05	2170.17	461.56
Cr (ppm)	39.86	41.99	111.21	192.54	325.6	59.34	231.11	26.56	198.92	335.65	19.47	16.09	2128.39	307.87
Co (ppm)	97.62	78.63	41.24	117.65	115.3	42.63	73.06	24.58	34	84.93	15.19	85.85	204.48	84.21
Ni (ppm)	130.8	124.42	43.46	231.7	304.87	51.77	146.17	23.58	55.12	128.56	20.33	185.24	790.83	523.98
Cu (ppm)	445.04	398.45	26.84	429.23	610.16	25.68	190.26	24.81	92.87	81.56	33.78	300.48	1344.85	2370.83
Zn (ppm)	115.91	113.88	81.52	156.78	168.73	66.17	81.25	48.8	54.25	91.86	39.99	79.9	169.45	98.78
Ga (ppm)	23.64	20.79	20.63	20.59	32.41	19.55	18.55	23.05	22.11	18.66	22.6	17.58	17.21	19.9
Rb (ppm)	1.92	11.63	14.43	2.3	0.61	11.69	2.8	17.94	5.77	2.19	28.52	4.96	18.24	3.16
Sr (ppm)	228.2	232.49	321.38	204.57	228.4	326.3	244.9	378.92	292.2	216.59	399.63	301.02	41.91	306.05
Y (ppm)	7.96	11.5	7.93	3.91	2.91	10.61	9.05	5.23	10.94	8.32	6.88	5.06	5.24	0.94
Zr (ppm)	21.69	33.55	33.96	21.87	24.33	29.79	22.05	33.55	24.6	16.48	44.27	18.25	13.02	12.51
Nb (ppm)	1.96	1.74	1.92	6.04	6.66	3.13	3.87	3.25	2.46	2.87	2.91	2.37	3.73	0.25
Mo (ppm)	BDL	0.13	BDL	0.49	1.21	0.22	0.9	0.57	BDL	0.66	0.29	BDL	0.96	0.72
Ba (ppm)	111.94	142.82	200.1	81.67	109.07	198.28	110.57	229.81	158.1	100.58	347.28	134.57	29.48	130.25
Pb (ppm)	3.99	2.08	4.55	2.85	2.17	7.01	1.32	5.1	2.84	3.18	6.17	6.58	11.53	17.28
Th (ppm)	BDL	BDL	BDL	BDL	BDL	BDL	BDL	BDL	BDL	BDL	0.02	BDL	BDL	BDL
U (ppm)	BDL	BDL	BDL	BDL	BDL	BDL	BDL	BDL	BDL	BDL	BDL	BDL	BDL	BDL
SiO_2/Al_2O_3	2.85	3.05	2.49	2.84	2.25	2.49	2.94	2.16	2.56	3.15	2.05	2.41	5.82	2.32
Mg#	18.21	21.91	23.11	19.56	10.47	28.73	30.79	27.54	29.07	33.42	20.09	31.77	25.78	26.40
Al_2O_3/FeO + MgO	0.47	0.60	1.15	0.39	0.45	1.40	0.84	3.10	1.33	0.60	3.83	1.12	0.12	0.95
CaO/Al_2O_3	0.70	0.75	0.55	0.56	0.53	0.54	0.66	0.45	0.65	0.69	0.45	0.46	0.59	0.45
Sr/Al_2O_3	16.43	16.16	17.08	15.20	15.13	16.55	14.96	16.14	15.42	14.81	16.50	15.47	7.26	16.02

Sample	TW1-15	TW1-16	TW1-17	TW1-18	TW1-19	TW1-20	TW1-21	TW1-22	TW1-23	TW1-24	TW1-25	TW1-26	TW1-27	TW1-28
SiO_2 (wt%)	44.19	47.59	50.28	49.99	49.71	48.65	48.69	44.69	48.40	48.55	46.19	50.36	48.29	48.62
TiO_2 (wt%)	1.52	1.19	0.36	0.37	0.22	0.39	0.57	0.11	0.17	0.54	1.72	0.61	0.47	0.13
Al_2O_3 (wt%)	18.58	20.01	17.19	16.72	20.39	17.85	19.83	9.35	16.59	26.28	17.90	14.97	13.46	14.67
Fe_2O_3 (wt%)	16.06	10.92	9.59	10.87	6.59	10.31	9.14	16.00	10.02	4.44	14.00	12.75	15.24	8.11
MnO (wt%)	0.14	0.13	0.15	0.17	0.11	0.15	0.14	0.22	0.16	0.08	0.19	0.19	0.22	0.15
MgO (wt%)	5.06	3.92	7.71	8.29	5.84	7.15	6.75	22.66	11.79	1.90	5.70	10.06	11.81	13.35
CaO (wt%)	10.28	11.07	9.68	10.43	13.07	11.37	10.92	6.12	9.79	12.74	12.70	9.13	8.36	12.97
Na_2O (wt%)	2.38	2.92	2.29	1.97	2.24	2.08	2.09	0.78	1.46	3.08	1.94	1.59	1.19	1.06
K_2O (wt%)	0.25	0.44	0.26	0.18	0.27	0.14	0.37	0.08	0.11	0.47	0.21	0.34	0.13	0.11
P_2O_5 (wt%)	0.03	0.02	0.03	0.04	0.02	0.03	0.03	0.02	0.02	0.05	0.05	0.06	0.03	0.01
Cr_2O_3 (wt%)	0.08	0.01	0.07	0.08	0.05	0.01	0.05	0.07	0.00	0.00	0.10	0.09	0.05	0.15
NiO (wt%)	0.04	0.01	0.02	0.02	0.01	0.02	0.01	0.19	0.05	0.01	0.02	0.03	0.10	0.05
LOI (wt%)	1.49	1.33	1.78	0.47	0.63	1.48	1.68	0.95	2.02	1.77	0.39	0.72	0.85	0.98
Total (wt%)	100.10	99.54	99.41	99.59	99.15	99.64	100.27	101.25	100.56	99.88	101.11	100.88	100.20	100.35
Sc (ppm)	28.15	35.19	28.77	35.43	34.15	34.19	27.44	19.97	26.03	17.94	37.82	35.29	32.17	33.11
V (ppm)	938.96	505.11	180.91	175.78	129.28	190.09	184.61	61.73	99.96	142.88	617.62	237.27	186.87	112.52
Cr (ppm)	389.64	68.53	407.31	499.42	308.48	129.22	376.03	409.38	167.33	7.56	586.28	526.2	342.86	799.65
Co (ppm)	73.5	43.41	46.66	49.79	35.57	51.21	41.45	143.91	64.48	18.89	47.82	61.41	94.85	70
Ni (ppm)	260.01	73.41	149.82	163.17	108.03	172.77	113.4	1476.41	360.81	51.4	158.44	201.27	744.53	378.42
Cu (ppm)	801.18	160.22	130.75	144.15	104.59	167.91	74.56	329.44	151.54	71.84	124.7	142.75	831	25.87
Zn (ppm)	77.51	80.58	67.79	74.69	39.93	72.11	63.58	99.86	63.72	32.06	80.28	83.5	103.67	43.13
Ga (ppm)	21.1	20.14	15.09	15.77	14.82	15.12	16.62	8.1	12.57	19.12	18.97	13.42	11.52	11.97
Rb (ppm)	1.71	6.86	3.02	1.68	2.53	-1.93	5.78	-1.67	-1.57	10.26	1.63	10.34	0.61	0.63
Sr (ppm)	299.75	344.23	263.79	204.43	219.61	184.8	209.38	102.25	179.75	318.86	189.4	151.04	136.36	143.62
Y (ppm)	4.44	5.75	6.95	8.39	6.41	7.51	7.03	1.85	5.12	5.23	11.36	10.17	9.3	5.66
Zr (ppm)	19.34	23.46	19.61	20.48	17.73	13.65	23.04	6.74	13.07	14.83	29.61	27.43	16.25	8.27
Nb (ppm)	1.75	0.76	1.1	0.88	2.42	2.3	3.56	2.16	2.43	2.82	5.88	3.13	3.38	2.01
Mo (ppm)	0.96	0.36	0.59	0.49	0.89	1.08	1.03	0.31	0.74	1.59	1.19	BDL	BDL	0.82
Ba (ppm)	121.92	196.73	94.48	76.29	111.07	74.55	121.41	31.18	44.47	168.9	89.4	89.7	49.29	19.03
Pb (ppm)	6.31	3.3	3.77	1.86	2.18	2.99	3.2	3.91	5.49	3.18	3.09	1.8	4.59	4.01
Th (ppm)	BDL	BDL	BDL	BDL	BDL	BDL	BDL	BDL	BDL	0.72	BDL	BDL	BDL	BDL
U (ppm)	BDL	BDL	BDL	BDL	BDL	BDL	BDL	BDL	2.00	BDL	BDL	BDL	BDL	BDL
SiO_2/Al_2O_3	2.38	2.38	2.92	2.99	2.44	2.73	2.46	4.78	2.92	1.85	2.58	3.36	3.59	3.31
Mg#	23.96	26.42	44.57	43.27	46.98	40.95	42.48	58.61	54.06	29.97	28.93	44.10	43.66	62.21
Al_2O_3/FeO + MgO	0.95	1.46	1.05	0.93	1.73	1.09	1.32	0.25	0.80	4.46	0.98	0.70	0.53	0.71
CaO/Al_2O_3	0.55	0.55	0.56	0.62	0.64	0.64	0.55	0.65	0.59	0.48	0.71	0.61	0.62	0.88
Sr/Al_2O_3	16.13	17.20	15.35	12.23	10.77	10.35	10.56	10.94	10.83	12.13	10.58	10.09	10.13	9.79

Sample	TW1-29	TW1-30	TW1-31	TW1-32	TW1-33	TW1-34	TW1-35	TW1-36	TW1-37	TW1-38	TW1-39	TW1-40
SiO_2 (wt%)	46.88	43.59	50.08	53.14	48.21	47.50	47.97	48.12	44.60	46.63	46.97	71.82
TiO_2 (wt%)	0.15	0.16	0.13	0.19	0.14	0.13	0.13	0.16	0.18	0.14	1.18	0.10
Al_2O_3 (wt%)	17.37	5.61	21.16	13.97	22.05	21.01	21.95	22.22	16.49	23.28	4.27	15.03
Fe_2O_3 (wt%)	7.26	17.16	6.29	10.66	4.79	5.95	5.97	5.77	14.39	6.56	20.65	1.46
MnO (wt%)	0.13	0.24	0.11	0.17	0.09	0.10	0.09	0.09	0.17	0.09	0.31	0.02
MgO (wt%)	9.94	25.08	6.46	7.65	5.29	5.25	5.09	4.92	12.37	6.30	12.77	0.43
CaO (wt%)	14.49	5.08	12.51	9.04	13.69	12.90	13.77	13.89	9.29	12.89	12.55	1.94
Na_2O (wt%)	1.04	0.58	2.18	2.47	2.15	2.29	2.08	2.08	1.16	1.66	0.48	6.13
K_2O (wt%)	0.08	0.16	0.21	0.29	0.31	0.45	0.33	0.34	0.22	0.21	0.06	0.73
P_2O_5 (wt%)	0.02	0.03	0.02	0.22	0.02	0.02	0.02	0.02	0.02	0.02	0.14	0.05
Cr_2O_3 (wt%)	0.16	0.08	0.01	0.01	0.02	0.02	0.02	0.03	0.01	0.01	0.05	0.00
NiO (wt%)	0.04	0.18	0.02	0.03	0.02	0.14	0.15	0.13	0.21	0.10	0.09	0.00
LOI (wt%)	2.48	3.01	0.57	2.01	2.76	3.41	1.98	1.69	1.34	1.88	1.33	0.84
Total (wt%)	100.03	100.96	99.73	99.87	99.54	99.16	99.55	99.45	100.46	99.78	100.84	98.52
Sc (ppm)	34.58	25.46	28.65	40.64	24.07	27.2	28.15	31.58	19.7	20.85	86.92	1.25
V (ppm)	107.42	93.87	84.19	118.7	76.32	81.8	95.6	101.02	90.47	54.03	542.23	12.95
Cr (ppm)	839.35	463.82	158.71	107.7	180.55	182.7	215.43	200.89	136.49	159.4	311.97	0.38
Co (ppm)	52.29	156.98	37.62	72.82	35.35	59.76	62.09	61.06	127.51	54.72	138.28	2.23
Ni (ppm)	287.79	1413.71	160.71	259.17	164.17	1035.24	1142.87	971.46	1668.82	744.77	720.63	4.7
Cu (ppm)	76.36	816.83	127.9	434.61	213.96	2546.66	2391.56	1839.64	2204.56	1015.55	2709.51	9.06
Zn (ppm)	41.44	114.18	41.11	93.95	34.5	39.21	36.66	37.72	75.62	33.61	151.9	21.77
Ga (ppm)	11.91	5.3	17.24	14.95	15.3	15.71	16.4	16.16	15.46	16.13	9.38	16.95
Rb (ppm)	0.37	4.54	2.55	10.15	7.91	12.72	6.87	6.99	3.65	3.67	-0.7	15.96
Sr (ppm)	151.5	64.51	264.84	263.26	275.68	258.8	284.46	288.56	214.19	282.31	57.84	470.35
Y (ppm)	4.5	6.06	4.41	20.7	4.17	3.69	4.24	4.53	3.37	3.39	38.13	2.83
Zr (ppm)	32.51	11.03	9.14	21.04	13.5	12.9	11.73	13.42	11.74	12.94	38.43	83.65
Nb (ppm)	1.71	2.6	1.44	2.87	1.16	BDL	0.09	BDL	0.76	0.56	4.54	BDL
Mo (ppm)	0.92	0.85	BDL	1.42	0.88	BDL	0.4	0.33	0.45	BDL	0.59	BDL
Ba (ppm)	39.95	45.34	73.47	85.8	109.71	135.35	125.95	128.13	81.94	80.63	18.1	247.16
Pb (ppm)	2.02	4.52	3.73	1.92	1.55	7.96	6.43	5.23	6.57	5.35	4.9	4.61
Th (ppm)	BDL	BDL	BDL	BDL	BDL	BDL	BDL	BDL	BDL	BDL	BDL	BDL
U (ppm)	BDL	BDL	BDL	BDL	BDL	BDL	BDL	BDL	BDL	BDL	BDL	BDL
SiO_2/Al_2O_3	2.70	7.77	2.37	3.80	2.19	2.26	2.19	2.17	2.70	2.00	11.00	4.78
Mg#	57.79	59.38	50.67	41.78	52.48	46.88	46.02	46.02	46.23	48.99	38.21	22.75
Al_2O_3/FeO + MgO	1.05	0.14	1.75	0.81	2.30	1.98	2.10	2.20	0.65	1.91	0.14	8.62
CaO/Al_2O_3	0.83	0.91	0.59	0.65	0.62	0.61	0.63	0.63	0.56	0.55	2.94	0.13
Sr/Al_2O_3	8.72	11.50	12.52	18.84	12.50	12.32	12.96	12.99	12.99	12.13	13.55	31.29